“Structural alteration of nucleic acids in bacteria and hepatitis C virus by quinoxaline small molecules”

Thesis submitted for the degree of
Doctor of Philosophy (Science)
In Biochemistry

By
JEET CHAKRABORTY

Department of Biochemistry
University of Calcutta

2021

Acknowledgement

The pages of this Thesis not only represent my research work here at CSIR Indian Institute of Chemical Biology but also reflect the wonderful people I have come across, the wonderful memories that I have shared with them during this time, and the lifelong impression they have left which I will always carry with me all my life. There is a saying that **"Life is a journey with problems to solve and lessons to learn but most of all. Experiences to enjoy"** and it was a remarkable experience indeed, one I would cherish all my life.

When I was just a new kid on the block, my PI would often say that Ph.D. would change me as a person. Little did I know back then the meaning of those words but as I stand at the very edge of this journey I realized it was my toughest journey yet. Life does change us to some extent, and like the great Heraclitus said, **"Change is the only constant"** so changes are always good as long as they are constructive in life. The list of people that have played a big part in making this journey worthwhile is long but I adore every contribution to my development as a scientific researcher.

First and foremost, I would like to convey my sincere gratitude to my Ph.D. supervisor **Dr. Sanjay Dutta**, without whom my research work here at IICB would have been impossible. He has always inspired and motivated me to push myself harder but at the same time to enjoy my work. He has an immense ability to remain calm even in the most tense environment something that has inspired me. He has always given me the freedom to carry out my research work at my own pace, and has always encouraged the incorporation

of my ideas in those projects. I feel very lucky to have found a mentor like him who has helped me evolve as a researcher and also as a person.

I am grateful to the former directors of IICB **Prof. Siddhartha Roy**, **Prof Chitra Mandal**, **Prof. Samit Chattopadhyay,** and the current director **Prof. Arun Bandhyopadhyay** for giving me the platform to carry out my research work here at IICB and providing me all the institutional facilities for the last few years. I would also like to acknowledge The Council of Scientific and Industrial Research (CSIR) for providing me the Junior and senior research fellowship and contingency funds for the last 5 years.

I would like to especially thank **Payel Di** under whom I did my summer training at IICB. It was the first time I worked on a scientific project and my interest in science grew further after working under her guidance in the lab. She was one of the most hardworking people I have ever met in my life.

I have met a lot of great people during this time and they have made this journey a memorable one. I would first like to thank my lab seniors **Ajay Da**, **Tridib Da**, **Sayanika Di**, **Sanghamitra Di,** and **Abhi Di** for the wonderful moments I shared with them in the lab. You guys were always fun to be around and we had a lot of scientific as well as discussions on other topics, which was a great learning experience for me. Also thank you for tolerating me. I would also like to thank some other seniors like **Krishnendu Da**, **Abdus Da**, **Shyam Da**, **Asim Da**, **Asad Da**, **Atul Da,** and **Chinmoy Da** with whom I shared a very good bond and I have learned a lot from discussing scientific problems with you guys.

I have always been a big admirer of **Dr. APJ Abdul Kalam Azad** and to quote him "**One best book is equal to a hundred good friends but one**

good friend is equal to a library". I consider myself lucky to have found such great friends during this period. I would like to especially thank you guys **Snehasis**, **Anand**, **Dheerendra**, **Debajyoti**, **Kamran**, **Dipayan Da**, **Kaushik Da**, **Saroj**, **Suvendu,** and **Kajol** for making my life happier and stress-free. I always had a great time with you guys, constantly discussing funny and nonsensical things that really took a lot of pressure at work.

I would like this opportunity to specially thank **Ritesh** and **Sayef** for being my two best buddies at work and we together formed the inseparable trio. We had so many scientific and off-topic discussions, arguments, goofy and fun-filled moments, which I would always cherish all my life. Three of us share similar passions and interests and it was such a great experience to watch three of us grow as a researcher as well as in person. It really was a memorable journey.

I would like to thank my colleagues **Subhadeep Da**, **Amit**, **Dipendu**, **Bhim**, **Chandrasova**, and to all the active members of **Lab 144/148**, my trainee **Parinita**, and other trainees **Bijaya**, **Haseena**, **Sravani**, **Sangappa**, **Oindrila,** and my lab juniors **Rimita**, **Achyut** and **Aymen** for the wonderful memories. I wish you guys a wonderful future.

I would also like to acknowledge **Jishu Da**, **Murugan Da**, **Tanmoy Da** and **Debalina** for helping me out during my experiments and providing the much-needed technical support.

I would also like to extend my appreciation to all other IICB friends and seniors who have helped me with chemicals, reagents and cell lines (the most in-demand thing at IICB). My acknowledgement to **Eshani**, **Satadeepa**, **Krishna**, **Sambit**, **Sunny (Md Abul)**, **Samrat**, **Sumit**, **Shiladitya**, **Sonali**, **Arijit**,

Pratiti, **Mahesh Da**, **Dipika Di**, **Nidhi**, **Gaurab**, **Chittran Da**, **Rajeev Da**, **Shadab Da**, **Shameel Da**, **Mainak Da**, **Deepsikha Di**, **Mainak Da** (SNB Sir's lab), **Yogaditya Da**, **Animesh** and **Deepak Da** for helping me out whenever I needed help.

I would also like to acknowledge **Abhishek Da** (Canteen), **Niranjan Da** (Store and Purchase), and **Shibu Da** (Janitor) with whom I also share a great bond.

One can't have enough words to acknowledge their parents so all I want to say is I feel extremely proud to have the best parents in this world. They are my biggest strength in life, my constant support, my two best friends and I love them to the moon and back.

Finally, I would like to mention the two people who are very close to my heart my **Dida** and **Choto Mashi**. I lost both of them a few years back. I know that I will always have their blessings in life. I really miss you guys.

My sincere apologies to all the people I have missed to acknowledge. I wish you all the best in life.

Date: 12/4/2021 **Jeet Chakraborty**

CONTENTS

LIST OF ABBREVIATIONS	**I-II**
REVIEW OF LITERATURE	**1-39**
References	27-39
AIMS AND OBJECTIVES	**40**
CHAPTER 1:	**41-64**
1.1 Introduction	42-43
1.2 Materials and Methods	44-49
1.3 Result and Discussion	50-61
1.4 Conclusion	62-64
1.5 References	
CHAPTER 2:	**65-95**
2.1A Introduction	66-67
2.1B Introduction	68
2.2 Materials and Methods	68-72
2.3A Result and Discussion	72-86
2.3B Result and Discussion	87-91
2.4 Conclusion	91-92
2.5 References	92-95
SUMMARY OF WORK	**96-97**
PUBLICATIONS	**98-101**

Abbreviations

dsDNA	double stranded Deoxyribonucleic acid
RNA	Ribonucleic acid
ctDNA	Calf Thymus DNA
UV	Ultraviolet
NMR	Nuclear Magnetic Resonance
IC50	Half Maximal Inhibitory Concentration
CC50	Cytotoxic Concentration
μM	Micromolar
nM	Nanomolar
mM	Millimolar
DPB	Diffuse Panbronchiolitis
Ca	Calcium
FDA	Food and Drug Association
THF	Tetrahydrofolate
LPS	Lipopolysaccharide
FabI	1-phosphatidylinositol 3-phosphate 5-kinase
EF	Elongation Factor
Mtb	Mycobacterium tuberculosis
IFN-α	Interferon alpha
HCV	Hepatitis c Virus
IRES	Internal Ribosome Entry Site
UTR	Untranslated Region
CD	Circular Dichroism
NaCl	Sodium Chloride
APTES	3-aminopropyltriethoxysilane
EDTA	Ethylene diamine tetra acetic acid
EtBr	Ethidium Bromide
RT	Room Temperature
PAGE	Poly acrylamide gel electrophoresis
DMEM	Dulbecco's Modified Eagles Medium

PBS	Phosphate Buffer Saline
TAE	Tris-acetate-EDTA
TBE	Tris-Borate-EDTA
PCR	Polymerase Chain reaction
m-RNA	Messenger RNA
FRET	Forster Resonance Energy Tranfer
NAP	Nucleoid Associated Proteins
HU	Heat Unstable
HNS	Histone like Nucleoid Structuring
Fis	Factor for inversion stimulation
IHF	Integration host factor
ChIP	Chromatin immunoprecipitation
XS	Xenogenic Silencing

REVIEW OF LITERATURE:

A. 1. Quinoxaline therapeutics

Quinoxaline antibiotics are a name given to a family of heterodetic cyclodepsipeptide antibiotics and comprise of a group of secondary metabolites that are manufactured by different bacterial species like Streptomyces, Actinomadura, and Micromonospora, etc.[1] Quinoxaline antibiotics comprise of an octadepsipeptide ring attached to two quinoxaline rings that have the capacity to intercalate into ds DNA by inserting between the adjacent bases. These antibiotics have been found to be really active against a wide range of gram-positive bacteria, viruses, and different types of cancers.[2] Some of them are quite well characterized quionoxaline antibiotics are Triostin A, Echinomycin, Thiocoraline etc.

Triostins:

Triostins are potent antitumor and antibacterial agents derived from *Streptomyces aureus* and other *Streptomyces* species. Triostins are comprised of three different types Triostin A, B, and C and they differ from other quinoxaline molecules by the presence of disulfide crosslinks confirmed by NMR studies. Triostin A was found to be very active against cultured mammalian cancerous cell lines like HT-29 (Colon carcinoma), NSCLC A549 (Lung carcinoma), and MDA-MB-231 (Breast cancer) with Inhibitory concentration (IC50) values around 100 nM. Triostin A was also found to intercalate into ds DNA and displayed high GC preference. A synthetic derivative of Triostin A known as TAMDEM (des-N-tetramethyl-triostin A) has been found to have a high preference for AT-rich DNA.

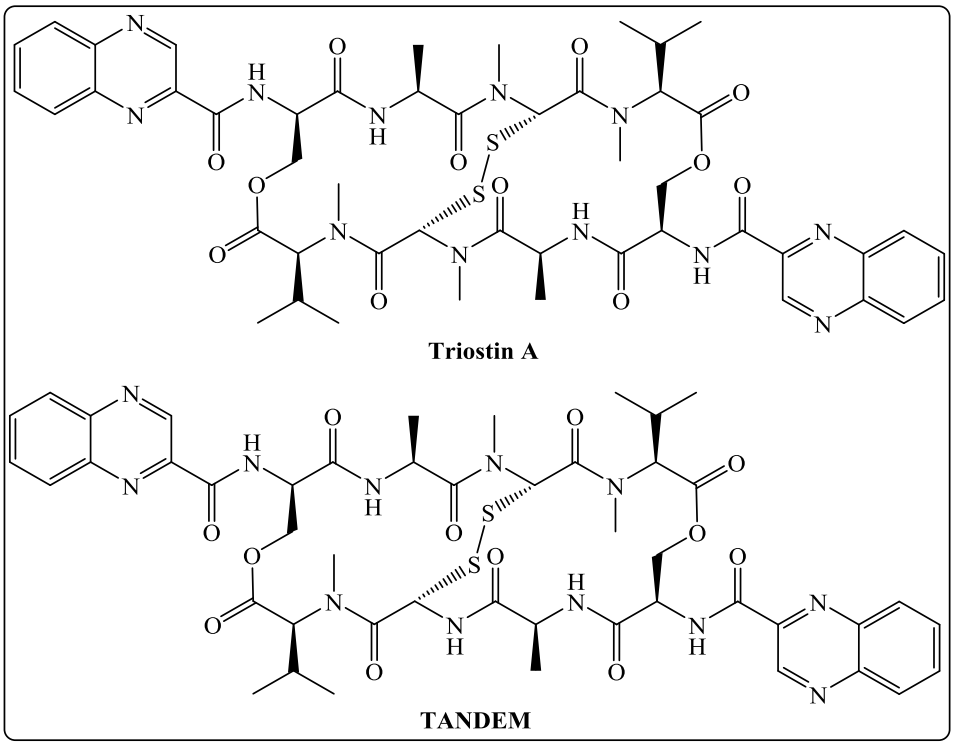

Figure I: Structures of various Quinoxaline antibiotics.

Echinomycin:

Echinomycin, a natural derivative was isolated from different *Streptomyces* species like *Streptomyces echinatus*, *Streptomyces lasalienis*, etc.[3] Echinomycin has an asymmetrical structure with an octadepsipeptide ring that contains L-alanine, N-methyl-L-valine, N-methyl-L-cysteine, N-methyl-L-serine and also a 2-carbonylquinoxaline group.[4] It has high activity against different gram-positive and gram-negative bacteria. It is also active against several types of cancers. Previous reports have shown that binding of Echinomycin to ds DNA occurs by bisintercalation, where the quinoxaline part slots between the DNA bases and the depsipeptide ring lies in the minor groove and they interfere with transcription by blocking RNA Polymerase progression.[5-7] Crystal and NMR studies have shown that DNA-echinomycin interaction is stabilized by Hoogsteen base pairing. Echinomycin has high GC specificity as seen from DNA footprinting experiments and it binds to 5_-[d(TCGATCGA)$_2$] by the non-cooperative way and to 5_-[d(ACGTACGT)$_2$] cooperatively.[8-9] Other biophysical studies like differential scanning calorimetry, UV melting studies have shown that the DNA-Echinomycin interaction was driven by entropy. [10]

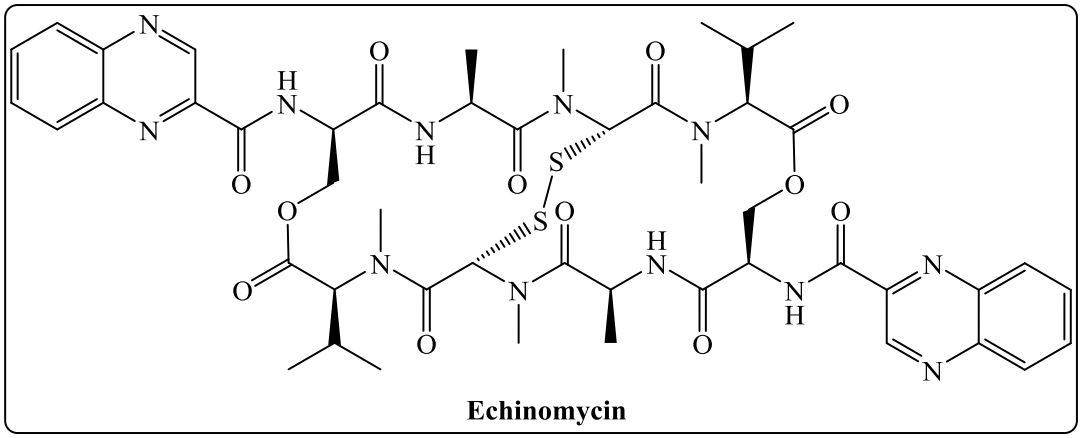

Figure II: Structure of the quinoxaline antibiotic Echinomycin.

B. Antibiotics Review:

Antibiotics have been a life savior for the last few decades and it is because of them the average life span of individuals has increased over time. But the increasing resistance against antibiotics by a wide group of pathogenic microorganisms has raised a serious alarming situation for the development of new antibiotics with different targets and mechanisms to the existing ones. To date the different classes of Antibiotics and their targets are summarized in Figure III and Table I below:

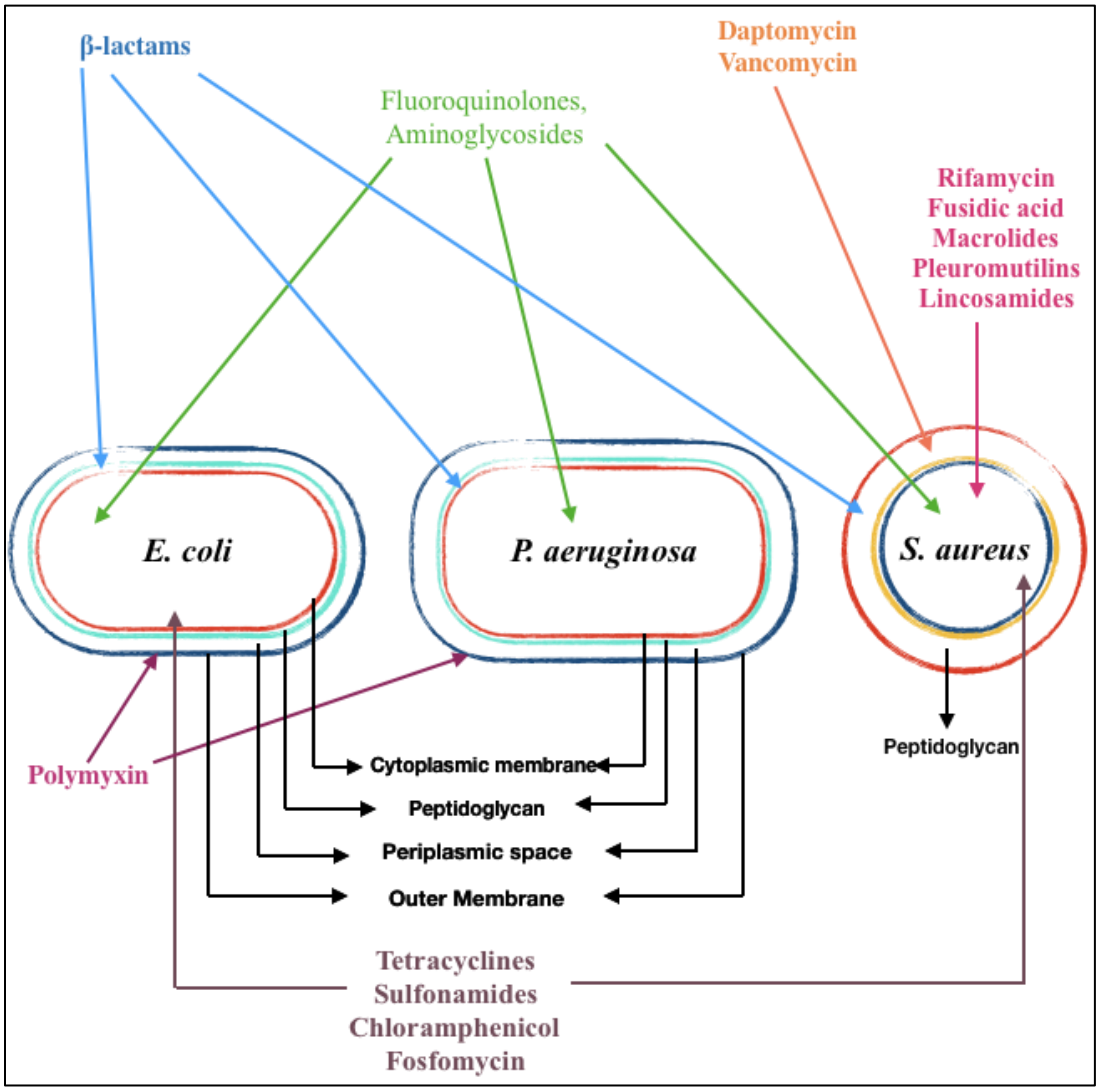

Figure III: The different antibiotic targets across gram-negative bacteria (*P. aeruginosa*), (*E. coli)*, *and* gram-positive (*S. aureus*).

Drug class	Target	Resistance Invitro	Major Clinical Resistance
β-Lactams	Penicillin binding proteins	porin loss, efflux	HGT (Horizontal gene transfer) β-lactamases, endogenous β-lactamases, porin loss, efflux
Glycopeptides	Lipid II	Rare	HGT vancomycin-resistance cassettes; stepwise cell-wall changes.
Macrolides,Chloramphenicol	50S RNA	Rare	HGT MLSB ribosome methylation, efflux
Tetracyclines,Aminoglycosides	30S RNA	Low (some efflux)	HGT efflux, ribosome protection
Fluoroquinolones	Gyrase, Topo IV	Low (ribosomal proteins)	HGT modification
Daptomycin Polymyxins	Membranes	Low (mutations modifying LPS)	Stepwise LPS changes, HGT modification
Metronidazole	DNA	Low (loss of reductase, entry)	HGT nim (alternate reductase) genes
Rifampicin	RNA polymerase	Changes in rpoB at many sites	Changes in rpoB at fewer sites
Trimethoprim	Dihydrofolate reductase	Altered DHFR (folA)	Altered DHFR, HGTaltered DHFR
Sulfonamides	Dihydropterate synthase	Altered DHPS (folP)	Altered folP, HGT altered DHPS
Fosfomycin	MurA	Loss of permeases	HGT-modifying enzymes
Fusidic acid	Elongation factor G	Mutations in fusA (EfG)	Mutations in fusA; HGT target protection FusB,C,D
LpxC inhibitors	Lipid A deacetylase	Mutations in fabZ, efflux, lpxC	Mutations in fabZ, efflux
Fab I inhibitors	Enoyl (acyl carrier protein) reductase	Mutations in fabI	Mutations in fabI

Cold Spring Harb Perspect Med 2016;6:a030239

Table I. Antibacterial class and their targets.

β-Lactam Antibiotics:

In the year 1928, while studying the relationship between Staphylococcus morphology and their virulence, Alexander Fleming accidentally contaminated them with Penicillium molds and found out that they inhibited the growth of *Staphylococcus* colonies around them.[11] He later subcultured the *Penicillium notatum* and isolated the lytic agent which he termed "penicillin" and designed an extraction process as well as an antimicrobial assay.[12] Using serial dilutions of the extract against different bacteria it was found that penicillin was active against, *Streptococcus pyrogenes*, *Staphylococci*, and *Pneumococcus* cultures and was inactive against *Vibrio cholerae*, *Bacillus proteus*, *Pseudomonas aeruginosa*, *Salmonella typhi*, and *Escherichia coli*.

Penicillin extracted in the US was crystallized successfully and analyzed by Squibb and Sons[13] and the strain used for clinical trials in England was crystallized by Florey's group.[14] It was later shown by Florey and colleagues that penicillin contained β-lactam rings. observed that at low penicillin concentrations, bacteria formed filament-like structures an indication that penicillin interferes with the bacterial cell wall.[15] Druid illustrated that penicillin could interfere with bacterial cell division and cell structure maintainance.[16]

Over the years a lot of derivatives containing the β-Lactam nucleus have been synthesized. Methicillin that was approved in the US for clinical use was the first semi-synthetic penicillin.[17] Carbenicillin, which was a semi-synthetic penicillin analog, was found to be effective against *Pseudomonas aeruginosa* was introduced in the year 1967.[18]

In recent years around 65% of prescribed antibiotics are β-Lactam antibiotics and Cephalosporin comprising half of them.

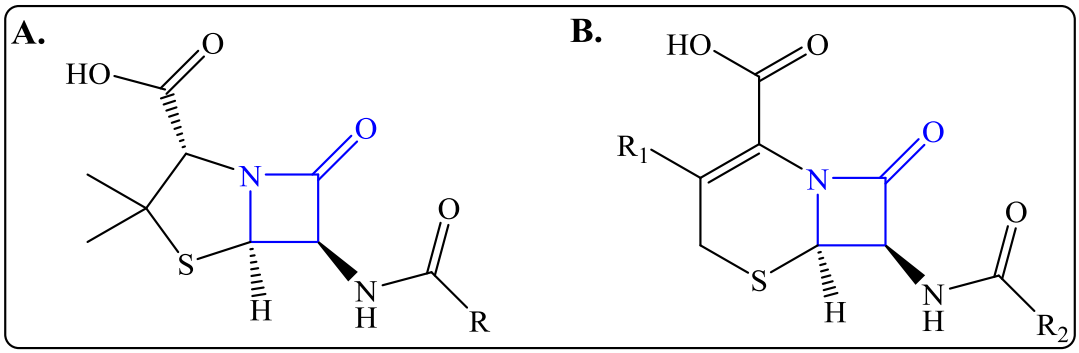

Figure IV: Structure (core) of Penicillins (A) and Cephalosporins (B). The β-Lactam ring is marked with red.

Glycopeptides

Glycopeptides comprise a class of glycosylated polycyclic peptides, which have inhibitory activity against cell-wall synthesis of Gram-positive bacteria. Some of the members of this group like teicoplanin and vancomycin and semisynthetic derivatives such as dalbavancin, telavancin etc work by preventing crosslinking of the peptidoglycan layer in the cell wall by binding with D-alanyl-D-alanine terminus.

The oldest glycopeptide-based antibiotic used for clinical purposes to date is Vancomycin, isolated from *Amycolaptosis orientalis* in 1953. Vancomycin was later approved by FDA to treat penicillin-resistant *staphylococci*.[19] Other Lipid II binding Glycopeptides include Teicoplanin, Dalbavancin, Oritavancin, Telavancin, etc whose activities are given in Table 2 below.

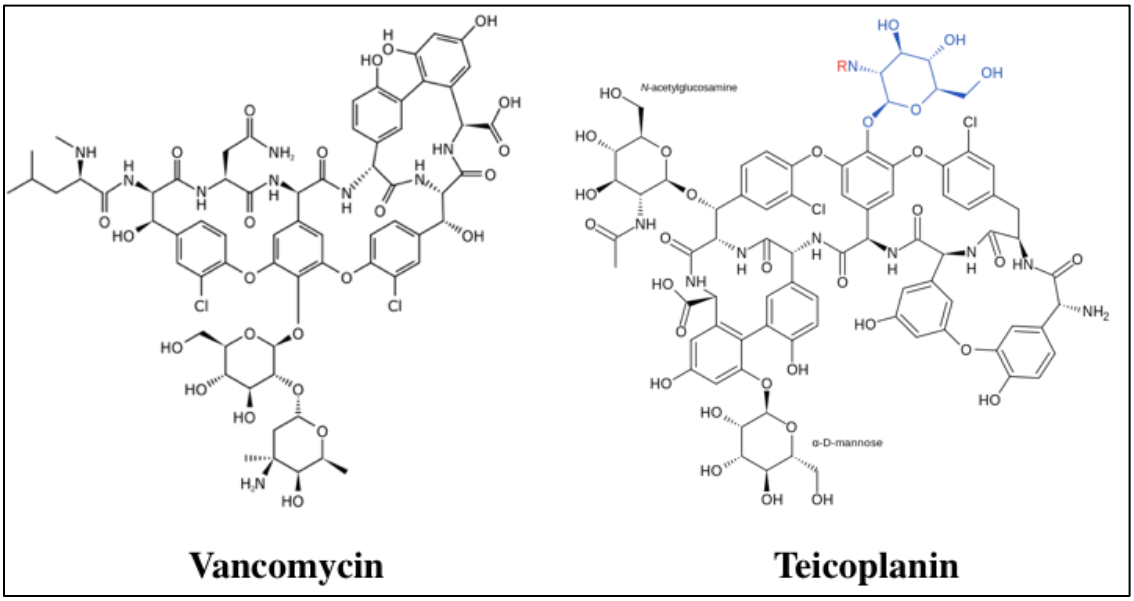

Figure V: Structures of Glycopeptides like vancomycin and teicoplanin.

MECHANISM OF ACTION			
LIPID II-binding			
Antibiotic	Membrane Anchoring	Transpeptidation (Enzymatic)	Membrane (permeabilization - depolarization)
Vancomycin	No	No	No
Teicoplanin	Yes	No	No
Dalbavancin	Yes	No	No
Oritavancin	Yes	Yes	Yes
Telavancin	Yes	——	Yes

Cold Spring Harb Perspect Med 2016;6:a026989

Table II: List of different Glycopeptide antibiotics.

Macrolides:

They constitute antibiotics with a macrocyclic lactone ring comprising..[20] They have very good antibacterial activity against Gram-positive cocci and also have good tissue penetration abilities.[21] One of the oldest member of this class is Erythromycin A, a 14-member macrolide was the first one to be introduced in clinical practice. It was isolated from *Streptomyces*.[22-23] Macrolides were found to be very effective in treating diffuse panbronchiolitis (DPB).[24] They helped in increasing the ten-year longevity percentage from 40% to 90% in DPB patients from the year 1970 to 1979.[25] The 16 member macrolides have shown much better activity against resistant strains, better gastrointestinal tolerance, minimal drug-drug interaction in comparison to the 14 membered ones like the erythromycins. [26-28]

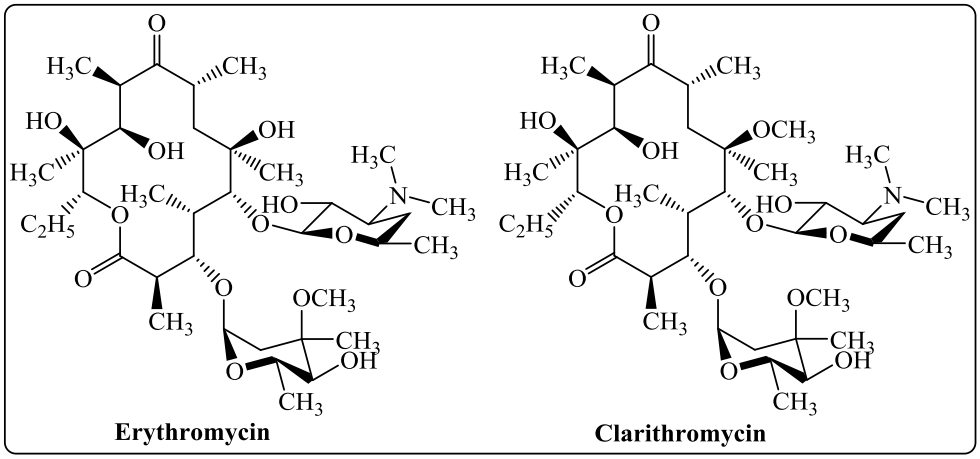

Figure VI: Structure of Macrolide Erythromycin and Clarithromycin.

Aminoglycosides

Aminoglycosides are broad-spectrum antibiotics that work by inhibiting protein synthesis. They are one of the most widely used groups for antibacterial chemotherapy since streptomycin. Other members of the class include neomycin, kanamycin, gentamycin, tobramycin, amikacin, etc. Since Aminoglycosides possessed high toxicity levels, therefore new molecules such as arbekacin, plazomicin, etc was developed to overcome the toxicity as well as resistance by multidrug-resistant pathogens.

Aminoglycosides show the best potency against the Enterobacteriaceae family members like *E. aerogenes, E.coli, K oxytoca, K. pneumonia and* Serratia species etc.[29-30] They are also active against *Yersinia pestis, Staph aureus, P. aeruginosa,* and *Mycobacterium tuberculosis, M. fortuitum,* etc.[31-33] The aminoglycosides were inactive against anaerobic bacteria since they required active electron transport for uptake into cells. The activity of aminoglycosides can be further enhanced by synergy with other antimicrobial classes. Aminoglycosides target bacterial translation through codon misreading by binding to A-site on 16S ribosomal RNA of 30S ribosomal subunit.[34] Aminoglycosides enter cells by electrostatic interaction of their polycationic charge with the negatively charged components like Teichoic acids and lipopolysaccharides in the bacterial cell membrane. [35-36] Once the aminoglycosides enter the cell and lead to mistranslation of proteins, this leads to alteration of the bacterial membrane and facilitates the uptake of more aminoglycoside molecules into the cell leading to more mistranslation and ultimately death of the microorganism. [35]

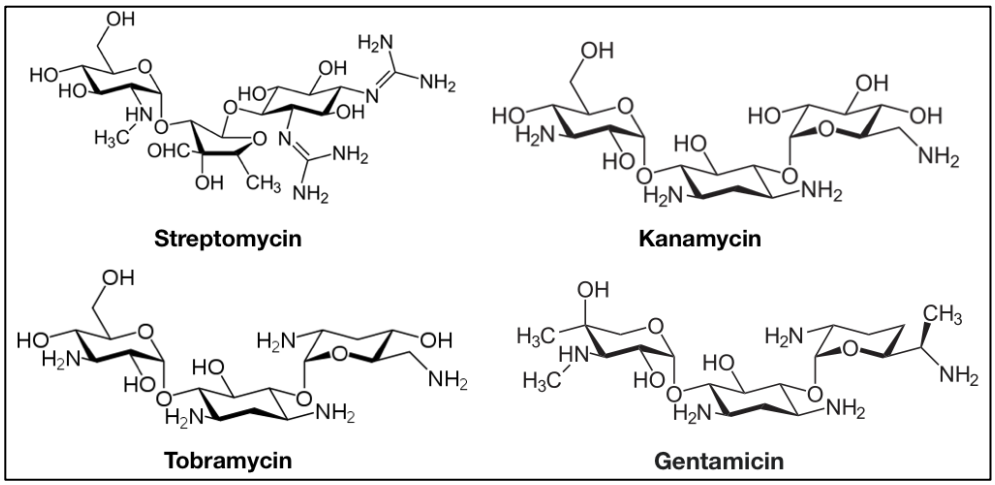

Figure VII: Structures of different aminoglycosides.

Quinolones

Quinolones comprise a family of antibiotics that contains a bicyclic core, structurally similar to the compound 4-quinolone.[37] Nalidixic acid was the first reported quinolone in the year 1962.[38] During the 1970s and 1980s, a new quinolone class emerged that displayed a broader spectrum in comparison to the first generation.[39-40] Quinolones are selected over other antibiotics in the last five decades due to their broad-spectrum

activity, high potency, and relatively low side effects and good bioavailability. Quinolones are broadly classified into four different generations depending on their antimicrobial activities. They are summarized in Table 3. Since the quinolones had an extensive gram-negative activity range, they were initially used for the treatment of urinary tract infections.[41-42]

Generation of Quinolone	Antimicrobial activity against	Administration and characteristics
First Generation		
Nalidixic acid	*Enterobacteriaceae*	Oral administration. Low serum and tissue drug concentrations
Second Generation		
Class I		
Lomefloxacin	*Enterobacteriaceae*	Oral administration. Low serum and tissue drug concentrations
Norfloxacin	*Enterobacteriaceae*	Improved gram-negative coverage compared to 1st generations
Class II		
Oloxacin Ciplofloxacin	*Enterobacteriaceae* *Pseudomonas aeruginosa* (Ciplofloxacin only)	Oral and intravenous administration. Higher serum, tissue and intracellular drug concentration compared to class I
Third Generation		
Levofloxacin,Sparfloxacin Gatrifloxacin,Moxifloxacin	*Enterobacteriaceae*, atypical pathogens, *streptococci*	Oral and intravenous administration. Similar to class II second generation quinolone. Increased hepatic metabolism (sparfloxacin and moxifloxacin)
Fourth Generation		
Trovafloxacin	*Enterobacteriaceae, Pseudomonas aeruginosa,* methicillin susceptible *S. aureus, Streptococci*	Oral and intravenous administration. Similar to third generation quinolone with improved gram-positive activity.

Oliphant, C. M., & Green, G. (2002). Quinolones: a comprehensive review. *American family physician*, *65*(3), 455.

Table III: The different generations of Quinolones antibiotics.

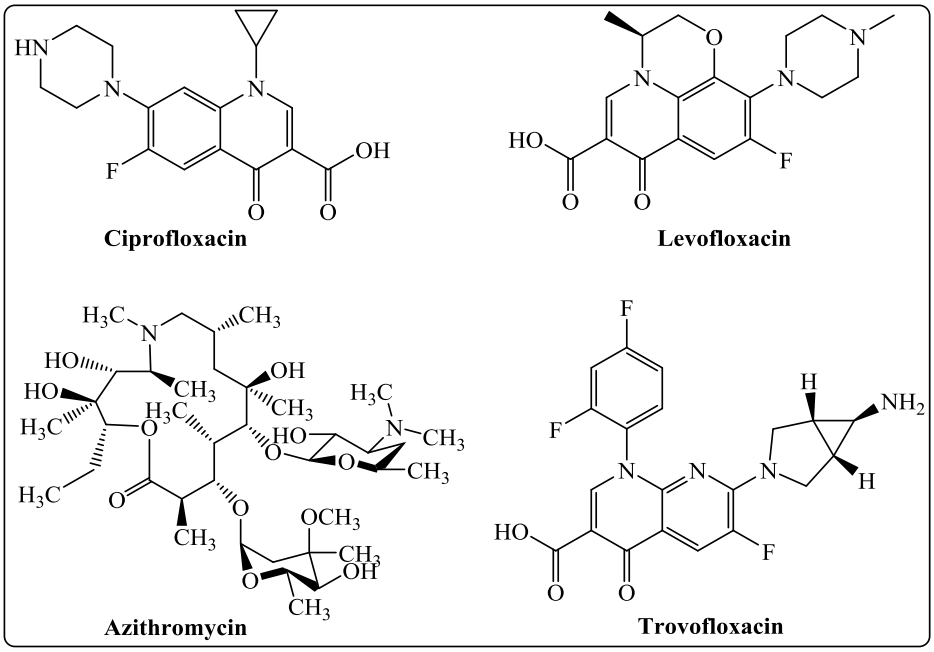

Figure VIII: The different types of Quinolone antibiotics.

Daptomycin

Daptomycin is a cyclic lipopeptide antibiotic assembled by adding decanoic acid on the growth medium of *Streptomyces roseosporus* during the process of fermentation. Daptomycin has antibacterial activity against gram-positive strains against which there are limited alternatives for therapy. They are also used effectively against meningitis, sepsis, urinary tract infections, and bacteremia. Daptomycin shares some structural similarity to the antimicrobial cationic peptides made by our immune system. Daptomycin is believed to enter bacterial cell cytoplasm using Ca dependent process and lead to depolarization of the membrane and subsequent loss of ions from the intracellular components.[43-45] Daptomycin causes leakage of Potassium Ions from the membrane of *S. aureus* and *B. megaterium*.[46]

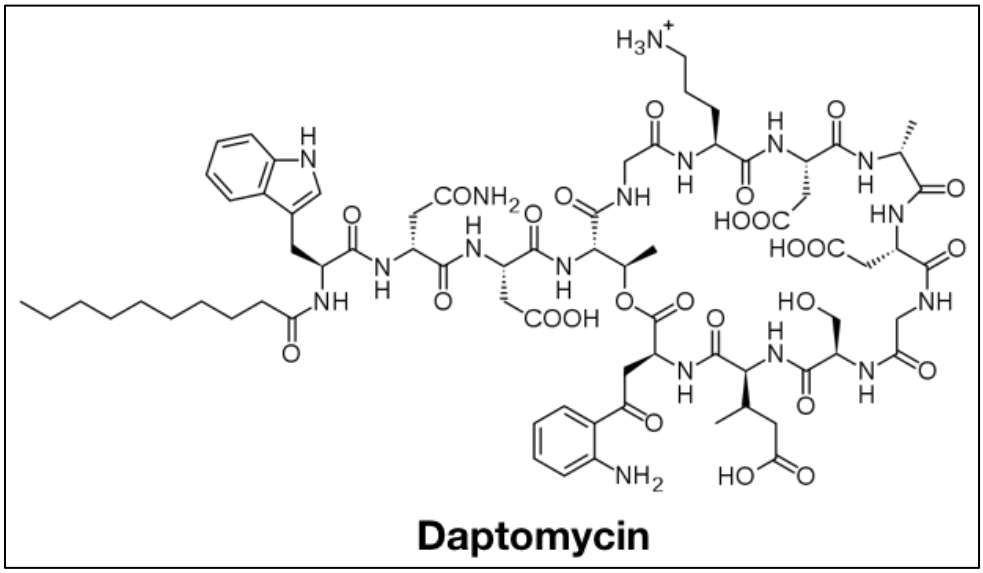

Figure IX: Structure of Daptomycin.

Polymyxins

Polymyxins comprise the class of antibiotics that exhibit antibacterial activity by binding with the lipopolysaccharides and phospholipids on the outer membrane of gram-negative bacteria. They displace divalent ions that stabilize the phosphate group in phospholipids thus leading to disruption of outer cell membrane and leakage of cellular components leading to bacterial cell death.[47-48] They have re-emerged in recent times due to the increasing prevalence of multidrug-resistant bacteria that causes nosocomial infections. Polymyxin B has high bactericidal activity against MDR gram-negative *Pseudomonas aeruginosa*, *Acinetobacter baumannii*, etc.

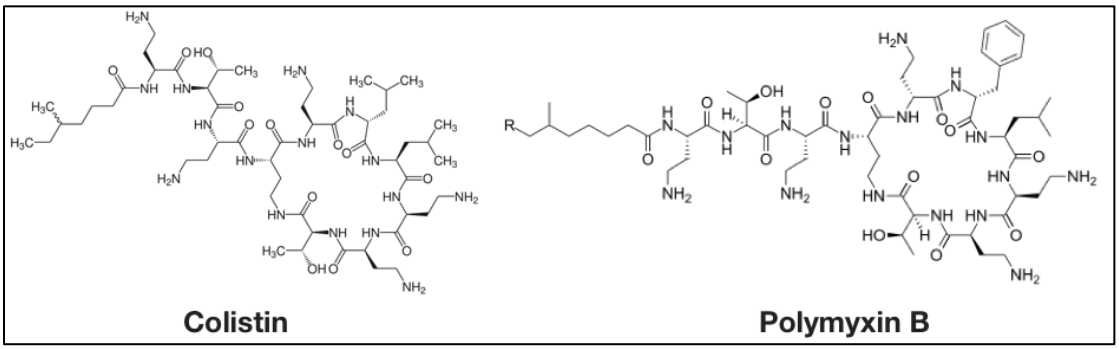

Figure X: Structure of Polymixins.

Metronidazole

It is one of the mainstream drugs used to treat protozoal infections, anaerobic bacterial infections, and facultative bacteria etc. Metronidazole has been approved by FDA for the treatment of protozoal infections like *Entamoeba histolytica*, *Trichomoniasis vaginalis*, *Giardia lamblia* etc and anaerobic bacteria like *Helicobactor pylori*, *Gardnerella vaginalis*, *clostridium* species, *Biophilia wadsworth*, etc.[49] Metronidazole have a rapid concentration-dependent anti bactericidal effect against Trichomonas vaginalis and Entamoeba histolytica and can also cross the blood-brain barrier.[50-51]

Metronidazole inhibits protein synthesis by binding with the DNA and causes disruption of helicase from the DNA and DNA strand breakage causing the death of the target organism. Although the antimicrobial effects of Metronidazole are limited to anaerobic organism.[52]

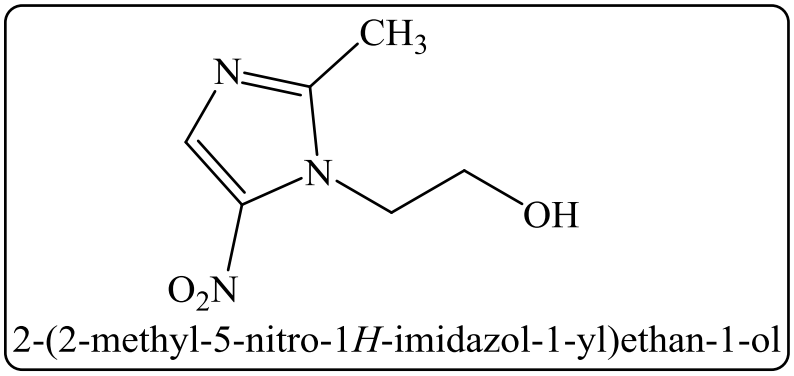

Figure XI: Structure of Metronidazole.

Rifampicin

Rifampicin is active against a wide range of gram-positive cocci, Clostridium difficile, Mycobacteria, and gram-negative species like Hemophilus influenza, Niesseria gonorrhoeae etc. Rifampicin is used clinically for the treatment of Leprosy, latent and active tuberculosis, endocarditis, meningitis, osteomyelitis, etc.

The antimicrobial effect of Rifampicin stems from their inhibitory action on DNA-dependent RNA Polymerase. They can either sterically block the elongation of RNA at the 5' end or decrease the affinity of RNA Pol towards the short RNA transcripts. [53-55]

They have no affinity towards the mammalian RNA polymerase thus having no adverse effect on humans.

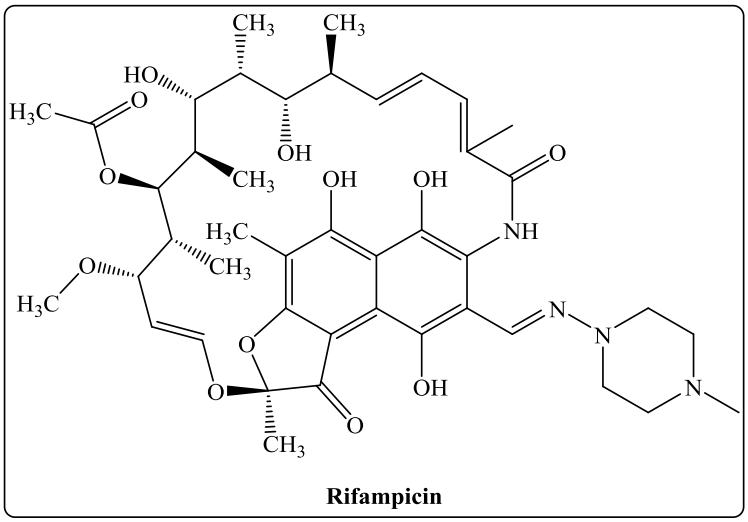

Figure XII: Structure of Rifampicin.

Trimethoprim and Sulfonamides

It is a synthetic chemotherapeutic compound, recently used for the treatment of symptomatic urinary tract infections. It works well in synergy with sulfamethoxazole. Trimethoprim acts by blocking Tetrahydrofolate (THF) production, the active folic acid form in organisms. Since microorganisms only rely on endogenous THF production from dihydrofolate therefore competitive inhibition of Trimethoprim on dihydrofolate reductase enzyme leads to a reduction in THF production. This leads to derangement in nucleic acid and protein synthesis thereby leading to bacterial cell death.[56-57] Trimethoprim shows inhibitory activity against bacteria like *S. aureus*, *S. pneumonia*, *S. viridans*, and gram-negative bacteria like *E. coli*, *K. pneumoniae*, *Salmonella* sp, *Serratia* sp, etc. [57]

Sulfonamides act by competitively inhibiting the enzyme dihydropteroate synthase, another enzyme involved in folate synthesis. Sulfonamides, therefore are bacteriostatic i.e. they inhibit bacterial growth but do not kill them. Sulfonamides have strong activity against a wide range of bacteria.

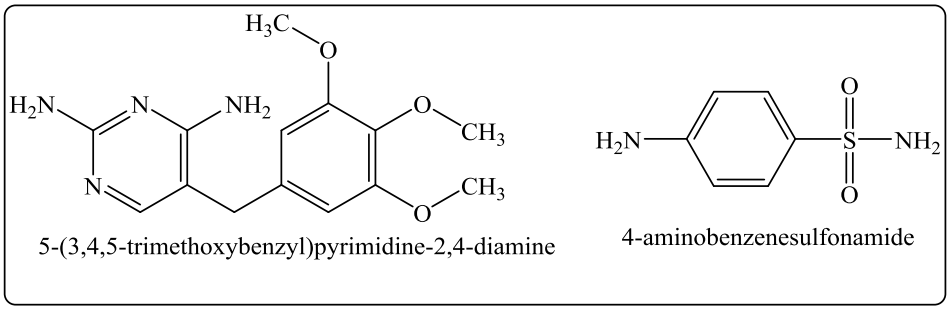

Figure XIII: Structure of Trimethoprim and Sulfanilamide (a cyclic Sulfonamide)

Fosfomycin

Fosfomycin was discovered in 1969.[58] It is an analog of phosphoenolpyruvate produced by Streptomyces spp and can be synthesized synthetically.[59] Fosfomycin exerts its inhibitory effect by interfering with the formation of UDP-N-acetylmuramic acid, the precursor of peptidoglycan thereby interfering with cell wall formation.[60-61] Fosfomycin binds covalently to the thiol group of the cysteine 115 present in the enzyme MurA (UDP-N-Acetylglucosamine enol pyruvate transferase) active site.[62] Fosfomycin also have the ability to penetrate inside biofilms and that clinically significant bacteria can be eradicated from biofilms by fosfomycin alone or in coordination with other antibiotics.[63-64]

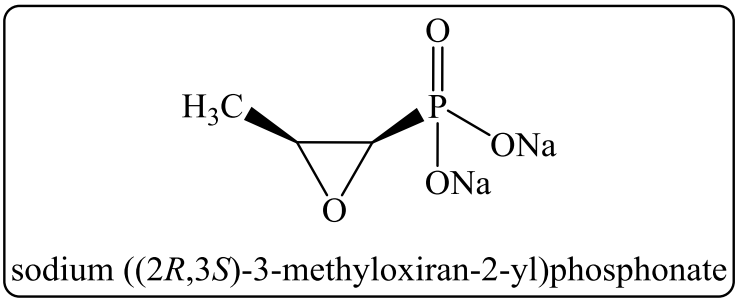

Figure XIV: Fosfomycin structure.

Fusidic acid

Fusidic acid is structurally related to cephalosporin P1 and is derived from the fungus *Fusidium coccineum*. Fusidic acid has good activity against both sensitive and methicillin-resistant *staphylococci*. It also has good activity against *B. Pertussis*, *Neisseria* spp, *Clostridium difficile*, *C. perfringens*, *Propionibacterium acnes*, etc.[65]

Fusidic acid functions by interfering with the elongation factor G(EF-G) thus resulting in inhibition in protein synthesis. In Fusidic acid's presence, the EF-G keeps bound to ribosome after GTP hydrolysis and cannot translocate the peptidyl-tRNA into the P site on the 50S ribosomal subunit thus blocking the synthesis of protein.

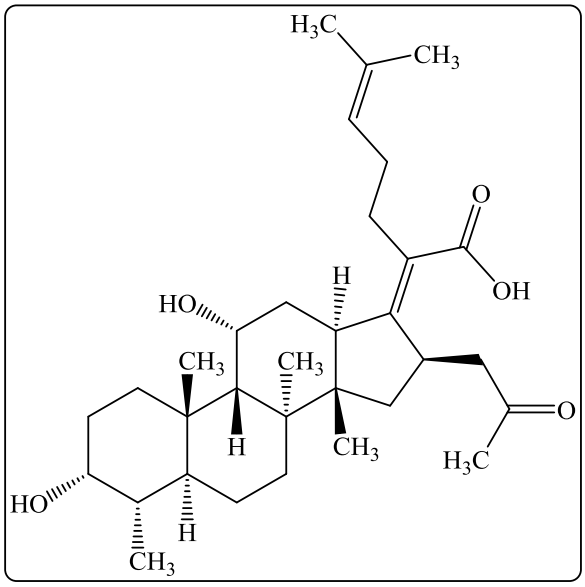

Figure XV: Structure of Fusidic acid.

LpxC inhibitors

LpxC(UDP-3-o-(R3-hydroxymyristoyl)-N-acetylglucosamine deacetylase) is an enzyme found across Gram-negative bacteria which is a key player in lipid A synthesis, the Lipopolysaccharide(LPS) membrane anchor. Scientific and industrial research has been conducted on the search for LpxC inhibitors since the mid-1980s. A lot of molecules were screened using *P. aeruginosa* LpxC.[66-67]

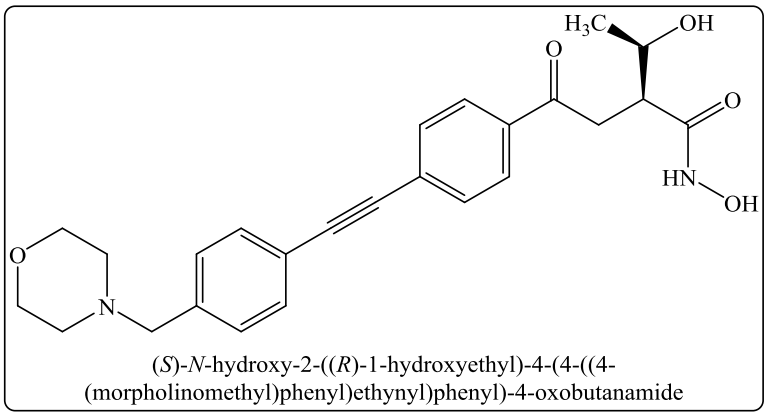

Figure XVI: Structure of LpxC inhibitor CHIR-090.

FabI Inhibitors

The fatty acid biosynthesis pathway in bacteria is a new target since fatty acids are essential for the growth of bacteria. Fatty acids cannot be absorbed by the bacteria from the host and have to be synthesized inside the cell hence it's a good drug target.[68-69] The enzyme FabI (Enoyl reductase) is involved in the reduction of enoyl-ACP, the ultimate step of every elongation cycle of bacterial type II fatty acid synthesis, and they are essential for the viability of bacteria.[70] Fab I inhibitors like Triclosan interact with the Enzyme-cofactor complex non-covalently leading to stabilization of the ecFabI complex and inhibiting fatty acid biosynthesis. [71-72]

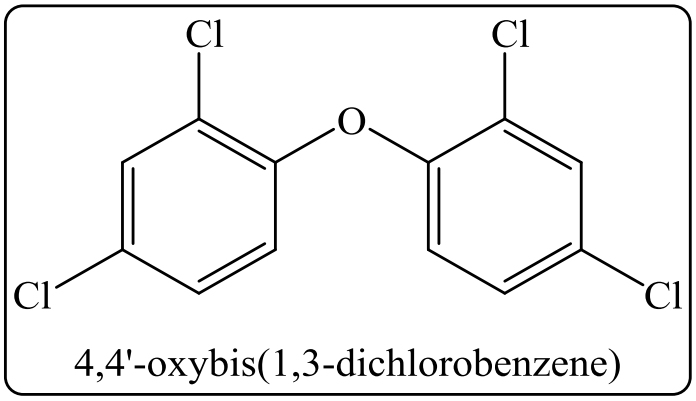

Figure XVII: Structure of Triclosan

Bifunctional Inhibitors:

With the growing emergence of antibiotic resistance in the pathogenic organism, new concepts of targeting microbes are coming up. One of them is the design of dual-functional inhibitors that normally involve designing molecules that target similar domains or folds in two different targets or conjugating two different antibiotics with different targets. The conjugated antibiotics are then further modified so that they retain inhibitory activities from both antibiotics towards their respective targets. This leads to a more potent antibiotic that has fewer chances of getting resistant to the bacterium. One example includes the synthesis of inhibitors that target Mycobacterium tuberculosis (Mtb) Dna G primase and DNA gyrase by targeting the conserved TOPRIM fold.[73] TD-1607 and Cefilavancin are hybrid antibiotics that can target a wide range of Gram-positive bacteria.[74] Fluoroquinolones are another group that targets two bacterial enzymes, DNA gyrase and topoisomerase IV thus inhibiting both transcription and replication.[75] The antibiotic Cefilavancin is a heterodimer comprising of cephalosporin and vancomycin linked covalently by a linker.[76] Naringen hybrid with ciprofloxacin has a 23 times higher activity in inhibiting DNA Gyrase than ciprofloxacin alone and have been found to be active against few MRSA strains.[77]

C. Summary on Hepatitis C virus:

Hepatitis C virus (HCV) is the causative agent of hepatitis C, one of the prime liver diseases and a serious global health concern.[78] Hepatitis C infection can result in severe acute hepatitis or may lead to progression into chronic liver disease. This can lead to cirrhosis in the liver and ultimately some patients may develop hepatocellular carcinoma and liver failure. Around 3.5 to 5 million people are infected worldwide with HCV with new HCV cases and around 70-80% of the patients develop chronic liver infections.[79] Hepatitis infection poses a serious burden on the world economy and a significant concern on public health. The ever-presence of HCV infections in countries such as Southeast countries, east Mediterranean, Africa, Egypt, etc. constitutes around 14-15% of HCV-infected individuals.[80]

HCV is one of the members of the Flaviviridae family and consists of a positive sensed RNA genome of 9.6 kb in length (Figure XVIII). The HCV genome comprises of two

Structural and highly conserved UTR (untranslated regions) 5' UTR and 3'UTR as part of regulatory elements that control HCV translation and replication. [81] The genome also comprises a single ORF (Open reading frame), which encodes a polyprotein that is cleaved and processed by proteases to generate 10 different functional proteins that include the Envelope, Capsid, and non-structural proteins. HCV possesses an IRES (Internal ribosome entry site) as part of the 5' UTR region, which plays a key role in directing the translation of the HCV genome by binding with the 40S subunit of the ribosome.[82]

HCV is transmitted from one person to another through blood transfusions or by the use of the same surgical needles from an infected person to a healthy individual. The therapeutic strategies employed mainly focus on reducing the viral load from the blood and reduce cirrhosis risk. The most widely used therapies use immunostimulatory combinations of pegylated interferon-alpha (IFN-α) with ribavirin, a nucleoside analog that boosts the IFN-α effect. [83] This therapy leads to the elimination of the virus in around 40-50% of patients but has some side effects.[84] Thus there is a pressing requirement for the development of new antiviral drugs against HCV with high efficacy that can block HCV IRES-mediated translation and replication in host cells.

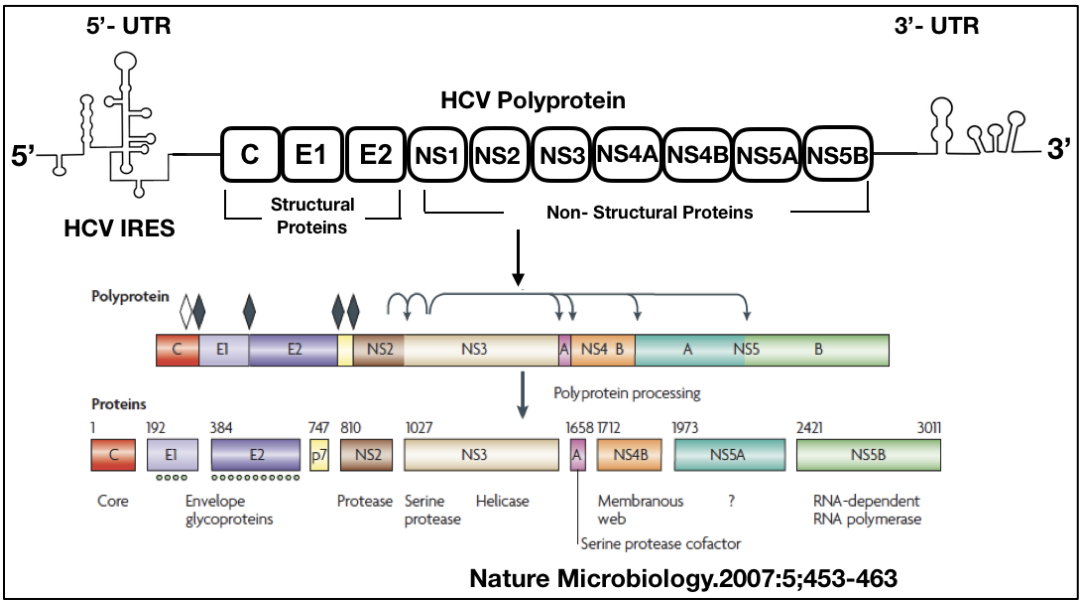

Figure XVIII: The genetic makeup and processing of the Hepatitis c virus polyprotein.

Hepatitis C Virus IRES:

The HCV IRES comprises of the 5'-UTR of the HCV RNA genome and is involved in the initiation of cap-independent translation in the host by the virus. The 5'UTR does not require the cap for translation initiation and can directly recruit the mammalian ribosomal subunits hence they are called Internal ribosome entry site. The total length of the HCV IRES is around 341 nucleotides and comprises of mainly four domains (I, II, III, and IV).[85] Under physiological conditions the tertiary structure of HCV IRES is maintained by divalent metal ions like Mg^{2+}, and Mn^{2+}. The HCV IRES secondary structure shows that this structure is well conserved across different flavivirus and they play an important part in cap-independent translation by recruiting the translational machinery very efficiently.

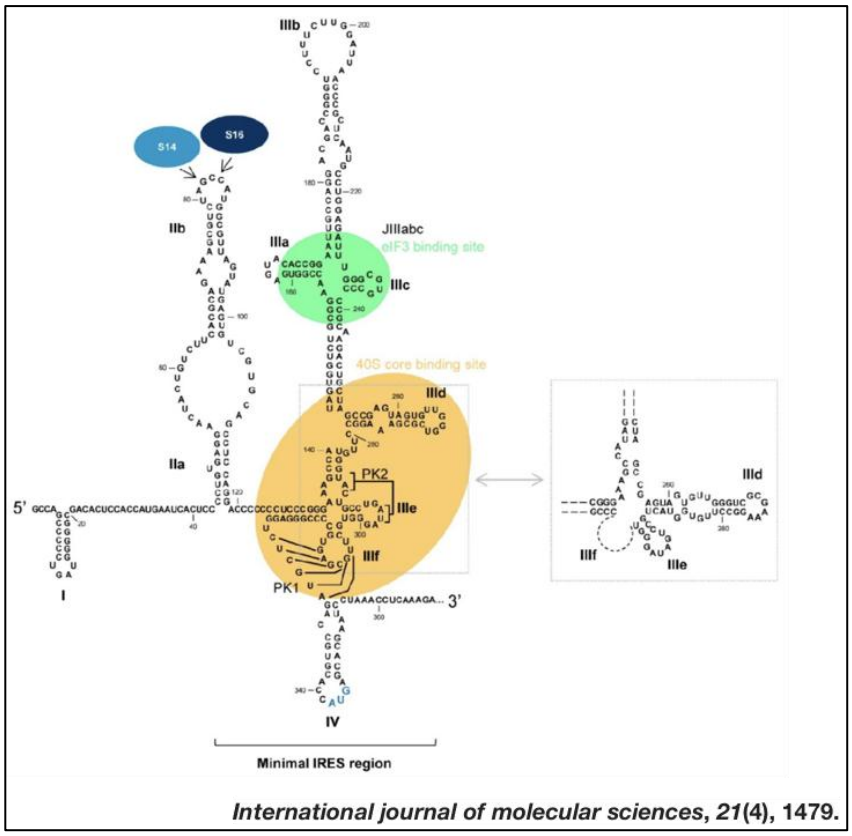

Figure XIX: HCV IRES sequence and secondary structure with the role of different domains interacting with different translational machinery. S14 and S16 are ribosomal proteins shown in blue, eIF3 binding site shown in green and 40S subunit shown in orange. Alternative folding of domain III(inset).

HCV IRES domains and their structural and functional characterizations:

There have been extensive studies on the structural role of the various HCV IRES domains in the non-canonical cap independent translation process. Mutational studies have thrown light on the high conserved nature of domain II that is mainly comprised of IIa and IIb as the two sub-domains. NMR studies have shown that domain II adopts an L-shaped structure three-dimensional structure and this bent structure helps in orienting itself to the E site of the ribosome.[86] The studies using X-ray crystallography have further shown that the domain IIa takes a 90° bent architecture that is crucial for the activity of the HCV IRES. [87-88] This bent structure is stabilized by metal ions like Mg^{2+} and Mn^{2+} and H-bonding along with base stacking interaction involving A53, A54, A57, U56, and C55. [88] The Uracil residue (U86) present in the apical loop of subdomain IIb is highly conserved across many different HCV clinical isolates and it interacts with 40S subunit of ribosome through the two ribosomal proteins S14 and S16.[85] Through mutational experiments with domain IIa it has been found that IIa can interact with the domain IV and together they help in the correct placement of the start codon AUG after the HCV-IRES and ribosome 40S complex formation.[89] The subdomain IIa also is important in recruiting Translation Initiation factors such as eIF5 and eIF2-TC along with the 40s subunit and the subsequent release of eIF2-GDP after the hydrolysis of GTP. This helps in the attachment of the 60s subunit to form the complete 80s initiation complex.[90-91]

The HCV IRES domain III is the largest and comprises various subdomains like IIIa, IIIb, IIIc, IIId, IIIe, and IIIf. Domain III is crucial in recruiting the 40s ribosomal subunit and the initiation factor eIF3. The junction of IIIabc along with the loop of IIIa, IIIb, and IIIc also are important for the interaction of the eIF3 multisubunit initiation factor. They also help in the formation of the 80s initiation complex by stabilizing the methionine tRNA-eIF2 complex.[83,85] Cryo-EM experiments have shown that domain IIIe binds to ribosomal proteins to initiate the process of translation.[92] The pseudoknot in domain IIIf interacts with the ribosomal protein eS28 and helps in the insertion and positioning of the viral mRNA into the 40s subunit at the start codon. After elongation, the HCV mRNA exits the channel by displacing subdomain IIIf from the exit site.[93-94]

Cap-independent Translation by HCV IRES

Translation initiation by HCV IRES does not require the 7-methyl guanosine cap present on the 5' end of mRNA. Toe printing assay showed that the 40s ribosomal subunit was directly recruited by the HCV IRES to the initiator codon. Interaction of HCV IRES with the 40s subunit by the domain II and III leads to a conformational change in 40s after which eIF2-Met-tRNA$_i$-GTP ternary complex and eIF3 binds to the 40s-IRES complex. The eIF3 mediates the hydrolysis of GTP that induces the merging of the 60s subunit and to form the complete 80s complex which now initiates the cap-independent IRES driven translation.[85,91]

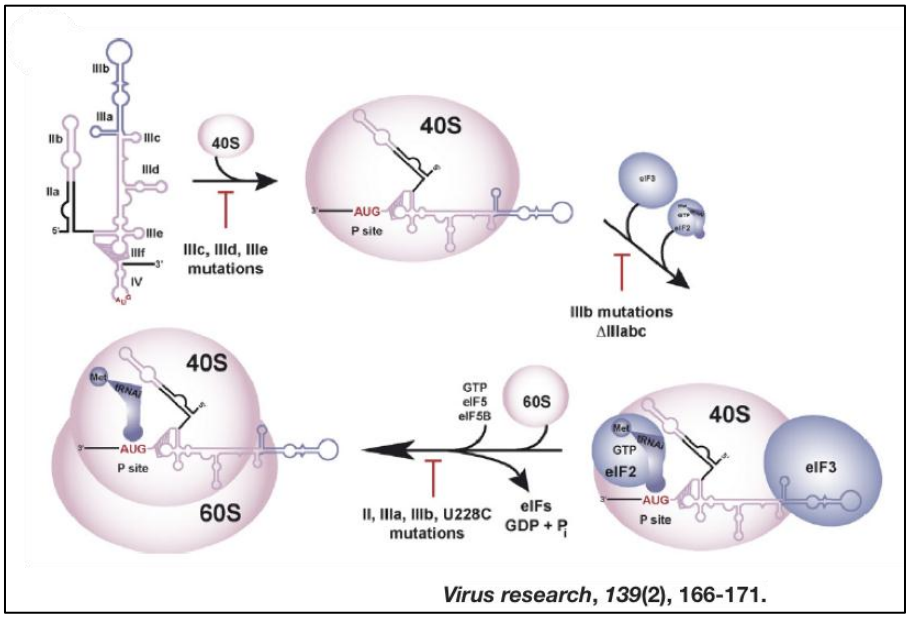

Figure XX: Cap Independent translation initiation by HCV IRES.

Targeting HCV IRES

The conserved nature of the subdomains in the HCV IRES make it a very attractive target and could pave a path for the new antiviral therapeutics against HCV using RNA targeting small molecules described below.[95]

Small Molecule Inhibitors of HCV IRES-mediated translation in the host cell

Small molecules targeting the translation driven by HCV IRES were screened using high throughput assays. One of the inhibitors, Phenazine was identified using In vitro translation experiments and inhibits translation driven by IRES at lower specificity. [96] Using Forster resonance energy transfer (FRET) and dual luciferase-based assays using bicistronic plasmid DNA constructs transfected in host cell lines, two HCV-driven translation inhibitors were identified. They were benzimidazoles[97-98] and diaminopiperidines. [99]

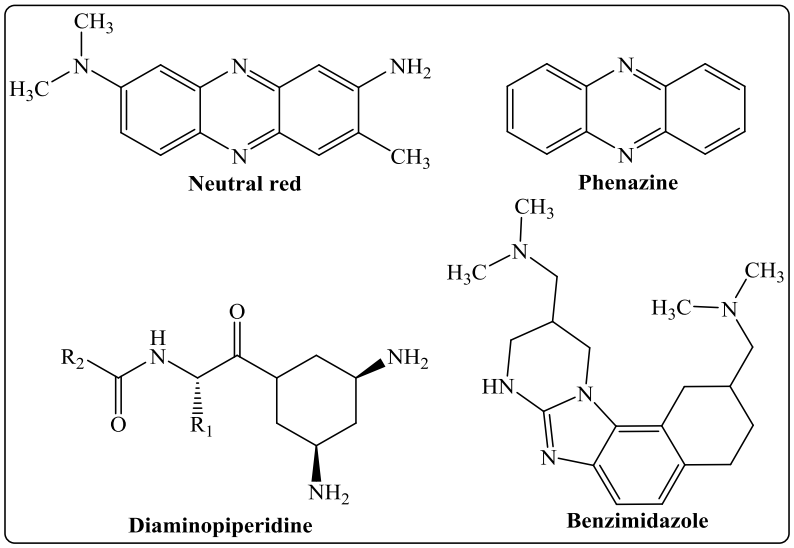

Figure XXI: Structure of HCV IRES small molecule inhibitors.

Crystallography, NMR, and cry-EM studies have established that an L-shaped structure is adopted by the subdomain IIa.[87] This L-shaped bent architecture is stabilized with the help of stacking interaction, hydrogen bonds, and divalent metal ions like Mg^2. The domain IIa then assists in incorporating subdomain IIa to the E site of the 40S subunit of the ribosome to initiate translation.[92] X-ray Crystallography, FRET, and NMR studies have discovered that the small molecule benzimidazole binds with the subdomain IIa and leads to widening of the interhelical angle. This widened interhelical angle can no longer dock itself inside the 40s ribosomal subunit thus the 80s initiation complex does not form.[88] The interaction of benzimidazole to the subdomain IIa was found to be very

specific and was unaffected even when treated with high salt concentration and competitive RNA. [95]

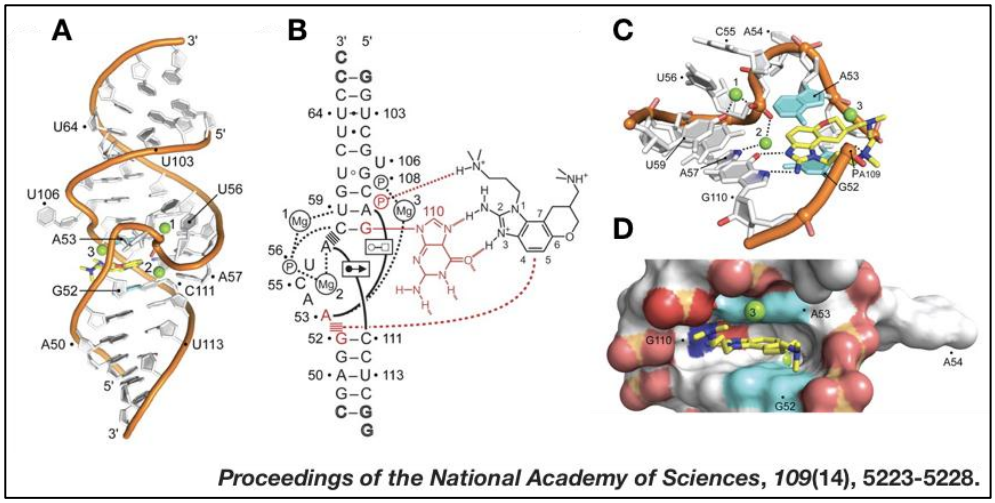

Figure XXII: Crystal structure of Benzimidazole-HCV IRES inhibitor complex (A) Overall view of the complex. Benzimidazole is marked in yellow and green spheres represent Mg^{2+} ions. (B) Schematic representation of the interaction. (C) A detailed view of the binding site of the ligand. (D) Surface representation showing the ligand-binding pocket.

Using Circular Dichroism to study RNA structural change

Nucleic acids can exist in left-handed or right-handed helical structures. The most predominant structures of RNA include right-handed A-form and left-handed Z-form and in DNA include right-handed helical A and B-DNA and left-handed Z DNA.[100-102] These structures can be interchanged using temperature and high salt concentrations, which can have biological implications.[103-107] Circular dichroism is a very effective tool to study the structural change in nucleic acids.[108-109] The two most predominant form of RNA i.e. the A and Z form has different characteristic signature ellipticity peaks which are unique to each form and can be used to differentiate between different forms very well. The CD spectrum of A-form of RNA comprises of mainly two peaks. A negative peak at around 230 nm indicates helicity and a positive peak at around 265 nm stacking interaction of the RNA bases. Disruption of base stacking or alteration of the native RNA structure can lead to various consequences.

D. Nucleoid Associated Proteins

Bacteria contain proteins that are very functionally similar to the histone proteins present in eukaryotes. In bacteria, these histone-like proteins plays a crucial part in regulating the expression of various genes as well as controlling other processes like DNA replication, recombination, etc.[110-111] They also play a key role in the structural organization of the bacterial nucleoid. Some of the examples include H-NS (histone-like nucleoid structuring), HU (heat unstable), Fis (factor for inversion stimulation), and IHF (Integration host factor). IHF has the greatest specificity towards DNA binding.[112] The HU and HNS on the other hand are termed as nonspecific DNA binders.[113-115] These DNA binding proteins have differential expression patterns at different stages or time points of the bacterial growth cycle suggesting they play different roles. For example, IHF is in ample concentration in the stationary phase while Fis is mostly expressed in the log phase.[116] H-NS level remains more or less similar throughout the growth whereas HU level reduces with the onset of stationary phase.[117-118]

H-NS

H-NS is one of the most abundantly occurring nucleoid binding proteins present inside *E. coli*.[119] They help in preventing the global chromosomal unwinding following any occurrence of double-stranded DNA breaks.[120] H-NS over-expression can lead to the transcriptional silencing on a global level.[121-122] The whole-genome mapping and recent work have shown that H-NS acts as a global repressor in controlling the expression of a large number of bacterial genes.[114] H-NS are present as dimers at low concentrations and as tetramers or higher-order complexes at higher concentrations.[123-124] H-NS have a high affinity towards AT-rich DNA sequences and bind to an intrinsically curved region of the promoter of the gene to be repressed and that in turn leads to the binding of more H-NS proteins to the region.[125-127] This leads to looping of the DNA and the RNA polymerase gets trapped between the loops.[128-129] The oligomerization property of H-NS is imparted by its N-terminal region and it is connected to the C terminal DNA binding domain by a linker region.[130] To overcome the repression complex formed by H-NS often require the help of activators.[131] Many virulence factors under the influence of H-NS can respond to signals like change in osmolarity, temperature, pH, etc.[132]

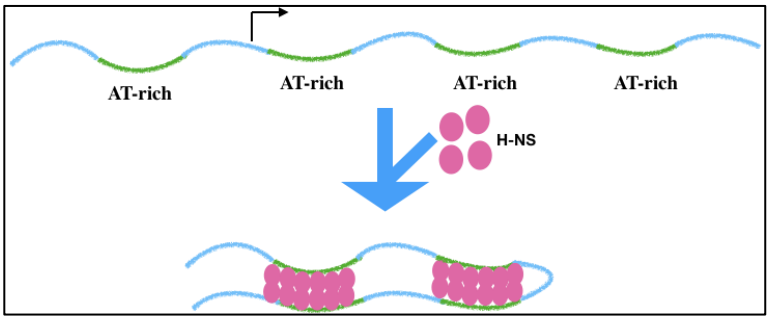

Figure XXIII: A model showing the mechanism of H-NS binding on the DNA.

Studies on H-NS mutant *Salmonella* with the help of cDNA microarray have revealed that most genes repressed by H-NS were rich in AT. It was found that around 400 AT-rich regions present in the chromosome of *Salmonella* were bound by H-NS. These include all five pathogenicity islands, the plasmid virulence factor, and nearly all AT-rich islets. The binding of H-NS was not just restricted to promoter regions but also to coding regions rich in AT as seen by oligonucleotide arrays.[129] Using CHIP-on-chip technology in *E.coli* it was found that H-NS targets AT DNA sequences as mentioned in *Salmonella* before. Although the protein has biases towards intergenic regions more, they also bind to coding regions frequently.

Recent studies have suggested that the primary role of H-NS is to silence any AT-rich DNA mainly as defense mechanism against foreign DNA sequences thus adding to the bacterial innate immunity.[133] The Xenogeneic Silencing (XS) model by H-NS is thus believed to have played a crucial role in shaping up the evolution of microbes.

HU

The HU (Heat unstable) protein has an affinity for DNA that contains structural aberrations like single-stranded lesions and four-way junctions. HU plays a key role in site-specific DNA recombination. They bind to DNA in the form of dimers and bends DNA nonspecifically without interacting with other DNA binding proteins or transcription factors. For the *e.coli gal P2* promoter, HU binds with the DNA and helps in assisting the tetrameric GalR protein to bind to the promoter and form the repression loop.[134] The HU then makes a transient interaction with the GalR protein called

'piggybacking' the first reported specific contact between HU and another protein.[134-135] The HU plays the role of an architect in aiding the weak dimer-dimer interaction between the GalR with the operator site.[135]

REFERENCES:

1. Zolova, O. E., Mady, A. S., & Garneau-Tsodikova, S. (2010). Recent developments in bisintercalator natural products. Biopolymers., 93(9), 777-790.

2. Dawson, S., Malkinson, J. P., Paumier, D., & Searcey, M. (2007). Bisintercalator natural products with potential therapeutic applications: isolation, structure determination, synthetic and biological studies. Nat. Prod. Rep., 24(1), 109-126.

3. Corbaz, R., Ettlinger, L., Gäumann, E., Schierlein, W. K., Kradolfer, F., Neipp, L., ... & Zähner, H. (1957). Stoffwechselprodukte von actinomyceten. 7. mitteilung. echinomycin. Helvetica Chim. Acta., 40(1), 199-204.

4. Keller-Schierlein, W., Mihailović, M. L., & Prelog, V. (1959). Stoffwechselprodukte von Actinomyceten. 15. Mitteilung. über die Konstitution von Echinomycin. Helv. Chim. Acta., 42(1), 305-322.

5. Ughetto, G., Wang, A. H., Quigley, G. J., van der Marel, G. A., van Boom, J. H., & Rich, A. (1985). A comparison of the structure of echinomycin and triostin A complexed to a DNA fragment. Nucleic Acids res., 13(7), 2305-2323.

6. Gilbert, D. E., & Feigon, J. (1991). The DNA sequence at echinomycin binding sites determines the structural changes induced by drug binding: NMR studies of echinomycin binding to [d (ACGTACGT)] 2 and [d (TCGATCGA)] 2. Biochemistry., 30(9), 2483-2494.

7. Gause Jr, G. G., Loshkareva, N. P., & Zbarsky, I. B. (1968). Effect of olivomycin and echinomycin on initiation and growth of RNA chains catalyzed by RNA polymerase. Biochim et Biophys Acta (BBA)-Nucleic Acids and Protein Synthesis., 166(3), 752-754.

8. Low, C. L., Drew, H. R., & Waring, M. J. (1984). Sequence-specific binding of echinomycin to DNA: evidence for conformational changes affecting flanking sequences. Nucleic Acids res., 12(12), 4865-4879.

9. Van Dyke, M. M., & Dervan, P. B. (1984). Echinomycin binding sites on DNA. Science., 225(4667), 1122-1127.

10. Gilbert, D. E., Van Der Marel, G. A., Van Boom, J. H., & Feigon, J. (1989). Unstable Hoogsteen base pairs adjacent to echinomycin binding sites within a DNA duplex. Proc. Natl. Acad. Sci., 86(9), 3006-3010.

11. Steffee, C. H. (1992). Alexander Fleming and penicillin. The chance of a lifetime? N. C. Med. J., 53(6), 308-310.

12. Fleming, A. (1929). On the antibacterial action of cultures of a penicillium, with special reference to their use in the isolation of B. influenzae. Br. J. Exp. Pathol., 10(3), 226.

13. Chain, E. (1979). The early years of the penicillin discovery. Trends Pharmacol. Sci., 1(1), 6-11.

14. Queener, S. F. (1986). History and origins of beta-lactam antibiotics. Clin. Pharmacol., 1986.

15. Gardner, A. D. (1940). Morphological effects of penicillin on bacteria. Nature., 146(3713), 837-838.

16. Duguid, J. P. (1946). The sensitivity of bacteria to the action of penicillin. Edin. Med. J., 53(8), 401.

17. Fairbrother, R. W., & Taylor, G. (1961). Sodium Methicillin in Routine Therapy. Lancet., 473-6.

18. Acred, P., BROWN, D. M., Knudsen, E. T., Rolinson, G. N., & Sutherland, R. (1967). New semi-synthetic penicillin active against Pseudomonas pyocyanea. Nature., 215(5096), 25-30.

19. Haley, T. J., & McCormick, W. G. (1957). Pharmacological effects produced by intracerebral injection of drugs in the conscious mouse. Brit. J of Pharmacol and Chemother., 12(1), 12-15.

20. Mazzei, T., Mini, E., Novelli, A., & Periti, P. (1993). Chemistry and mode of action of macrolides. J Antimicrob Chemother., 31(suppl_C), 1-9.

21. Bearden, D. T., & Rodvold, K. A. (1999). Penetration of macrolides into pulmonary sites of infection. Infect in Medici., 16(7), 480-+.

22. Mazzei, T., Mini, E., Novelli, A., & Periti, P. (1993). Chemistry and mode of action of macrolides. J Antimicrob Chemother., 31(suppl_C), 1-9.

23. Williams, J. D., & Sefton, A. M. (1993). Comparison of macrolide antibiotics. J Antimicrob Chemother., 31(suppl_C), 11-26.

24. Keicho, N., & Kudoh, S. (2002). Diffuse Panbronchiolitis. Am. J. Respir. Med., 1(2), 119-131.

25. Kudoh, S., Azuma, A., Yamamoto, M., Izumi, T., & Ando, M. (1998). Improvement of survival in patients with diffuse panbronchiolitis treated with low-dose erythromycin. Am. J. Respir. Crit. Care Med., 157(6), 1829-1832.

26. Zhao, Z., Jin, L., Xu, Y., Zhu, D., Liu, Y., Liu, C., & Lei, P. (2014). Synthesis and antibacterial activity of a series of novel 9-O-acetyl-4′-substituted 16-membered macrolides derived from josamycin. Bioorg. Med. Chem. Lett., 24(2), 480-484.

27. Fernandes, P. B., Baker, W. R., Freiberg, L. A., Hardy, D. J., & McDonald, E. J. (1989). New macrolides active against Streptococcus pyogenes with inducible or constitutive type of macrolide-lincosamide-streptogramin B resistance. Antimicrob. Agents Chemother., 33(1), 78-81.

28. Arenz, S., Ramu, H., Gupta, P., Berninghausen, O., Beckmann, R., Vázquez-Laslop, N., ... & Wilson, D. N. (2014). Molecular basis for erythromycin-dependent ribosome stalling during translation of the ErmBL leader peptide. Nat. Commun., 5(1), 1-8.

29. Ristuccia, A. M., & Cunha, B. A. (1985). An overview of amikacin. Ther. Drug. Monit., 7(1), 12-25.

30. Aggen, J. B., Armstrong, E. S., Goldblum, A. A., Dozzo, P., Linsell, M. S., Gliedt, M. J., ... & Moser, H. E. (2010). Synthesis and spectrum of the neoglycoside ACHN-490. Antimicrob Agents Chemother., 54(11), 4636-4642.

31. Heine, H. S., Hershfield, J., Marchand, C., Miller, L., Halasohoris, S., Purcell, B. K., & Worsham, P. L. (2015). In vitro antibiotic susceptibilities of Yersinia pestis determined by broth microdilution following CLSI methods. Antimicrob. Agents Chemother., 59(4), 1919-1921.

32. Ristuccia, A. M., & Cunha, B. A. (1985). An overview of amikacin. Ther. Drug. Monit., 7(1), 12-25.

33. Karlowsky, J. A., Draghi, D. C., Jones, M. E., Thornsberry, C., Friedland, I. R., & Sahm, D. F. (2003). Surveillance for antimicrobial susceptibility among clinical isolates of Pseudomonas aeruginosa and Acinetobacter baumannii from hospitalized patients in the United States, 1998 to 2001. Antimicrob Agents Chemother., 47(5), 1681-1688.

34. Kotra, L. P., Haddad, J., & Mobashery, S. (2000). Aminoglycosides: perspectives on mechanisms of action and resistance and strategies to counter resistance. Antimicrob Agents Chemother., 44(12), 3249-3256.

35. Taber, H. W., Mueller, J. P., Miller, P. F., & Arrow, A. S. (1987). Bacterial uptake of aminoglycoside antibiotics. Microbiol Rev., 51(4), 439.

36. Ramirez, M. S., & Tolmasky, M. E. (2010). Aminoglycoside modifying enzymes. Drug Resist Updat, 13(6), 151-171.

37. Bisacchi, G. S. (2015). Origins of the quinolone class of antibacterials: an expanded "discovery story" miniperspective. J. Med. Chem., 58(12), 4874-4882.

38. Lesher, G. Y., Froelich, E. J., Gruett, M. D., Bailey, J. H., & Brundage, R. P. (1962). 1, 8-Naphthyridine derivatives. A new class of chemotherapeutic agents. J. Med. Chem., 5(5), 1063-1065.

39. Adjei, M. D., Deck, J., Heinze, T. M., Freeman, J. P., Williams, A. J., & Sutherland, J. B. (2007). Identification of metabolites produced from N-phenylpiperazine by Mycobacterium spp. J. Ind Microbiol Biotechnol., 34(3), 219-224.

40. Andersson, M. I., & MacGowan, A. P. (2003). Development of the quinolones. J. Antimicrob Chemother., 51(suppl_1), 1-11.

41. Hooper, D. C., & Wolfson, J. S. (1991). Fluoroquinolone antimicrobial agents. N Eng J Med., 324(6), 384-394.

42. Hakanen, A., Kotilainen, P., Huovinen, P., Helenius, H., & Siitonen, A. (2001). Reduced fluoroquinolone susceptibility in Salmonella enterica serotypes in travelers returning from Southeast Asia. Emerg Infect Dis., 7(6), 996.

43. Marty, F. M., Yeh, W. W., Wennersten, C. B., Venkataraman, L., Albano, E., Alyea, E. P., ... & Pillai, S. K. (2006). Emergence of a clinical daptomycin-resistant Staphylococcus aureus isolate during treatment of methicillin-resistant Staphylococcus aureus bacteremia and osteomyelitis. J Clin Microbiol., 44(2), 595-597.

44. Poutsiaka, D. D., Skiffington, S., Miller, K. B., Hadley, S., & Snydman, D. R. (2007). Daptomycin in the treatment of vancomycin-resistant Enterococcus faecium bacteremia in neutropenic patients. J Infect., 54(6), 567-571

45. Ho, S. W., Jung, D., Calhoun, J. R., Lear, J. D., Okon, M., Scott, W. R., ... & Straus, S. K. (2008). Effect of divalent cations on the structure of the antibiotic daptomycin. Eur Biophys J., 37(4), 421-433.

46. Hobbs, J. K., Miller, K., O'neill, A. J., & Chopra, I. (2008). Consequences of daptomycin-mediated membrane damage in Staphylococcus aureus. J Antimicrob Chemother., 62(5), 1003-1008.

47. MacLaren, G., & Spelman, D. (2012). Polymyxins: an overview. Up to Date. Ed. Post TW, UpToDate, Waltham, MA. Disponible en: https://www. uptodate. com/contents/polymyxins-an-overview. Fecha de consulta, 5(2), 2020.

48. Evans, M. E., Feola, D. J., & Rapp, R. P. (1999). Polymyxin B sulfate and colistin: old antibiotics for emerging multiresistant gram-negative bacteria. Ann Pharmacother., 33(9), 960-967.

49. Pankuch, G. A., Jacobs, M. R., & Appelbaum, P. C. (1993). Susceptibilities of 428 gram-positive and-negative anaerobic bacteria to Bay y3118 compared with their susceptibilities to ciprofloxacin, clindamycin, metronidazole, piperacillin, piperacillin-tazobactam, and cefoxitin. Antimicrob Agents Chemother., 37(8), 1649-1654.

50. Ravdin, J. I., & Skilogiannis, J. (1989). In vitro susceptibilities of Entamoeba histolytica to azithromycin, CP-63,956, erythromycin, and metronidazole. Antimicrob Agents Chemother., 33(6), 960-962.

51. Nix, D. E., Tyrrell, R., & Müller, M. (1995). Pharmacodynamics of metronidazole determined by a time-kill assay for Trichomonas vaginalis. Antimicrob Agents Chemother., 39(8), 1848-1852.

52. Edwards, D. I. (1993). Nitroimidazole drugs-action and resistance mechanisms I. Mechanism of action. J Antimicrob Chemother., 31(1), 9-20.

53. Campbell, E. A., Korzheva, N., Mustaev, A., Murakami, K., Nair, S., Goldfarb, A., & Darst, S. A. (2001). Structural mechanism for rifampicin inhibition of bacterial RNA polymerase. Cell., 104(6), 901-912.

54. McClure, W. R., & Cech, C. L. (1978). On the mechanism of rifampicin inhibition of RNA synthesis. J Biol Chem., 253(24), 8949-8956.

55. Schulz, W., & Zillig, W. (1981). Rifampidn inhibition of RNA synthesis by destabilisation of DNA-RNA polymerase-oligonucleotide-complexes. Nucleic Acids Res., 9(24), 6889-6906.

56. Then, R., & Angehrn, P. (1973). Nature of the bactericidal action of sulfonamides and trimethoprim, alone and in combination. J Infect Dis., 128(Supplement_3), S498-S501.

57. Bach, M. C., Finland, M., Gold, O., & Wilcox, C. (1973). Susceptibility of recently isolated pathogenic bacteria to trimethoprim and sulfamethoxazole separately and combined. J Infect Dis., 128(Supplement_3), S508-S533.

58. Hendlin, D., Stapley, E. O., Jackson, M., Wallick, H., Miller, A. K., Wolf, F. J., ... & Mochales, S. (1969). Phosphonomycin, a new antibiotic produced by strains of Streptomyces. Science., 166(3901), 122-123.

59. Falagas, M. E., Giannopoulou, K. P., Kokolakis, G. N., & Rafailidis, P. I. (2008). Fosfomycin: use beyond urinary tract and gastrointestinal infections. Clin Infect Dis., 46(7), 1069-1077.

60. Skarzynski, T., Mistry, A., Wonacott, A., Hutchinson, S. E., Kelly, V. A., & Duncan, K. (1996). Structure of UDP-N-acetylglucosamine enolpyruvyl transferase, an enzyme essential for the synthesis of bacterial peptidoglycan, complexed with substrate UDP-N-acetylglucosamine and the drug fosfomycin. Structure., 4(12), 1465-1474.

61. Borisova, M., Gisin, J., & Mayer, C. (2014). Blocking peptidoglycan recycling in Pseudomonas aeruginosa attenuates intrinsic resistance to fosfomycin. Microb Drug Resist., 20(3), 231-237.

62. Eschenburg, S., Priestman, M., & Schönbrunn, E. (2005). Evidence that the fosfomycin target Cys115 in UDP-N-acetylglucosamine enolpyruvyl transferase (MurA) is essential for product release. J Biol Chem., 280(5), 3757-3763.

63. Anderson, G. G., Kenney, T. F., MacLeod, D. L., Henig, N. R., & O'Toole, G. A. (2013). Eradication of Pseudomonas aeruginosa biofilms on cultured airway cells by a fosfomycin/tobramycin antibiotic combination. Pathog Dis., 67(1), 39-45.

64. Oliva, A., Tafin, U. F., Maiolo, E. M., Jeddari, S., Bétrisey, B., & Trampuz, A. (2014). Activities of fosfomycin and rifampin on planktonic and adherent Enterococcus faecalis strains in an experimental foreign-body infection model. Antimicrob Agents Chemother, 58(3), 1284-1293.

65. Barber, M., & Waterworth, P. M. (1962). Antibacterial activity in vitro of fucidin. Lancet., 931-2.

66. Onishi, H. R., Pelak, B. A., Gerckens, L. S., Silver, L. L., Kahan, F. M., Chen, M. H., ... & Raetz, C. R. (1996). Antibacterial agents that inhibit lipid A biosynthesis. Science., 274(5289), 980-982.

67. Erwin, A. L. (2016). Antibacterial drug discovery targeting the lipopolysaccharide biosynthetic enzyme LpxC. Cold Spring Harb Perpect Med., 6(7), a025304.

68. Payne, D. J., Warren, P. V., Holmes, D. J., Ji, Y., & Lonsdale, J. T. (2001). Bacterial fatty-acid biosynthesis: a genomics-driven target for antibacterial drug discovery. Drug Discov Today., 6(10), 537-544.

69. Chirala, S. S., Huang, W. Y., Jayakumar, A., Sakai, K., & Wakil, S. J. (1997). Animal fatty acid synthase: functional mapping and cloning and expression of the domain I constituent activities. Proc. Natl. Acad. Sci., 94(11), 5588-5593.

70. Bergler, H., Fuchsbichler, S., Högenauer, G., & Turnowsky, F. (1996). The enoyl-[acyl-carrier-protein] reductase (FabI) of Escherichia coli, which catalyzes a key regulatory step in fatty acid biosynthesis, accepts NADH and NADPH as cofactors and is inhibited by palmitoyl-CoA. Eur J Biochem., 242(3), 689-694.

71. Sivaraman, S., Sullivan, T. J., Johnson, F., Novichenok, P., Cui, G., Simmerling, C., & Tonge, P. J. (2004). Inhibition of the bacterial enoyl reductase FabI by triclosan: a structure− reactivity analysis of FabI inhibition by triclosan analogues. J Med Chem., 47(3), 509-518.

72. Sivaraman, S., Zwahlen, J., Bell, A. F., Hedstrom, L., & Tonge, P. J. (2003). Structure− activity studies of the inhibition of FabI, the Enoyl Reductase from Escherichia coli, by Triclosan: kinetic analysis of mutant FabIs. Biochemistry., 42(15), 4406-4413.

73. Singh, M., Ilic, S., Tam, B., Ben-Ishay, Y., Pappo, D., & Akabayov, B. (2020). Dual acting small-Molecule inhibitors targeting Mycobacterial DNA replication. bioRxiv, 561506.

74. Parkes, A. L., & Yule, I. A. (2016). Hybrid antibiotics–clinical progress and novel designs. Expert Opin Drug Discov., 11(7), 665-680.

75. Radzishevsky, I. S., Rotem, S., Bourdetsky, D., Navon-Venezia, S., Carmeli, Y., & Mor, A. (2007). Improved antimicrobial peptides based on acyl-lysine oligomers. Nat Biotechnol., 25(6), 657-659.

76. Blais, J., Lewis, S. R., Krause, K. M., & Benton, B. M. (2012). Antistaphylococcal activity of TD-1792, a multivalent glycopeptide-cephalosporin antibiotic. Antimicrob Agents Chemother, 56(3), 1584-1587.

77. Zhang, F. Y., Du, G. J., Zhang, L., Zhang, C. L., Lu, W. L., & Liang, W. (2009). Naringenin enhances the anti-tumor effect of doxorubicin through selectively inhibiting the activity of multidrug resistance-associated proteins but not P-glycoprotein. Pharm Res., 26(4), 914-925.

78. Tan, S. L., Pause, A., Shi, Y., & Sonenberg, N. H. C. (2002). therapeutics: current status and emerging strategies, Nat. Drug Discov., 1, 867-881.

79. Gravitz, L. (2011). Introduction: a smouldering public-health crisis. Nature., 474(7350), S2-S4.

80. Perz, J. F., Armstrong, G. L., Farrington, L. A., Hutin, Y. J., & Bell, B. P. (2006). The contributions of hepatitis B virus and hepatitis C virus infections to cirrhosis and primary liver cancer worldwide. J Hepatol., 45(4), 529-538.

81. Moradpour, D., Penin, F., & Rice, C. M. (2007). Replication of hepatitis C virus. Nat. Rev Microbiol., 5(6), 453-463.

82. Fraser, C. S., & Doudna, J. A. (2007). Structural and mechanistic insights into hepatitis C viral translation initiation. Nat. Rev Microbiol., 5(1), 29-38.

83. Sharma, S. D. (2010). Hepatitis C virus: molecular biology & current therapeutic options. Indian J Med Res, 131(1), 17-34.

84. Garber, K. (2007). HDAC inhibitors overcome first hurdle.

85. Khawaja, A., Vopalensky, V., & Pospisek, M. (2015). Understanding the potential of hepatitis C virus internal ribosome entry site domains to modulate translation initiation via their structure and function. Wiley Interdisciple.. RNA., 6(2), 211-224.

86. Lukavsky, P. J., Kim, I., Otto, G. A., & Puglisi, J. D. (2003). Structure of HCV IRES domain II determined by NMR. Nat Struct Mol Biol., 10(12), 1033-1038.

87. Dibrov, S. M., Johnston-Cox, H., Weng, Y. H., & Hermann, T. (2007). Functional architecture of HCV IRES domain II stabilized by divalent metal ions in the crystal and in solution. Angew Chem., 119(1-2), 230-233.

88. Zhao, Q., Han, Q., Kissinger, C. R., Hermann, T., & Thompson, P. A. (2008). Structure of hepatitis C virus IRES subdomain IIa. Acta Crystallogr Sect D Struct Biol, 64(4), 436-443.

89. Filbin, M. E., & Kieft, J. S. (2011). HCV IRES domain IIb affects the configuration of coding RNA in the 40S subunit's decoding groove. Rna, 17(7), 1258-1273.

90. Otto, G. A., & Puglisi, J. D. (2004). The pathway of HCV IRES-mediated translation initiation. Cell, 119(3), 369-380.

91. Ji, H., Fraser, C. S., Yu, Y., Leary, J., & Doudna, J. A. (2004). Coordinated assembly of human translation initiation complexes by the hepatitis C virus internal ribosome entry site RNA. Proc. Natl. Acad. Sci., 101(49), 16990-16995.

92. Spahn, C. M., Kieft, J. S., Grassucci, R. A., Penczek, P. A., Zhou, K., Doudna, J. A., & Frank, J. (2001). Hepatitis C virus IRES RNA-induced changes in the conformation of the 40s ribosomal subunit. Science., 291(5510), 1959-1962.

93. Kieft, J. S., Zhou, K. A. I. H. O. N. G., Jubin, R. O. N. A. L. D., & Doudna, J. A. (2001). Mechanism of ribosome recruitment by hepatitis C IRES RNA. Rna., 7(2), 194-206.

94. Berry, K. E., Waghray, S., Mortimer, S. A., Bai, Y., & Doudna, J. A. (2011). Crystal structure of the HCV IRES central domain reveals strategy for start-codon positioning. Structure., 19(10), 1456-1466.

95. Dibrov, S. M., Parsons, J., Carnevali, M., Zhou, S., Rynearson, K. D., Ding, K., ... & Hermann, T. (2014). Hepatitis C Virus Translation Inhibitors Targeting the Internal Ribosomal Entry Site: Miniperspective. J Med Chem., 57(5), 1694-1707.

96. Wang, W., Préville, P., Morin, N., Mounir, S., Cai, W., & Siddiqui, M. A. (2000). Hepatitis C viral IRES inhibition by phenazine and phenazine-like molecules. Bioord Med Chem Lett., 10(11), 1151-1154.

97. Parsons, J., Castaldi, M. P., Dutta, S., Dibrov, S. M., Wyles, D. L., & Hermann, T. (2009). Conformational inhibition of the hepatitis C virus internal ribosome entry site RNA. Nat Chem Biol., 5(11), 823-825.

98. Liu, S., Nelson, C. A., Xiao, L., Lu, L., Seth, P. P., Davis, D. R., & Hagedorn, C. H. (2011). Measuring antiviral activity of benzimidazole molecules that alter IRES RNA structure with an infectious hepatitis C virus chimera expressing Renilla luciferase. Antiviral Res., 89(1), 54-63.

99. Carnevali, M., Parsons, J., Wyles, D. L., & Hermann, T. (2010). A modular approach to synthetic RNA binders of the hepatitis C virus internal ribosome entry site. ChemBioChem, 11(10), 1364-1367.

100. Rich, A., Nordheim, A., & Wang, A. H. J. (1984). The chemistry and biology of left-handed Z-DNA. Annual Rev Biochem., 53(1), 791-846.

101. Tran-Dinh, S., Taboury, J., Neumann, J. M., Huynh-Dinh, T., Genissel, B., Langlois d'Estaintot, B., & Igolen, J. (1984). Proton NMR and circular dichroism studies of the B and Z conformations of the self-complementary deoxyhexanucleotide d (m5C-GCG-m5C-G): mechanism of the ZB-coil transitions. Biochemistry, 23(7), 1362-1371.

102. Kawai, K., Saito, I., & Sugiyama, H. (1999). Conformation-Dependent Photochemistry of 5-Halouracil-Containing DNA: Stereospecific 2 ‘α-Hydroxylation of Deoxyribose in Z-form DNA. J Am Chem Soc., 121(6), 1391-1392.

103. Miyahara, T., Nakatsuji, H., & Sugiyama, H. (2016). Similarities and Differences between RNA and DNA Double-Helical Structures in Circular Dichroism Spectroscopy: A SAC–CI Study. J Phys Chem A., 120(45), 9008-9018.

104. Oyoshi, T., Kawai, K., & Sugiyama, H. (2003). Efficient C2 ‘α-Hydroxylation of Deoxyribose in Protein-Induced Z-Form DNA. J Am Chem Soc., 125(6), 1526-1531.

105. Hall, K., Cruz, P., Tinoco, I., Jovin, T. M., & van de Sande, J. H. (1984). ‘Z-RNA’—a left-handed RNA double helix. Nature, 311(5986), 584-586.

106. Brown, B. A., Lowenhaupt, K., Wilbert, C. M., Hanlon, E. B., & Rich, A. (2000). The Zα domain of the editing enzyme dsRNA adenosine deaminase binds left-handed Z-RNA as well as Z-DNA. Proc. Natl. Acad. Sci., 97(25), 13532-13536.

107. Xu, Y., Ikeda, R., & Sugiyama, H. (2003). 8-Methylguanosine: a powerful Z-DNA stabilizer. Journal of the American Chemical Society, 125(44), 13519-13524.

108. Polavarapu, P. L. (2012). Determination of the structures of chiral natural products using vibrational circular dichroism. Comprehen chiropti spectro., 2, 387-420.

109. Berova, N., Nakanishi, K., & Woody, R. W. (Eds.). (2000). Circular dichroism: principles and applications. John Wiley & Sons.

110. Bahloul, A., Boubrik, F., & Rouviere-Yaniv, J. (2001). Roles of Escherichia coli histone-like protein HU in DNA replication: HU-beta suppresses the thermosensitivity of dnaA46ts. Biochimie., 83(2), 219-229.

111. Oberto, J., & Rouviere-Yaniv, J. (2001). Does the parallel evolution pattern between the replication-segregationproteins and HU have a biological significance?. Biochimie., 83(1), 61-66.

112. Ali, B. J., Amit, R., Braslavsky, I., Oppenheim, A. B., Gileadi, O., & Stavans, J. (2001). Compaction of single DNA molecules induced by binding of integration host factor (IHF). Proc. Natl. Acad. Sci., 98(19), 10658-10663.

113. Krylov, A. S., Zasedateleva, O. A., Prokopenko, D. V., Rouviere-Yaniv, J., & Mirzabekov, A. D. (2001). Massive parallel analysis of the binding specificity of histone-like protein HU to single-and double-stranded DNA with generic oligodeoxyribonucleotide microchips. Nucleic Acids Res., 29(12), 2654-2660.

114. Schröder, O., & Wagner, R. (2002). The bacterial regulatory protein H-NS A versatile modulator of nucleic acid structures. Biol Chem., 383(6), 945-960.

115. Grove, A., & Saavedra, T. C. (2002). The role of surface-exposed lysines in wrapping DNA about the bacterial histone-like protein HU. Biochemistry, 41(24), 7597-7603.

116. Azam, T. A., Iwata, A., Nishimura, A., Ueda, S., & Ishihama, A. (1999). Growth phase-dependent variation in protein composition of the Escherichia coli nucleoid. J Bacteriol., 181(20), 6361-6370.

117. Free, A., & Dorman, C. J. (1995). Coupling of Escherichia coli hns mRNA levels to DNA synthesis by autoregulation: implications for growth phase control. Mol Microbiol., 18(1), 101-113.

118. Balandina, A., Claret, L., Hengge-Aronis, R., & Rouviere-Yaniv, J. (2001). The Escherichia coli histone-like protein HU regulates rpoS translation. Mol Microbiol., 39(4), 1069-1079.

119. Tupper, A. E., Owen-Hughes, T. A., Ussery, D. W., Santos, D. S., Ferguson, D. J., Sidebotham, J. M., ... & Higgins, C. F. (1994). The chromatin-associated protein H-NS alters DNA topology in vitro. EMBO J., 13(1), 258-268.

120. Hardy, C. D., & Cozzarelli, N. R. (2005). A genetic selection for supercoiling mutants of Escherichia coli reveals proteins implicated in chromosome structure. Mol Microbiol., 57(6), 1636-1652.

121. Spurio, R., Dürrenberger, M., Falconi, M., La Teana, A., Pon, C. L., & Gualerzi, C. O. (1992). Lethal overproduction of the Escherichia coli nucleoid protein H-NS: ultramicroscopic and molecular autopsy. Mol Gen Genet., 231(2), 201-211.

122. McGovern, V., Higgins, N. P., Chiz, R. S., & Jaworski, A. (1994). H-NS over-expression induces an artificial stationary phase by silencing global transcription. Biochimie, 76(10-11), 1019-1029.

123. Spurio, R., Dürrenberger, M., Falconi, M., La Teana, A., Pon, C. L., & Gualerzi, C. O. (1992). Lethal overproduction of the Escherichia coli nucleoid protein H-NS: ultramicroscopic and molecular autopsy. Mol Gen Genet., 231(2), 201-211.

124. Coletta, M., Ceschini, S., Lupidi, G., Pon, C. L., Fioretti, E., & Angeletti, M. (2000). Multimeric self-assembly equilibria Involving the histone-like protein H-NS: a thermodynamic study. J Biol Chem., 275(2), 729-734.

125. Owen-Hughes, T. A., Pavitt, G. D., Santos, D. S., Sidebotham, J. M., Hulton, C. S., Hinton, J. C., & Higgins, C. F. (1992). The chromatin-associated protein H-NS interacts with curved DNA to influence DNA topology and gene expression. Cell., 71(2), 255-265.

126. Tupper, A. E., Owen-Hughes, T. A., Ussery, D. W., Santos, D. S., Ferguson, D. J., Sidebotham, J. M., ... & Higgins, C. F. (1994). The chromatin-associated protein H-NS alters DNA topology in vitro. EMBO J., 13(1), 258-268.

127. Lucht, J. M., Dersch, P., Kempf, B., & Bremer, E. (1994). Interactions of the nucleoid-associated DNA-binding protein H-NS with the regulatory region of the osmotically controlled proU operon of Escherichia coli. J Biol Chem., 269(9), 6578.

128. Schröder, O., & Wagner, R. (2000). The bacterial DNA-binding protein H-NS represses ribosomal RNA transcription by trapping RNA polymerase in the initiation complex. J Mol Biol., 298(5), 737-748.

129. Dame, R. T., Wyman, C., Wurm, R., Wagner, R., & Goosen, N. (2002). Structural basis for H-NS-mediated trapping of RNA polymerase in the open initiation complex at the rrnB P1. J Biol Chem., 277(3), 2146-2150.

130. Dorman, C. J., Hinton, J. C., & Free, A. (1999). Domain organization and oligomerization among H-NS-like nucleoid-associated proteins in bacteria. Trends Microbiol., 7(3), 124-128.

131. Yu, R. R., & DiRita, V. J. (2002). Regulation of gene expression in Vibrio cholerae by ToxT involves both antirepression and RNA polymerase stimulation. Mol Microbiol., 43(1), 119-134.

132. Dorman, C. J., & Deighan, P. (2003). Regulation of gene expression by histone-like proteins in bacteria. Curr Opin Genet., 13(2), 179-184.

133. Navarre, W. W., McClelland, M., Libby, S. J., & Fang, F. C. (2007). Silencing of xenogeneic DNA by H-NS—facilitation of lateral gene transfer in bacteria by a defense system that recognizes foreign DNA. Genes Dev., 21(12), 1456-1471.

134. Kar, S., & Adhya, S. (2001). Recruitment of HU by piggyback: a special role of GalR in repressosome assembly. Genes Dev., 15(17), 2273-2281.

135. Semsey, S., Geanacopoulos, M., Lewis, D. E., & Adhya, S. (2002). Operator-bound GalR dimers close DNA loops by direct interaction: tetramerization and inducer binding. EMBO J., 21(16), 4349-4356.

AIMS AND OBJECTIVES:

Quinoxaline small molecules are DNA intercalating compounds that display sequence specificity and antibacterial and antitumor properties. They are challenging to synthesize and their complexity also contributes to the difficulty in understanding their mode of activity. To overcome these problem simple monoxinoxaline small molecules were synthesized by our lab by keeping some of the features of the parental molecule intact.

The first objective of my research work was to study the DNA structural alteration potential of few monoquinoxaline small molecules by using biophysical techniques like DNA gel-shift, Circular dichroism, Fluorescence intercalator displacement assay, Atomic force microscopy etc. and how this DNA structural change can lead to various DNA damaging responses in the bacterial cell.

The second objective was to study the antiviral potential of few monoquinoxaline molecules against Hepatitis c Virus by interacting with the 5'-UTR of the HCV IRES. The design of the molecules was based on the crystal structure of HCV subdomain IIA RNA and Benzimidazole (a potent HCV IRES binder) complex. Among the several molecules synthesized in our lab, the potent molecules could disrupt the base stacking interaction in the L-shaped loop of the HCV IRES subdomain IIa and lead to an inhibition of HCV IRES mediated translation and replication in HUH 7 mammalian cell line. The DNA binding activities of these molecules were studied to enquire about the nonspecific nature of the compounds if there were any.

Chapter 1

Antibacterial evaluation of designed mono quinoxalinesmall molecules.

1.1. INTRODUCTION:

Antibiotic resistance by bacteria has proved to be a severe threat to mankind in recent times, and this fortifies an urgency to design and develop potent antibacterial small molecules/compounds with nonconventional mechanisms than the conventional ones.[136] DNA carries the genetic signature of any organism and bacteria maintain their genomic DNA inside the cell in a well-regulated compact form with the help of various nucleoid-associated proteins like HU, HNS, etc.[137-139] These proteins control various fundamental processes like gene expression, replication, etc inside the cell.[140-142] Alteration of the native DNA structure of bacteria can lead to severe consequences in cellular processes inside the bacterial cell and result in the death of the organism. The change in the global DNA structure by small molecules initiates a plethora of cellular responses that have not been very well investigated. Echinomycin and Triostin-A are biologically active Quinoxaline small molecules typically consist of a quinoxaline chromophore attached with an octadepsipeptide ring. They bind to double-stranded DNA in a sequence-specific way and have high activity against a wide variety of bacteria mainly against Gram-positive ones.[143-145] To date several synthetic quinoxaline scaffolds were synthesized displaying antibacterial potential against a broad scale of pathogenic bacteria.[146-147] QNOs (Quinoxaline N-oxides) are known to target DNA and instigate reactive oxygen species (ROS) production in bacteria thereby exhibiting antibacterial properties.[148] Small molecules comprising of a Quionoxaline core have been used in the past for treating bacterial infections in animal husbandry and fisheries. Quinoxaline N-oxides like CBX has been used regularly as growth promoters in various poultry farms.[149-151] The divergent role of Quinoxaline small molecules in medicinal research qualifies them for the evaluation of their antimicrobial properties as a potential candidate. The previous study from our lab has given new insights on a 6-nitroquinoxaline derivative **1d** as an intercalator of DNA which induces conformational changes in DNA upon binding.[152] The binding event observed was dependent on the presence of a crucial benzyl substituent on the quinoxaline moiety. This was associated with a large induced CD (ICD) appearing in a sigmoidal pattern, upon the interaction of **1d** with dsDNA. The induction of DNA superstructures by **1d** at high Drug: DNA ratios were observed that ultimately led to DNA condensation. Eviction of in vitro assembled nucleosome upon treatment with a high dose of **1d** was also observed.[153] In this work monoquinoxaline derivatives of **1d**

were synthesized by various modifications of the **1d** scaffold. The set of synthesized 6-nitroquinoxaline derivatives along with **1d** were all subjected to antibacterial evaluation. Once the potent candidates showing good antibacterial activity were selected they were subjected to various biophysical and biological experiments to study their DNA structural alteration as well as their biological response in the bacterial cells.

1.2.MATERIALS AND METHODS:

1.2.1. Synthesis of Molecules:

All molecules used in Project 1 were synthesized by Ritesh Pal and Ajay kanungo. The molecules used in Project 2 were synthesized by Ajay kanungo, Ritesh Pal, Dipendu Patra, and Bhim Majhi.

Project 1:

1.2.2. Minimal Inhibitory Concentration:

To study the Minimal Inhibitory concentrations of all compounds (as per the protocol of CLSI) [154] Broth microdilution assay was used against gram-positive bacteria like (*Staphylococcus epidermidis* (MTCC3615), *Staphylococcus aureus* (MTCC737), *Arthrobacter chlorophenolicus* A6 (MTCC3706), and gram-negative bacteria (*Pseudomonas aeruginosa* (MTCC1688), *Escherichia coli* (MTCC1916). Luria-Bertani (LB) broth containing different Bacterial cultures was added per well in a 96 well plate at 5×10^5 CFU/mL. The compounds used were DMSO dissolved and different concentrations were added maintaining DMSO percentage under 0.6%. The plates were kept at the specific recommended temperature for each bacterial growth for 6 hours and at 600 nm Optical Density was measured.

1.2.3. Cytotoxicity studies in Mammalian cells

Cytotoxicity of the compounds was checked in HEK 293Human embryonic kidney) cell line (4000 cells/well in 96 well plate) using MTT (3-(4,5-dimethylthiazol-2-yl)-2,5-diphenyltetrazolium bromide). Cells in DMEM (Dulbecco Modified Eagles medium) supplemented with 10% Fetal Bovine Serum were seeded in 96 well in and kept in a CO_2 incubator at 37°C overnight. Treatment of Cells was done with different compound concentrations and kept in a CO_2 incubator for 24 hours. MTT solution was added at 1

mg/mL working concentration and incubated for 2-3 hours in the incubator until formazan crystals have suitably formed. Media was discarded after plates were taken out and DMSO was added to each well. Plates were placed in a shaker for 10-15 min for the formazan crystals to dissolve completely. Results were measured using absorbance at 595 nm in a plate reader. From the OD value obtained from triplicate experiments, the IC_{50} values were measured.

1.2.4. EtBr fluorescence quenching assay

EtBr (5 µM), *Staph. aureus* gDNA and CT DNA (10 µM) were added to 10 mM NaP buffer containing 1% DMSO and 10 mM NaCl was titrated with different concentrations (2.5 µM to 100 µM) of the respective compound. Horiba PTI QuantaMaster™ 8000 fluorescence spectrometer was used to measure the fluorescence intensity with a 480 nm excitation wavelength and 520 to 700 nm emission wavelength scan. Results were plot by normalizing the fluorescence intensity vs. concentration of respective compounds using Graphpad Prism 7.

1.2.5. Circular Dichroism Spectroscopy

CD Spectra was performed with CT-DNA and an increasing concentration of **3a** varying from 15 µM - 60 µM in an optically inactive CD cuvette with a 5mm path length. The CD spectral range was chosen from 230 to 450 nm at around 100-nm/min per scan. For the experiment with genomic DNA, *A. chlorophenolicus* and *S. aureus* gDNA isolated manually using Sigma-Aldrich's GenElute bacterial genomic DNA isolation kit was used. The concentration of gDNA was taken with a UV-VIS spectrophotometer.

1.2.6. Agarose DNA Gel-shift assay

Gel shift assay was done with pCDNA 3.1 plasmid vector isolated using plasmid DNA isolation kit after amplifying it in *E. coli* DH5α. For the reaction 40 µM pCDNA 3.1 plasmid in 50 mM NaP buffer pH 7 supplemented with 10mM NaCl were mixed and an increasing concentration of the selected compounds (measured in terms of compound concentration: DNA base pair ratio) was added. The reaction was kept at 37°C for 16

hours. A 1% agarose gel was used to run all samples for ~ 3 hours at 50 V and stained with EtBr (0.5µg/mL) kept for 5 mins at room temperature, visualized in Bio-Rad GelDoc Imaging System from and data was processed with the help of Image Lab™ software.

For gel-shift experiments with gDNA similar reaction was performed with minor changes where the working concentration of gDNA was kept at 20 µM per reaction. A 0.6% agarose gel was used to run all samples for 3.5-4 hours at constant 50 V and the gel was stained using working EtBr solution at (1 µg/mL) and analyzed in a Bio-Rad gel doc.

1.2.7. DNA condensation in *S. aureus* cells

Staphylococcus. aureus (~10^5 CFU/mL) grown for 6 hours after which cell pellet was washed using Phosphate Buffer Saline(pH 7.4). Treatment of Cells was done with **3a** at 10 µM concentration for 1 hour at 37°C in shaker incubator. The untreated and treated cells were then centrifuged and the pellet was washed using PBS. A 16% paraformaldehyde solution was used to fix the cells and kept at 4°C for 30 mins. DAPI was used to stain the fixed cells for 5 mins at 37°C, finally washed using PBS, and cells were smeared on a glass slide using mounting solution, and DPX was used as a sealing agent. A filter set for DAPI was used in a Carl-Ziess Axio Observer LSM 880 confocal laser scanning fluorescence microscope to visualize all samples.

The density threshold function of Image J Fiji software was used to calculate the Nucleoid and cell/cytoplasmic surface area. From three independent experiment sets the sample images were taken. For the Nucleoid and cytoplasmic surface area around 35 independent cells were selected from both control and treated sets.

1.2.8. Stress in DNA synthesis induced in *S. aureus* by 3a

S. aureus cell suspension ($10^5$to 10^6 CFU/mL) in the log phase was treated for 1 hour with **3a** at 37°C and pulsed with 10 µM BrdU for 30 mins. The cells were then fixed for 30 mins using 16% paraformaldehyde solution at 4°C and Triton X-100 (0.5 %) and lysostaphin (0.05 mg/mL) was used to permeabilize it for 10 mins at 4°C. The samples were incubated for 10 mins in 2N HCl for the DNA to denature and HCL was neutralized

using CP buffer (Citrate Phosphate) (50 mM) pH 7.4 buffer by incubating the cells at 25°C for 10 mins. Using FITC tagged anti-BrdU mouse monoclonal antibody cells were incubated for 30 mins in dark at 25°C and PBS was used to wash it. Cells were, smeared in L-lysine pre-coated glass slides and visualized using the FITC channel in Olympus FLUOVIEW fluorescence microscope.

In DNA synthesis assay 10^5 to10^6CFU/mL *S. aureus* cells in log phase were incubated at a varying concentrations of **3a**. Cells were harvested following a 30 mins pulse of ^{3H}Thymidine (1µCi/well), and after the addition of scintillation liquid (Cocktail O), the radioactive counts were calculated in Perkin Elmer Tri-Carb 2810TR liquid scintillation counter.

1.2.9. DNA fragmentation

LMA (low melting agarose) was used to mix *S.aureus* cells, and on glass slides pre-coated with agarose (1%), cells were spread, covered using coverslip, and transferred to a humidified chamber for 30 mins at 4°C. After removing coverslips, 1% agarose solution was used to coat the slides and dried in a humidified chamber for 20 mins so that the cells get sandwiched within the two-agarose layer once the agarose solidifies. Cell lysis was carried out in buffer containing Na_2-EDTA (100 mM), NaCl (1.2 M), 0.2 M NaOH (pH > 10), and Triton X-100 (1%), by placing all slides submerged in dark at 4°C overnight. Gel electrophoresis was carried out the next day by submerging the slides in electrophoresis buffer (30 mM NaOH, 2 mM Na_2-EDTA) for 25-30 mins at a constant 15 V (0.6 V/cm). A neutralizing solution comprising of 50 mM Tris-HCl buffer pH 7.5 was used to neutralize the slides and slides were further washed with deionized water. EtBr (1µg/mL) was used to stain the slides for 3-5 mins and visualized in Olympus confocal laser scanning fluorescence microscope under Texas Red filter set (~ 620 nm).

1.2.10. TUNEL Assay

S. aureus cells were grown in LB and treatment using 3a was done in log phase, centrifuged and PBS was used to wash pellets, cells fixed with 16 % paraformaldehyde by keeping them for 30 mins at 4°C. Cells were permeabilised with chilled Triton X-100

(0.2 %) and of lysostaphin (0.05 mg/mL) at 4°C for 5 mins. Equilibration buffer was used to resuspend cells, nucleotide mix and, TdT Enzyme was added to cells and incubated in a moist chamber for 60 mins in dark inside a 37°C incubator for tailing reaction to occur. Using 2X SSC buffer (Saline Sodium Citrate) at the tailing reaction was stopped after incubation for 15 mins at room temperature. PBS was used to wash cells and resuspended onto a glass slide, covered with coverslip, and sealed using DPX. Using fluorescein filter set (520 +/- 20 nm) the slides were visualized in Olympus confocal microscope.

1.2.11. Atomic Force Microscopy of bacteria:

S. aureus cells with or without treatment were suspended in Phosphate Buffer Saline after centrifugation. A 16% paraformaldehyde solution was used to fix cells and then cleaned using PBS. The fixed cells were smeared onto a glass coverslip and covered by another coverslip so that cells spread equally and adhere uniformly on the surface of the coverslip and washed by sterile water to remove any excess cells and then air-dried. Using a Pico plus 5500 AFM from Agilent Technologies USA, AFM (contact mode) was done with a piezo scanner having a maximum range of 100 μm. Images were processed using Pico view 1.10.1. Using Pico scan 5 software, the cell length, height, and width of bacteria were manually calculated.

1.2.12. Acridine Orange Staining:

Staph. aureus cells untreated or treated with **3a** were placed for 6 hours at 37°C. Using a 16% paraformaldehyde solution, cells were fixed and PBS resuspended. Using chilled Triton X-100 (0.2%) and lysostaphin (0.05 mg/mL) solution, cells were permeabilized for 10 mins at 4°C, centrifuged, and PBS resuspended. Acridine orange (3 μM) was used to stain cells, PBS washed and smeared onto a glass slide covered with coverslip and sealed using DPX. Acridine orange filter set was used to visualize the slides in a confocal microscope.

1.2.13. Analysis of cells using flow cytometer:

Compound **3a** treated *S. aureus* cells were incubated for 2 hours at 37°C. Using chilled 80% methanol cells were fixed and PBS resuspended. In a BD LSRFotressa™ cell analyzer cells were studied. Using the software FlowJo™ the results were examined.

1.2.14. Determination of Membrane permeability:

(i) Propidium iodide permeability assay:

Phosphate buffer saline was used to resuspend treated and untreated *S. aureus* cells after centrifugation. Propidium iodide (4 µg/mL) was used to stain cells and in PE/Texas red channel (610 +/- 10) nm analysis was made in cell analyzer from BD LSRFotressa™. Results were analyzed using FlowJo™ software.

(ii) Alkaline Phosphatase assay:

3a treated *S. aureus* cells were kept for 2 hours and incubated for 1 hour with PNPP (*p*-Nitrophenyl phosphate) at 37°C. Using an Elisa plate reader OD was taken at 410 nm.

1.2.15. Biofilm disruption assay:

In a 96 well plate *Staph. aureus* and *Streptococcus. epidermidis* cells (3×10^5) were seeded kept undisturbed for 24 hours at 37°C so that the biofilm can develop properly. Treatment of cells was done with **3a** at 37°C for 12 hours. For the removal of all planktonic bacterial cells i.e the non-biofilm formers, the plates were washed with sterile water. Using 1% crystal violet solution, plates were stained and kept at room temperature for 10 mins, washed with sterile water and paper towel dried. Plates were placed overnight to dry and using a 30% acetic acid solution the crystal violet was solubilized by incubating at room temperature for 20 minutes. Using a multichannel plate reader, absorbance was recorded at 550 nm. Plates were visualized under the light microscope at 20X magnification and images were also taken using a Digital camera.

1.3. RESULTS AND DISCUSSION:

1.3.1. Design and Synthesis of the quinoxaline derivatives used to target DNA and provide antimicrobial property:

The compounds used in this study (Figure 1.1C) were based on the modification of the compound **1d** (Figure 1.1A). The substituents at the C2 and C3 positions of the 6-nitroquinoxaline moieties were altered (Figure 1.1B) to get the above sets of compounds for this study. The set-1 d (**3a**, **3h- 3u)** include of different benzylamine group at C2 position of the scaffold where C3 position was kept intact with *N*,*N*-dimethylaminopropylamine tail. The set-2 (**3b-3f**) contains distinct amine substituents in C-3 location of the quinoxaline core while keeping intact the *p*-trifluoromethylbenzylamine substituent at the C-2 position. All compounds were checked for any antibacterial potential. Ritesh Pal synthesized all the compounds used in this study.

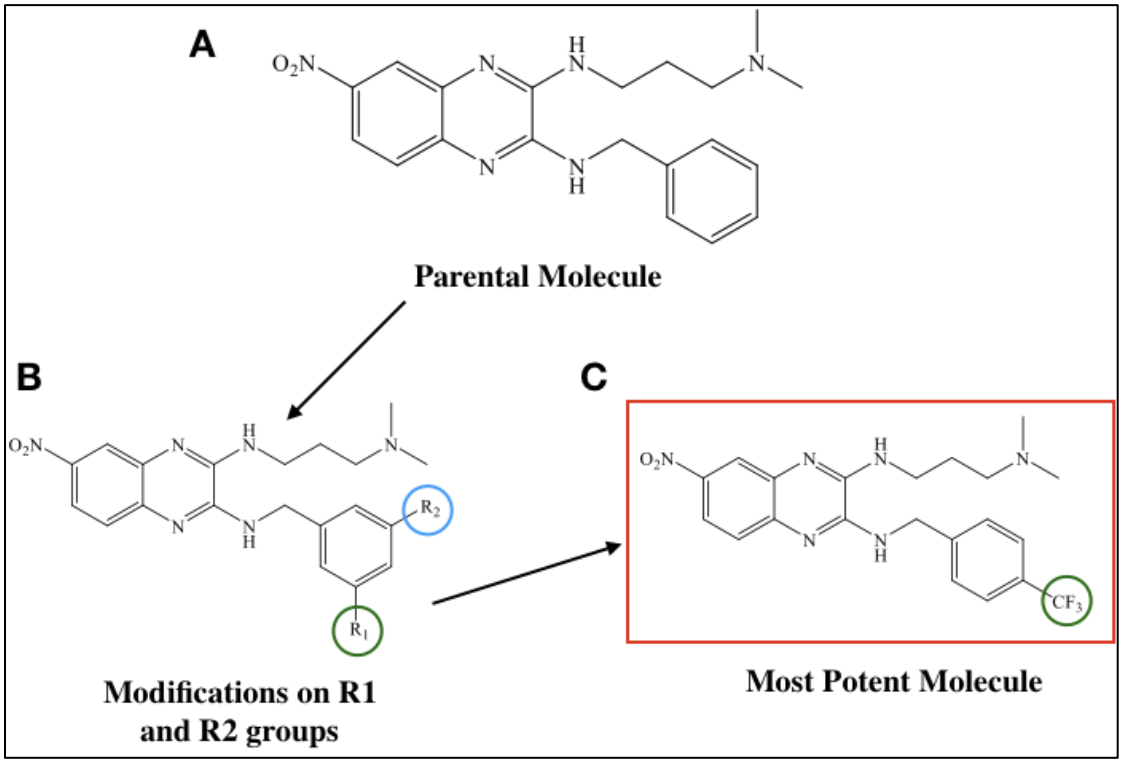

Figure 1.1: A) Parental molecule 1d used for modifications. B) The modification made at the C2 and C3 positions on the parental molecule. C) The most potent molecule used in the study.

1.3.2. Screening of compounds for their antibacterial activity:

All the compounds used were screened initially using the Paper-disk agar plate method against gram-positive (*Arthrobacter chlorophenolicus* A6 MTCC3706), *Staphylococcus epidermidis* MTCC3615, and *Staphylococcus aureus* MTCC737, as well as gram-negative bacteria (*Escherichia coli* MTCC1916, *Pseudomonas aeruginosa* MTCC1688) along with two known antibiotics Ampicillin and kanamycin (Table 1.1). The compounds displaying any zone of inhibition were further subjected to Minimal inhibitory concentration (MIC) evaluation following CLSI guidelines in the above-mentioned bacterial strains. The compound **3a** that showed the best MIC across all five bacteria and **3u** and **3q** was further subjected to biophysical evaluation.

Compounds		MIC (µg/mL)					IC_{50} (µg/mL) HEK 293
		Gram positive bacteria			Gram negative bacteria		
		S.aureus	*S. epidermidis*	*A. chlorophenolicus*	*E. coli*	*P. aeruginosa*	
	3a	1.79 ± 0.25	2.24 ± 0.64	0.897 ± 0.38	3.36 ± 0.64	6.73 ± 0.65	5.66 ± 0.77
	3q	0.89 ± 0.34	0.89 ± 0.22	1.57 ± 0.34	34.3 ± 3.40	>200	7.99 ± 1.29
	3u	1.03 ± 0.14	0.52 ± 0.19	1.81 ± 0.64	>250	>250	4.32 ± 1.03
Control	**Kanamycin**	1..85 ± 0.13	1.98 ± 0.22	3.2 ± 0.25	2.08 ± 0.38	>125	>500
	Echinomycin	0.04 ±0.005	0.02 ± 0.0043	0.07 ± 0.01	21 ± 3.60	>200	0.014±0.005

Table 1.1. MIC (Minimal Inhibitory Concentration) of active molecules and control antibiotics against the above-mentioned bacteria and cell cytotoxicity determination against mammalian HEK 293 cell line.

1.3.3. DNA-molecule interaction:

1.3.3.1. DNA Binding Properties:

Competitive DNA binding properties of **3q, 3u**, and **3a were** all checked by fluorescence quenching experiment with Ethidium Bromide (EtBr). When EtBr bound CT-DNA was titrated with increasing concentrations of the compounds, there was a significant reduction of the fluorescent intensity of EtBr as measured by fluorimeter. The reduction in fluorescent intensity of EtBr was examined using the quenching plot of Stern Volmer

(SV) (Figure 1.2B1-B3). The potency of the quencher is indicated by the K_{sv} (SV constant) value from the stern volmer plot. The compounds **3q**, **3u** and **3a** had K_{sv} values of 1.7 x 10^4 $M^{-}1$, 2 x 10^4 M^{-1} and 1 x 10^4 M^{-1}, and respectively. Since fluorescence quenching studies do not always reflect the true binding nature or properties of the quencher compound, therefore Isothermal titration calorimetric studies were also performed to show that the molecules do bind DNA with high affinity. The ITC experiment resulted in, K_a (binding affinity) values of compound **3q**, **3u,** and **3a** were found to be 3.06 x 10^4 M^{-1}, 9.9 x 10^4 M^{-1} and 2.27 x 10^4 M^{-1} respectively (Figure 1.2C1-C4). Both ITC and FID assay show that compounds bound to DNA with high affinity.

DNA intercalators can induce a change in the ds DNA structures by unwinding of supercoils and unstacking of bases. This change in the structure of the DNA can alter its mobility in an Agarose gel, which is referred to as the DNA gel shift. The compounds **3q**, **3u** and **3a** were all capable of significantly causing a shift in the migration of PBR 322 plasmid DNA (Figure 1.2A1-A3) as well as *S. aureus* genomic DNA (Figure 1.2A4) suggesting DNA binding and intercalation properties of the compounds like their parental compound **1d** but the change was much higher when compared to **1d.**

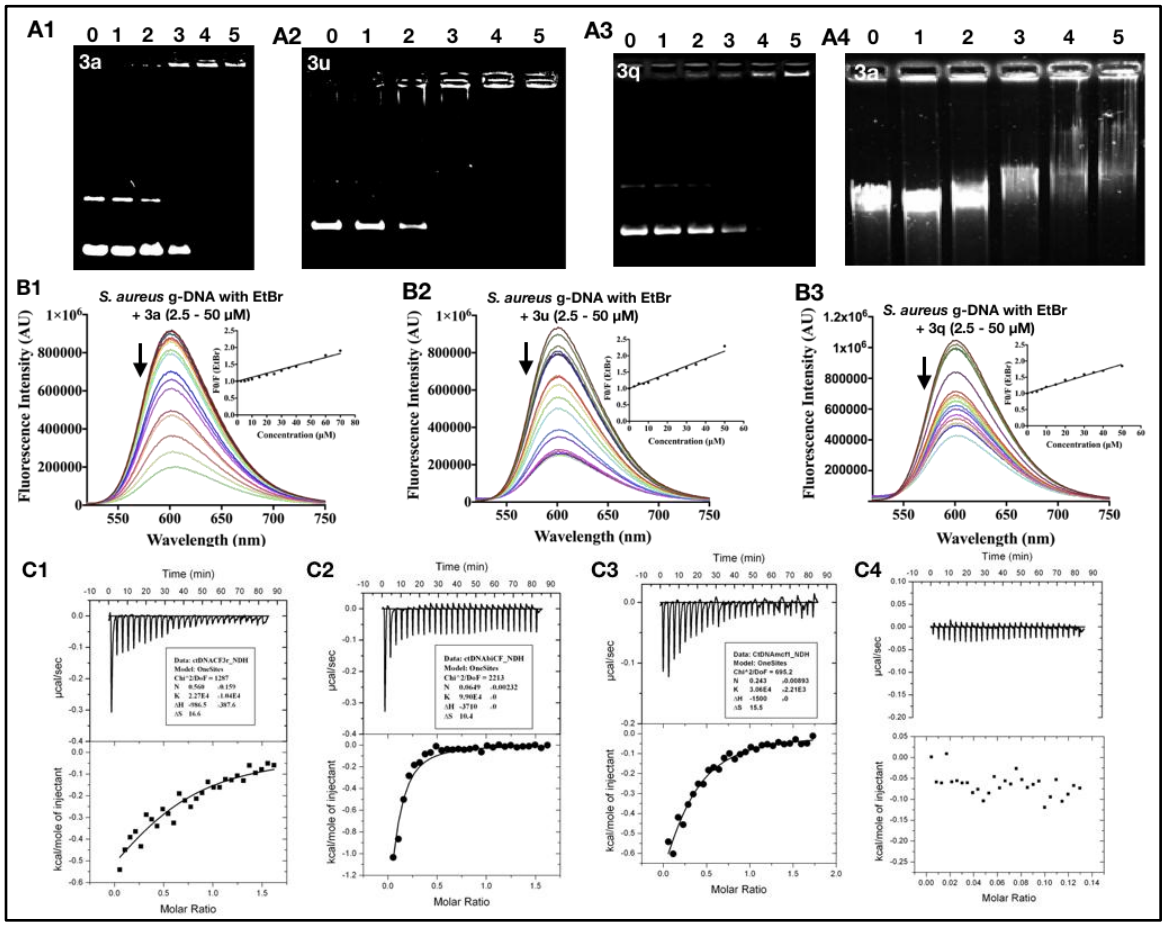

Figure 1.2: pCDNA3.1 Plasmid DNA gel shift assay of upon treatment with **3a**(A1), **3u**(A2), **3q**(A3) and *S. aureus* gDNA treated with **3a** (A4). FID assay with *S. aureus* gDNA with **3a**(B1), **3u**(B2) and **3q**(B3). ITC of calf thymus DNA treated with **3a**(C1), **3u**(C2), **3q**(C3), and buffer correction (C4).

1.3.3.2. <u>DNA structural change:</u>

The structural alteration properties of the compounds were further checked using Circular Dichroism spectroscopy. Upon titration of the compounds **3a**, **3q,** and **3u** with CT DNA as well as bacterial genomic DNA, there was a reduction in the ellipticity at 260 nm that indicates base unstacking as well as generation of an induced CD at around 320 nm which indicates an occurrence of DNA structural change induced by intercalation of the small molecule into the ds DNA (Figure 1.3A-3E). Also, the structural change inducing properties of the compounds was found to be more promising for GC rich *A. chlorophenolicus* genomic DNA than AT-rich *S. aureus* genomic DNA (Figure 1.3F) and

for GC rich DNA sequence (Poly GC) when compared to AT-rich sequence (Poly AT) (Figure1. 3G-3H).

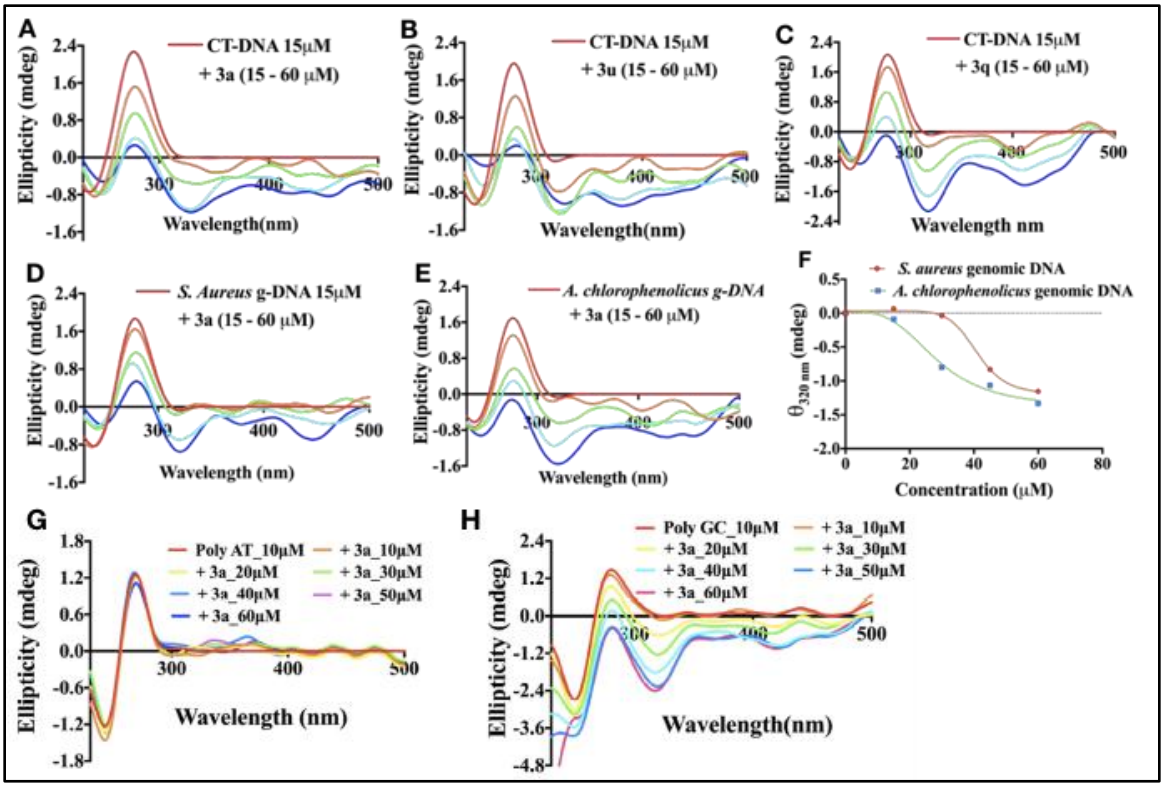

Figure 1.3: (A−C) Circular dichroism spectra of CTDNA (15 μM) with **3q**, **3u,** and **3a** from concentration range 15 μM to 60 μM. (D, E) CD of *S. aureus* gDNA (15 μM) (D) and *A. chlorophenolicus* gDNA (15 μM) (E) treated with **3a** from 15 μM − 60 μM). (F) Plot of ellipticity (320 nm) from *A. chlorophenolicus* (green) and *S. aureus* (red) and **3a** from 15 μM − 60 μM) titration plot. (G) CD of Poly AT (10 μM) with **3a(**10 μM − 60 μM**).** (H) CD of Poly GC (10 μM) with **3a(**10 μM − 60 μM**).**

The structural change was visualized using Atomic Force Microscopy (Figure 1.4A-4G). At lower **DNA**:**3a** (1:0.5 to 1:1) ratios the compound **3a** binds to the DNA locally and induces unwinding of the bases and supercoiling and partially alters the DNA structure (Figure 1.4B-4C). Upon gradually increasing the **DNA**:**3a** ratios (1:1.5 to 1:3) the DNA strands are bought in close proximity and looping of strands occur which lead to a significant structural change in the DNA and ultimately lead to the formation of DNA superstructures and finally, condensation of DNA occurs thereby leading to a global change in the DNA structure (Figure 1.4D-4F).. Similar kinds of DNA superstructures were seen for Doxorubicin, a known intercalator of DNA.

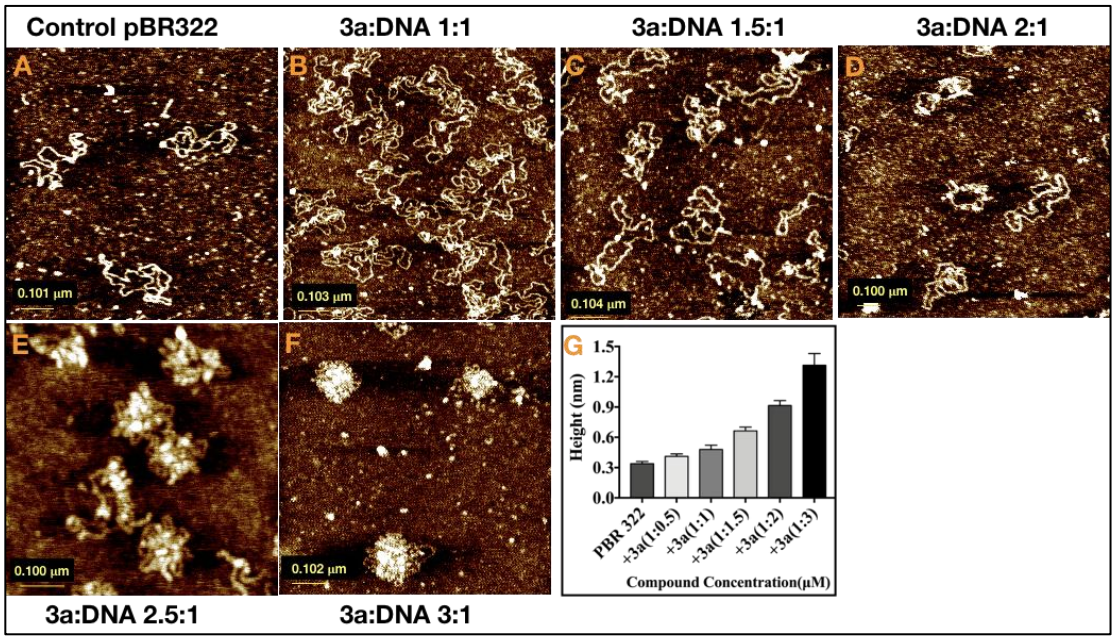

Figure 1.4: AFM of (A) Untreated pBR322 plasmid DNA, (B−F) pBR322 treated with varying **[3a]/[**DNA base pair] ratio. (G) AFM of 3d treated pBR322 in 5:1[3d]/[Pbr322 base pair] ratio. (H) The plot of height for treated and untreated PBR 322 DNA.

1.3.4. Bacterial chromosome condensation

The interaction of *Stapylococcus. aureus* gDNA with the representative compound **3a** also leads to the formation of oversupercoiled DNA structures (Figure 1.5A) similar to those observed for PBR 322 Plasmid DNA. The formation of these structures seems to be intolerable for the bacteria as they might hinder the binding of Nucleoid Associated Proteins (NAPS) present in the bacterial cell, which ultimately results in bacterial cell death.

The Nucleoid condensation event inside the bacterial cell was also observed using super-resolution confocal microscopy. *S. aureus* cells both treated and untreated ones were subjected to staining with DAPI (nucleoid stain) and the cells were observed using super-resolution confocal microscopy (Figure 1.5B). Nucleoid area and cytoplasmic area for each treated and untreated cells were calculated and density contour plots for the N/C ratio showed a significant reduction (~30%) for **3a** treated *S. aureus* cells when compared to untreated ones (Figure 1.5C-5D). This suggests that the global structural change

leading to condensation by **3a** can also occur in a single bacterial cell that might lead to replication stress and DNA damage thereby ultimately resulting in cell death.

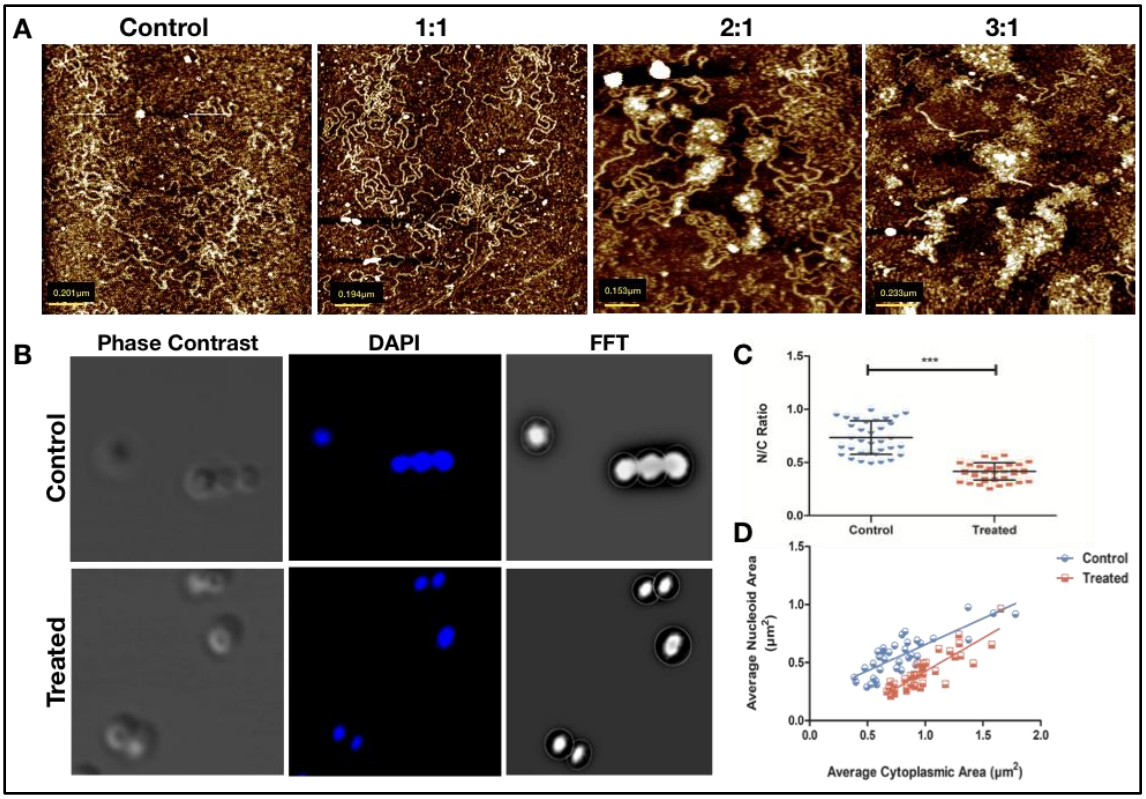

Figure 1.5: (A) AFM **of** *S. aureus* untreated/treated gDNA with **3a**. (B) **3a** treated ***S***. *aureus* cells placed in phase contrast microscope to observe the cytoplasmic area and fluorescence was recorded for DAPI stained nucleoid to measure the nucleoid area). Fast Fourier Transform (FFT) was done to show the image of the cytoplasmic area (denoted by circles) and nucleoid area (denoted by white regions) interior of the cytoplasmic circle. (C) Total N/C ratio from individual 35 samples was taken and plotted for treated and control samples that display a quite significant reduction in the N/C ratio for Treated samples when compared to control.

1.3.5. DNA synthesis Inhibition:

DNA replication occurs very rapidly in bacterial cells during the log phase. Replication stress during this phase can lead to the inhibition of growth. The compound **3a** was capable of inducing replication stress as observed by the reduced incorporation of BrdU (bromodeoxyuridine) when compared to DMSO treated control cells (Figure 1.6A). The replication stress was also crosschecked using ^{3H}Thymidine incorporation by the cells (Figure 1.6B). A reduction in the radioactive signal of ^{3H}Thymidine in **3a** treated *S.*

aureus cells in comparison to control suggests that compound **3a** induces replicative stress in *S. aureus* cells and leads to the halting of replication.

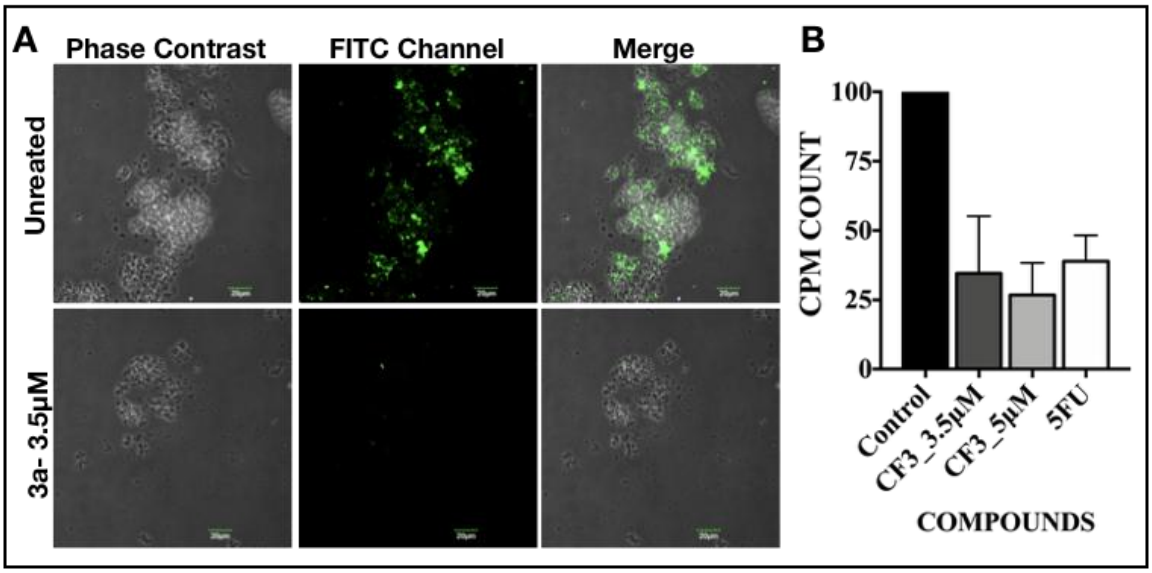

Figure 1.6: DNA synthesis studied in *S. aureus* using fluorescence microscopy. Cells treated with DMSO (Control) or 3.5 µM **of 3a** were pulsed using BrdU, incubated using anti-BrdU antibody. FITC channel was used to capture images at a magnification of 60Å~ and scale bar, 20 µm. (B) Global DNA replication amount was calculated in *S. aureus* cells by 3H-thymidine incorporation in dividing/replicating cells DNA. 5FU-2 µM (5-Fluorouracil) was chosen as the positive control.

1.3.6. Bacterial DNA fragmentation:

Programmed cell death is a well-studied phenomenon in Eukaryotes whereas recent reports have also shown that bacteria can undergo a similar PCD like phenomenon upon treatment with antibiotics [155-156] that results in DNA fragmentation ultimately leading to cell death. To study this, untreated and **3a** treated *S. aureus* cells were subjected to single-cell nucleoid diffusion-based technique. Results suggest that untreated cells appear as a dense and single nucleoid structure whereas for the **3a** treated cells, the nucleoid appears distorted, fragmented, and scattered across the agarose layer (Figure 1.7A). To further confirm the presence of DNA breaks in the *S. aureus* cells, TUNEL assay was performed following standard protocol. Results clearly show that there was significantly higher incorporation of the fluorescent nucleotide in the **3a** treated cells suggesting the induction of genomic DNA fragmentation upon treatment with compound **3a** (Figure 1.7B).

Although **3a** was also able to induce DNA fragmentation in mammalian cells (Hek 293) albeit at higher concentrations (Figure 1.7C).

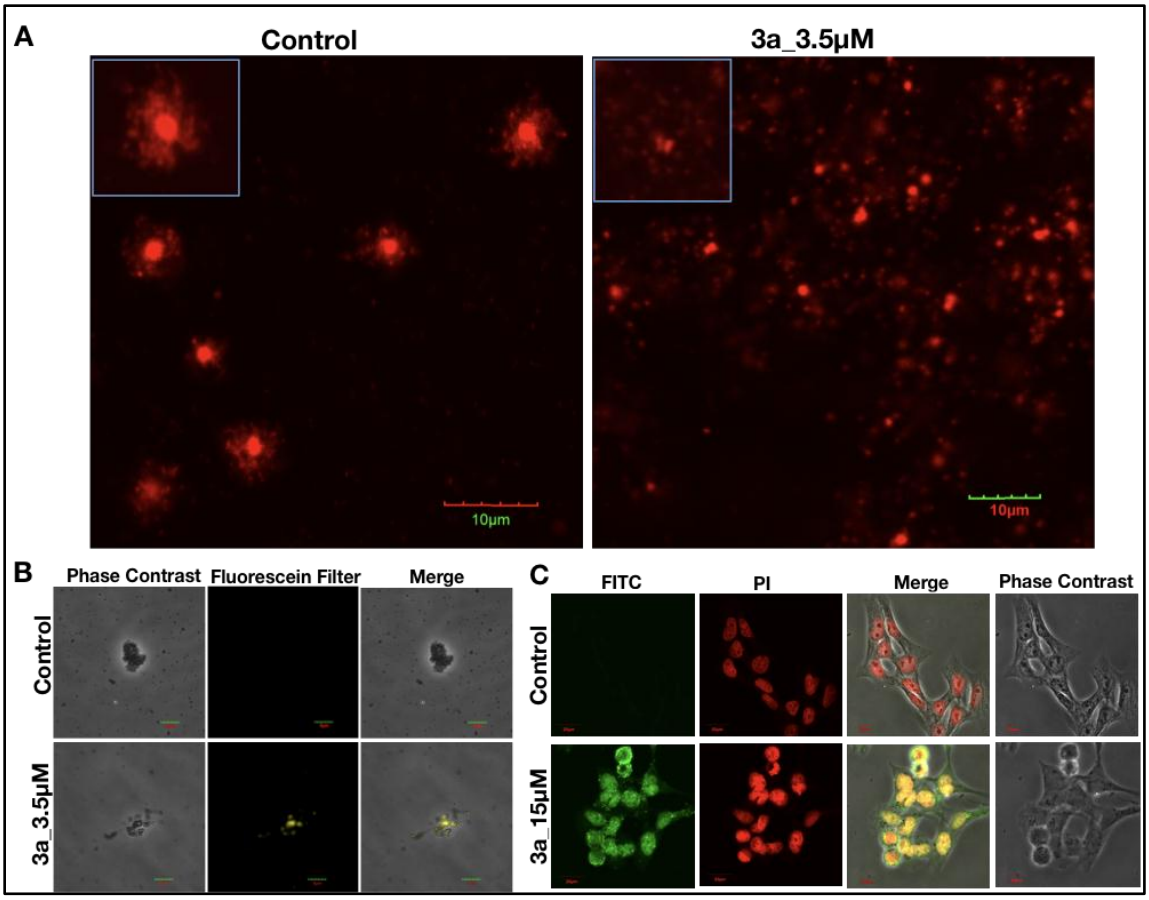

Figure 1.7: *S. aureus* DNA breaks: (A) Detection of Single-cell nucleoid fragmentation after treatment with 3a (3.5 µM) and EtBr staining.. (B) Treatment of Cells with **3a** or DMSO treated control and terminal deoxynucleotidyl transferase (TdT) enzyme was added so that incorporation of fluorescent nucleotides occurred.(C) TUNEL assay in HEK 293 cells treated with **3a** (15 µM).

1.3.7. Morphology plasticity induced by 3a:

The alteration of morphology in bacteria is a common phenomenon, which is often observed in response to various stimuli like stress, pH change, temperature change etc. Bacteria often adapt certain survival policies by altering their cell size or shape in order to escape host defenses [157-159]. Upon treatment of *S. aureus* cells with sub-MIC (3.5 µM) and dose higher than MIC (5 µM), and observed in AFM, there was a change in the cell shape from a round grape-like to elongated rod-like structures. Cell size also increased

from 1.37 ±0.09 for control cells to 2.30 ± 0.22 µm and 2.36 ±0.22 for 3.5 µM and 5 µM treated cells (Figure 1.8A)

The increase in cell size was also verified by visualization in confocal microscopy after Acridine orange staining (Figure 1.8B) and using flow cytometry (Figure 1.8C).

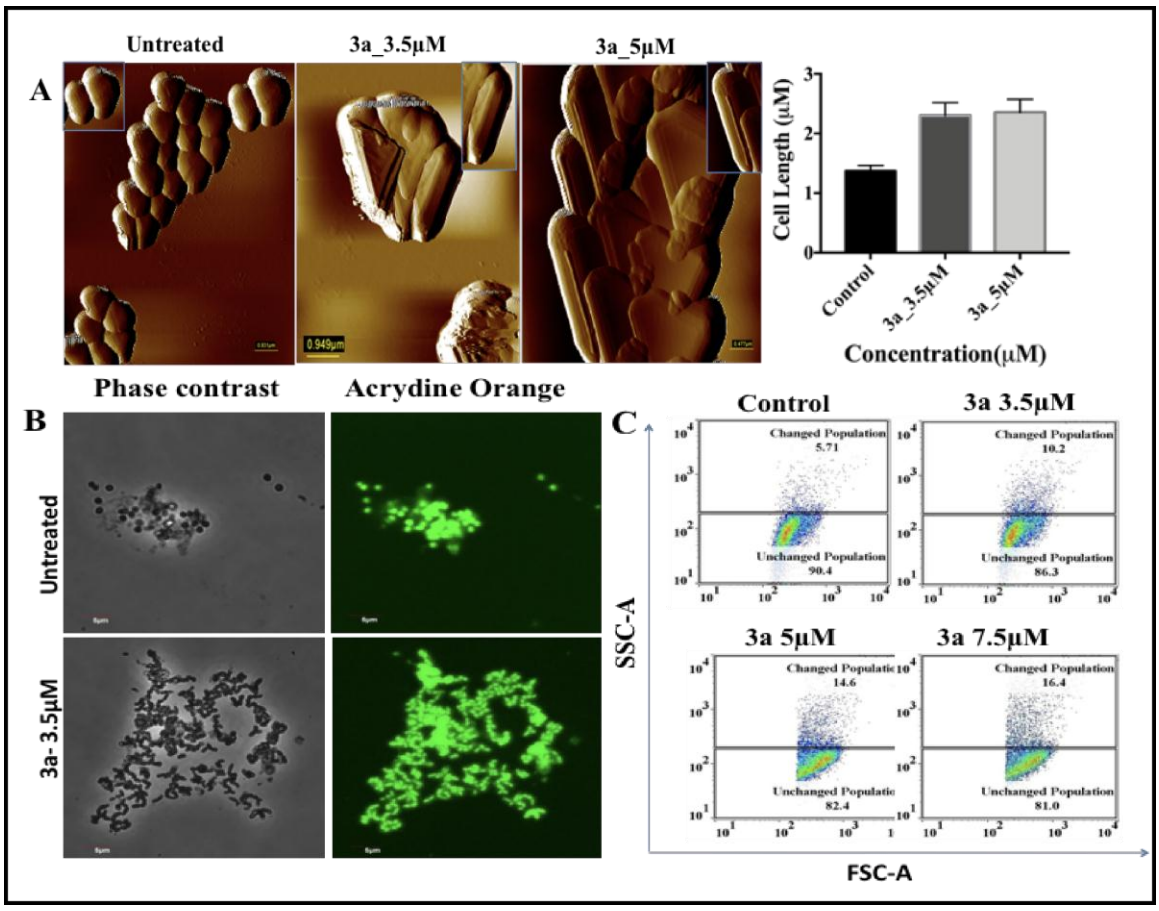

Figure 1.8: Change in *S. aureus* cells morphology upon induction of stress by **3a**. (A) AFM of *S. aureus* cells treated with **3a** (B) *S. aureus* cells after treatment was stained with Acridine orange (AO) and observed in semi confocal microscopy. (C) Separation and Quantification of the cell population that was morphologically different after treatment with **3a** (3.5, 5, or 7.5 µM) using flow cytometry.

1.3.8. Measurement of Membrane permeability/integrity:

Halting of DNA replication leading to incomplete cell division may lead to the ceasing of peptidoglycan synthesis, a very important component of the bacterial cell membrane that adds to the integrity of the membrane. The loss of membrane integrity leads to cell death

since the cells are now prone to osmotic stress, ph change, etc. Membrane integrity loss was observed for *S. aureus* cells treated with 3a in comparison to untreated ones (Figure 1.9A). *S. aureus* cells that were treated with **3a** showed increased permeability to Propidium Iodide (PI) stain which is impermeable in normal cells with an intact membrane. Loss of membrane integrity was also confirmed in *E. coli* cells using alkaline phosphatase (ALP) assay. ALP is an enzyme that is situated in the periplasmic space of *E. coli* and upon treatment of *E.coli* cells with **3a** there was an increase in the amount of ALP in the medium suggesting membrane integrity loss (Figure 1.9B).

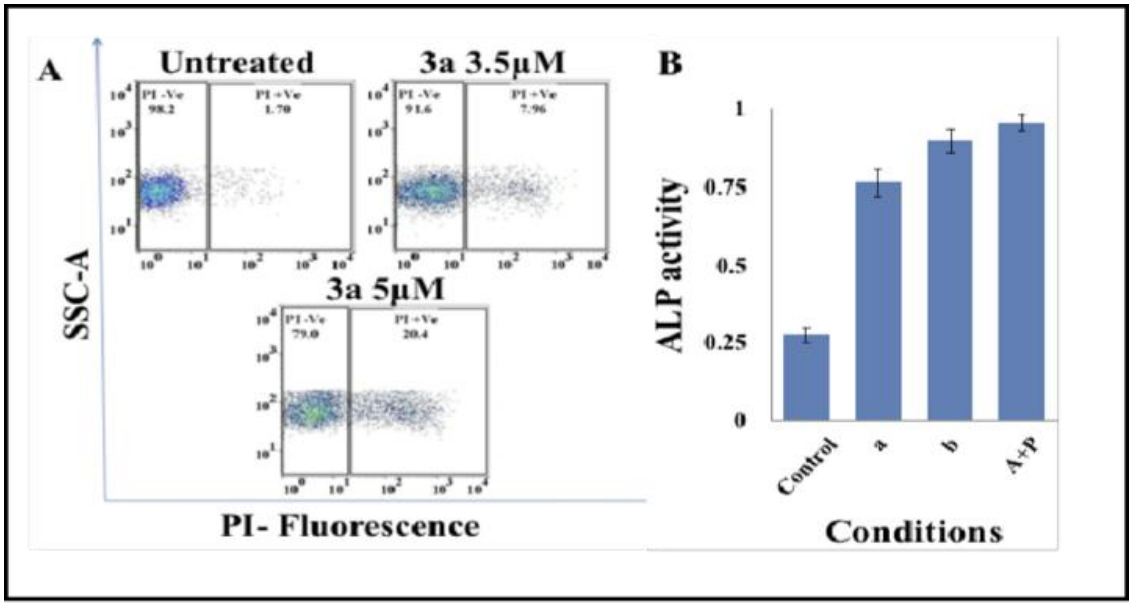

Figure 1.9: (A) Permeability of bacterial cell membrane observed using Flow cytometry after treatment with **3a** (3.5 or 5 µM) or DMSO control and PI (Propidium Iodide) staining. (B) Membrane integrity loss effect after treatment with **3a** detected by extracellular ALP level for both treated and untreated sets. For the positive control purified ALP was taken and for the substrate, p-nitrophenylphosphate (PNPP) was selected.

1.3.9. Disruption of preformed *S. aureus* and *S. epidermidis* biofilms:

Biofilm formation by many bacteria are proving to be the greatest challenges for any antibiotics nowadays and is one of the major cause for the development of antibiotic resistance among a large number of species. Preformed *S. epidermidis* and *S. aureus* biofilms were treated with compound **3a** for 24 hours and stained with crystal violet. It

was observed that **3a** was capable of disrupting both the *S. epidermidis* (Figure 1.10A-10B) and *S. aureus* (Figure 1.10C- 10D) biofilms up to 99% at 4 MIC value of **3a.**

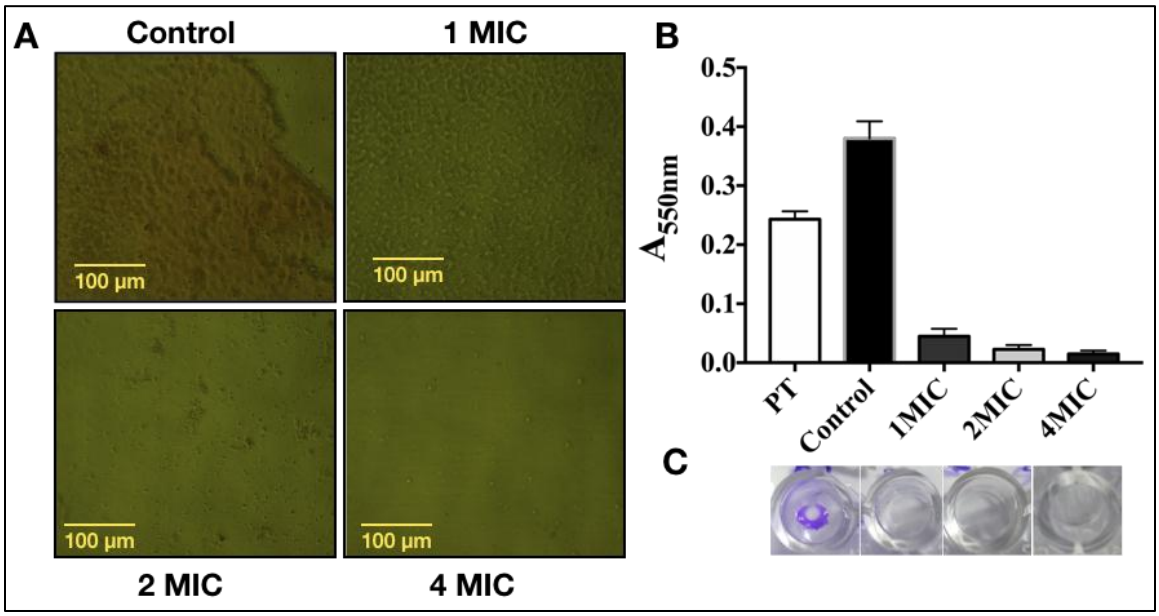

Figure 1.10: Biofilm disruption. (A) Visualization of *S. aureus* biofilm after treatment with **3a** (different concentrations) or untreated with the aid of light microscope. (B) Visualization and quantitative estimation of *S. aureus* biofilm formation with crystal violet stain. (C) Picture of the Biofilm stained with crystal violet.

1.4. CONCLUSION:

The study shows that a group of designed and synthesized monoquinoxaline derivatives was successfully synthesized that alters the native structure of Bacteria and displayed antibacterial properties. One of the most potent among the set was **3a** with a MIC value of 1.8 ± 0.25 µg/mL against *Staphylococcus aureus* bacteria. Biophysical studies using Agarose DNA gel shift assay, Circular Dichroism studies, Flurescence Intercalator displacement assay showed that the compound could intercalate into ds DNA very efficiently and showed GC preference. Atomic force Microscopic studies showed that the change in DNA structure upon treatment with compound **3a** was a local to global event, which ultimately led to condensation of DNA via superstructure formation. Regional condensation of purified *S. aureus*

genomic DNA was observed upon treatment with **3a.** Treatment of *S. aureus* with high doses of **3a** led to the formation of in cell nucleoid condensation as visualized by super resolution confocal microscopy.

When *S. aureus* cells were treated with a sub MIC dose of **3a**, an inhibition of DNA synthesis was observed in cells. Bacterial DNA fragmentation was also observed in**3a** treated *S. aureus* cells when compared to the control population. A change in the morphology of *S. aureus* cells from round to rod like structures was observed at sub MIC doses of **3a** along with disruption of the membrane architecture and loss in membrane permeability. The compound **3a** was also capable of disrupting preformed *S. aureus* biofilms.

Overall this study provides a good platform for the development of new antibacterials that can target the genome architecture by intercalating into DNA and inhibiting factors like the Nucleoid Associated Proteins and other factors that are associated in the maintenance of the bacterial chromosome.

1.5. REFERENCES

136. Blair, J. M., Webber, M. A., Baylay, A. J., Ogbolu, D. O., & Piddock, L. J. (2015). Molecular mechanisms of antibiotic resistance. Nat. Rev. Microbiol, 13(1), 42-51.

137. Thanbichler, M., Wang, S. C., & Shapiro, L. (2005). The bacterial nucleoid: a highly organized and dynamic structure. J. Cell. Biochem, 96(3), 506-521.

138. Dillon, S. C., & Dorman, C. J. (2010). Bacterial nucleoid-associated proteins, nucleoid structure and gene expression. Nat. Rev. Microbiol, 8(3), 185-195.

139. Luijsterburg, M. S., Noom, M. C., Wuite, G. J., & Dame, R. T. (2006). The architectural role of nucleoid-associated proteins in the organization of bacterial chromatin: a molecular perspective. J. Struct. Biol, 156(2), 262-272.

140. Dorman, C. J., & Dorman, M. J. (2016). DNA supercoiling is a fundamental regulatory principle in the control of bacterial gene expression. Biophys. Rev, 8(1), 89-100.

141. Schechter, L. M., Jain, S., Akbar, S., & Lee, C. A. (2003). The small nucleoid-binding proteins H-NS, HU, and Fis affect hilA expression in Salmonella enterica serovar Typhimurium. Infect. Immun, 71(9), 5432-5435.

142. Bahloul, A., Boubrik, F., & Rouviere-Yaniv, J. (2001). Roles of Escherichia coli histone-like protein HU in DNA replication: HU-beta suppresses the thermosensitivity of dnaA46ts. Biochimie, 83(2), 219-229.

143. Lee, J. S., & Waring, M. J. (1978). Bifunctional intercalation and sequence specificity in the binding of quinomycin and triostin antibiotics to deoxyribonucleic acid. Biochem. J, 173(1), 115-128.

144. Waring, M. J., Ben-Hadda, T., Kotchevar, A. T., Ramdani, A., Touzani, R., Elkadiri, S., ... & Ellis, T. (2002). 2, 3-Bifunctionalized quinoxalines: synthesis, DNA interactions and evaluation of anticancer, anti-tuberculosis and antifungal activity. Molecules, 7(8), 641-656.

145. Bailly, C., & Waring, J. M. (1998). DNA recognition by quinoxaline antibiotics: use of base-modified DNA molecules to investigate determinants of sequence-specific binding of triostin A and TANDEM. Biochem. J, 330(1), 81-87.

146. Tariq, S., Somakala, K., & Amir, M. (2018). Quinoxaline: An insight into the recent pharmacological advances. Eur. J. Med. Chem., 143, 542-557.

147. Seitz, L. E., Suling, W. J., & Reynolds, R. C. (2002). Synthesis and antimycobacterial activity of pyrazine and quinoxaline derivatives. J. Med. Chem, 45(25), 5604-5606.

148. Xu, F., Cheng, G., Hao, H., Wang, Y., Wang, X., Chen, D., ... & Dai, M. (2016). Mechanisms of Antibacterial Action of Quinoxaline 1, 4-di-N-oxides against Clostridium perfringens and Brachyspira hyodysenteriae. Front. Microbiol., 7, 1948.

149. Carta, A., Corona, P., & Loriga, M. (2005). Quinoxaline 1, 4-dioxide: a versatile scaffold endowed with manifold activities. Curr. Med. Chem, 12(19), 2259-2272.

150. Wilhelmsson, L. M., Kingi, N., & Bergman, J. (2008). Interactions of antiviral indolo [2, 3-b] quinoxaline derivatives with DNA. J. Med. Chem, 51(24), 7744-7750.

151. Zegar, I., Gräslund, A., Bergman, J., Eriksson, M., & Nordén, B. (1989). Interaction of ellipticine and an indolo [2, 3b]-quinoxaline derivative with DNA and synthetic polynucleotides. Chem. Biol. Interact, 72(3), 277-293.

152. Mahata, T., Kanungo, A., Ganguly, S., Modugula, E. K., Choudhury, S., Pal, S. K., ... & Dutta, S. (2016). The Benzyl Moiety in a Quinoxaline-Based Scaffold Acts as a DNA Intercalation Switch. Angew. Chem. Int, 55(27), 7733-7736.

153. Mahata, T., Chakraborty, J., Kanungo, A., Patra, D., Basu, G., & Dutta, S. (2018). Intercalator-induced DNA superstructure formation: doxorubicin and a synthetic quinoxaline derivative. Biochem, 57(38), 5557-5563.

154. Wayne, P. (2006). Clinical and Laboratory Standarts Institute: methods for dilution antimicrobial susceptibility tests for bacteria that grow aerobically. Approved Standart M7-A7, CLSI, USA.

155. Dwyer, D. J., Camacho, D. M., Kohanski, M. A., Callura, J. M., & Collins, J. J. (2012). Antibiotic-induced bacterial cell death exhibits physiological and biochemical hallmarks of apoptosis. Mol cell., 46(5), 561-572.

156. Fernández, J. L., Cartelle, M., Muriel, L., Santiso, R., Tamayo, M., Goyanes, V., ... & Bou, G. (2008). DNA fragmentation in microorganisms assessed in situ. Appl. Environ. Microbiol, 74(19), 5925-5933.

157. Mulvey, M. A., Lopez-Boado, Y. S., Wilson, C. L., Roth, R., Parks, W. C., Heuser, J., & Hultgren, S. J. (1998). Induction and evasion of host defenses by type 1-piliated uropathogenic Escherichia coli. Science, 282(5393), 1494-1497.

158. Justice, S. S., Hung, C., Theriot, J. A., Fletcher, D. A., Anderson, G. G., Footer, M. J., & Hultgren, S. J. (2004). Differentiation and developmental pathways of uropathogenic Escherichia coli in urinary tract pathogenesis. Proceedings of the National Academy of Sciences, 101(5), 1333-1338.

159. Foxman, B. (2002). Epidemiology of urinary tract infections: incidence, morbidity, and economic costs. Am. J. Med., 113(1), 5-13.

Chapter 2

Designed quinoxaline small molecules lead to HCV IRES mediated translation and replication inhibition by virtue of base destacking at the subdomain IIa.

2.1. INTRODUCTION

2.1A PART A

HCV (Hepatitis C Virus) infection has been a prime liver disease in the past and continues to be so in the present, which is why it is a global health concern. The Physiopathological symptoms associated are liver failure, liver cirrhosis, and ultimately hepatocellular carcinoma.[160] HCV is a part of the Flaviviridae family and has single-stranded positively sensed RNA genome.[161-162] The global prevalence of HCV is estimated at around 177.5 million where the HCV genotype 1 is the most prevalent worldwide.[163] The 9.6 kb HCV RNA genome comprises of three structural parts C (Core) and Envelope E1, E2, and different nonstructural part NS2, NS3, NS4A, NS4B, NS5A, and NS5B given in Figure 1. The structured 5'-UTR (5'-untranslated region) of HCV-IRES (Hepatitis C Virus-Internal Ribosome Entry Site) RNA comprise of 341 nucleotides and has a crucial role in ribosome loading and translation initiation process by a cap-independent translation that is distinct from the canonical cap-dependent process of translation.[164-166] Subdomain IIa in the 5'-UTR has a conserved L-shaped structure and is an attractive antiviral target.[167] The HCV IRES RNA folding is principally guided by metal ions like Mg2+ and Mn2+ and has important implications in viral translation and replication processes inside the host cell.[168-169] Stacking of the RNA bases is also extremely crucial for its RNA folding process that helps in maintaining its secondary and tertiary structure during viral translation as well as replication.[170-172] Hence small molecules that can target the subdomain IIa of HCV RNA can provide a good antiviral alternative to existing drugs in treating Hepatitis C. Several quinoxaline antibiotics were developed and synthesized in our lab based on the structure of Benzimidazole, a potent inhibitor of HCV IRES subdomain IIa.[170] The molecules were screened based on their viral translational inhibition potential using a Dual-Luciferase based activation retention approach. Among many potential candidates **4d** was the most potent candidate and thus was subjected to further biophysical studies like Circular Dichroism to determine their type of interaction with the HCV domain IIa. Docking and Molecular Dynamic simulation studies further supported that **4d** binds in the loop of the subdomain IIa and

competes with mg2+ ions for their binding site. At higher concentrations of **4d**, the RNA base stacking and RNA structure are completely disrupted which leads to a reduction in viral translation and replication by several folds. CD and Molecular dynamics studies showed that **4d** is bound to a region, which is similar to the $MgCl_2$ binding site and disrupts the base stacking interaction in the L-shaped loop of the subdomain IIa. Mutational studies using an A57U (Adenine at the 57^{th} position interacts with $MgCl_2$ and helps in stabilizing the base stacking interaction in the L-shaped structure) mutant lead to abolishment in the activity of **4d.** The compound **4d** donot interact with ds DNA and have intermediate cell cytotoxicity against HEK 293 and Huh 7 cells.

2.1B PART B:

In the second part of the project quinoxaline, small molecules targeting HCV IRES were designed by our lab by several modifications like replacing the *N,N*-dimethyl propyl amine tail part from the molecule N^2-benzyl-N^3-(3-(dimethylamino)propyl)-6-nitroquinoxaline-2,3-diamine (Figure) with various cyclic rings and tails to avoid DNA intercalation and to reduce cytotoxicity. All the molecules were screened using Dual-Luciferase assay. The most active compound was found to be compound **25**. The molecule was further subjected to circular dichroism studies against IRES subdomain IIa and also CT DNA to study their specificity towards the HCV IRES RNA. Finally, the cytotoxicity of all molecules was checked using MTT assay in HuH 7 and Hek 293 cells.

2.2. MATERIAL AND METHODS:

2.2.1. Design and Synthesis:

The molecules were synthesized by Ajay Kanungo, Dipendu Patro, Ritesh Pal, and Bhim Majhi from our lab.

2.2.2. Cell culture:

Huh 7 cells (Hepatocellular carcinoma) were provided by Dr. Suvendranath Bhattacharyya lab. The adherent cells were maintained using DMEM (Dulbecco's Modified Eagle's medium) with 10% Fetal Bovine Serum, Sodium Pyruvate, L-Glutamine, and 1X Penicillin-Streptomycin and maintained in a humidified CO_2 incubator at 37ºC.

2.2.3. Dual Luciferase Assay

Huh 7 cells in DMEM medium and 10% FBS were added to 24 well plates, kept in a CO_2 incubator at 37°C overnight. Cells reaching around 70% confluency were transfected using a bicistronic HCV plasmid containing the HCV IRES with Lipofectamine 2000 following standard procedure for 4-5 hours in the CO_2 incubator. After 4 hours, Complete DMEM media was added to the cells after removal of the Transfecting medium and kept overnight for cells to recover and amplify the plasmid. Cells were then treated with compounds and further incubated for 24 hours after which they are washed and lysed using PBS and Passive Lysis buffer, respectively.

Luciferase activity was estimated using Promega Glomax Luminometer and plot with Graphpad Prism 7.

2.2.4. Mutational Studies

For the mutational study QuikChange II Site-directed Mutagenesis kit from Agilent was used. The Primers used to make the A57U mutation were: 5’CCCCTGTGAGGAACTTCTGTCTTCACGCAGA-3' (sense primer) and 5'-TCTGCGTGAAGACAGAAGTTCCTCACAGGGG-3' (antisense primer). Any mutation was confirmed by DNA sequencing. They were further studied using dual-luciferase based assay.

2.2.5. HCV Replication Inhibition

The replication inhibition study was accomplished with Huh7 cells carrying the sub-genomic replicon RNA of HCV (HCV-replicon cell line). The replicon HUH7 cells were subjected to the compound/DMSO for 5h in a CO_2 incubator. Cells were washed with PBS and a fresh medium was added and kept for 48h. Cells were lysed using Tri Reagent to collect the total RNA. Change in HCV RNA level was recorded with RT-qPCR where GAPDH acted as an internal control.

2.2.6. Annealing of HCV Domain IIa

RNA sequence (5' – GCGUGUCGUGCAGCCUCCGG – 3' and 5' – CGGAGGAACUACUGUCUUCACGCC –3') was ordered from Integrated DNA Technologies (IDT). Equal amounts of both oligos were mixed in Hepes buffer, warmed up to 91°C for 4-5 minutes, and cooled slowly for the RNA oligo to anneal with one another. Annealed RNA was then quantified with a spectrophotometer and stored at -80°C for further use.

2.2.7. Circular Dichroism

Jasco 814 CD Spectrometer was used for the CD measurement studies. 10 mM NaP buffer containing 1% DMSO and $MgCl_2$ was used for the titration studies. An increasing concentration of compounds was added to the annealed HCV IIa RNA oligo and measured. All data were analyzed with Graphpad Prism 7.

2.2.8. Cytotoxicity assay

Hek293 and Huh7 cells were plated in 96 well plates in complete DMEM and kept in a CO_2 incubator overnight. Cells were treated with compounds and kept in the incubator for 24 hours. After the treatment with MTT, cells were kept for 2-3 hours. DMSO was added to each well after discarding the media and kept in dark at room temperature for 20 mins. A multiplate reader was used to analyze the data. Absorbance was recorded at 595 nm.

2.2.9. DNA Gel-shift assay:

For the gel-shift assay, pBR 322 plasmid DNA was purchased from Thermofisher Scientific (Cat No- SD0041). A buffer containing NaP (50mM ph 7), 10mM NaCl, and 40 μM DNA was used for the experiment. The pBR 322 DNA was subjected to increasing concentrations compound concentration (measured as a compound

concentration:DNA base pair ratio) kept at 37°C for 16 hours. The specimen were run in 1% Agarose gel for 2-3 hours at constant voltage of 50 V and stained with EtBr (0.5-1 μg/mL) at room temperature. The gels were visualized in a Biorad ChemiDoc MP Imaging System and the result was analyzed using Image Lab software.

2.2.10. Molecular docking simulations:

Molecular docking and simulations were performed by Krishna Kumar at CSIR-IICB TRUE Campus. The crystal structure of the IRES domain of HCV (PDB ID: 2NOK) [169] was taken from PDB [172]. Protein preparation wizard of Schrodinger suite [173] was used to assemble the receptor. Using Ligprep wizard [174] of Schrodinger suite the ligands were prepared which generates energy-minimized structures with different ionization states, stereochemistries, ring conformations and tautomers. Using rDock [175-176] docking tool docking was performed. During docking to get distinct docking solutions the receptor kept rigid and all ligands were flexible. For the improvement of each docking pose, Post-docking minimization was performed. Using rDock score best-docked poses were ranked and the best docking pose was chosen.

2.2.11. Molecular dynamics simulations:

Molecular dynamic simulations were performed by Krishna Kumar at CSIR-IICB TRUE Campus. To understand the change in the HCV IRES domain IIa structure by compound **4d**, MD simulations were performed using the receptor-ligand complex obtained from docking analysis. Using GROMACSv4.5.3 simulation package the MD simulation was performed.[177] The topology and coordinates of receptor was generated with Amberff99bsc0χ0L3 force field.[178] A simulation cubic box was defined by filling with TIP3P-water molecules.[179] Receptor-ligand complex was kept at 1.0 nm away from the box edge and Na^+ was added to neutralize the system. Equilibration of sample was done under unchanged particle number, volume and temperature (NVT) and unchanged particle number, pressure and temperature (NPT) conditions at 300K temperature with pressure of 1 atm using Berendsen temperature coupling method [180] and Parrinello-

Rahman barostat method.[181] The final runs were performed under NPT conditions at 300K for 30 ns and 1 atm pressure. The leapfrog algorithm [182] was used during production run for integrating the Newton's equations of motion. By the Particle-Mesh Ewald (PME) algorithm [183], the long-range electrostatics was calculated. To contrain the length of the bonds, LINCS (LINear Contrainst Solver) [184] algorithm was used. The trajectories and coordinates of atoms were recorded every 0.002 ps. After MD simulation completion, *g_dist* utility of GROMACS package was used to calculate the distance between the terminal bases.

2.3A. RESULTS AND DISCUSSION:

2.3A.1. Design and Sythesis of the monoquinoxaline derivatives:

The monoquinoxaline derivatives targeting IRES domain IIa RNA were designed from the crystal structure of the complex between benzimidazole and subdomain IIa RNA (Figure 2.2B). From the structure it was hypothesized that the RNA bases will form stacking interaction with the quinoxaline part, the guanine residues in IRES will form hoogsteen pairing with the nitrogen atoms of the quinoxaline core and the RNA Phosphate backbone will interact with the protonated N,N-dimethylaminopropylamine chain thus the molecule should have an increased affinity for the IRES RNA subdomain IIa (Figure 2.2D). To achieve the above objectives the substituents at the C2, C3 and the C6 positions of the quinoxaline core were varied (Figure 2.2E).

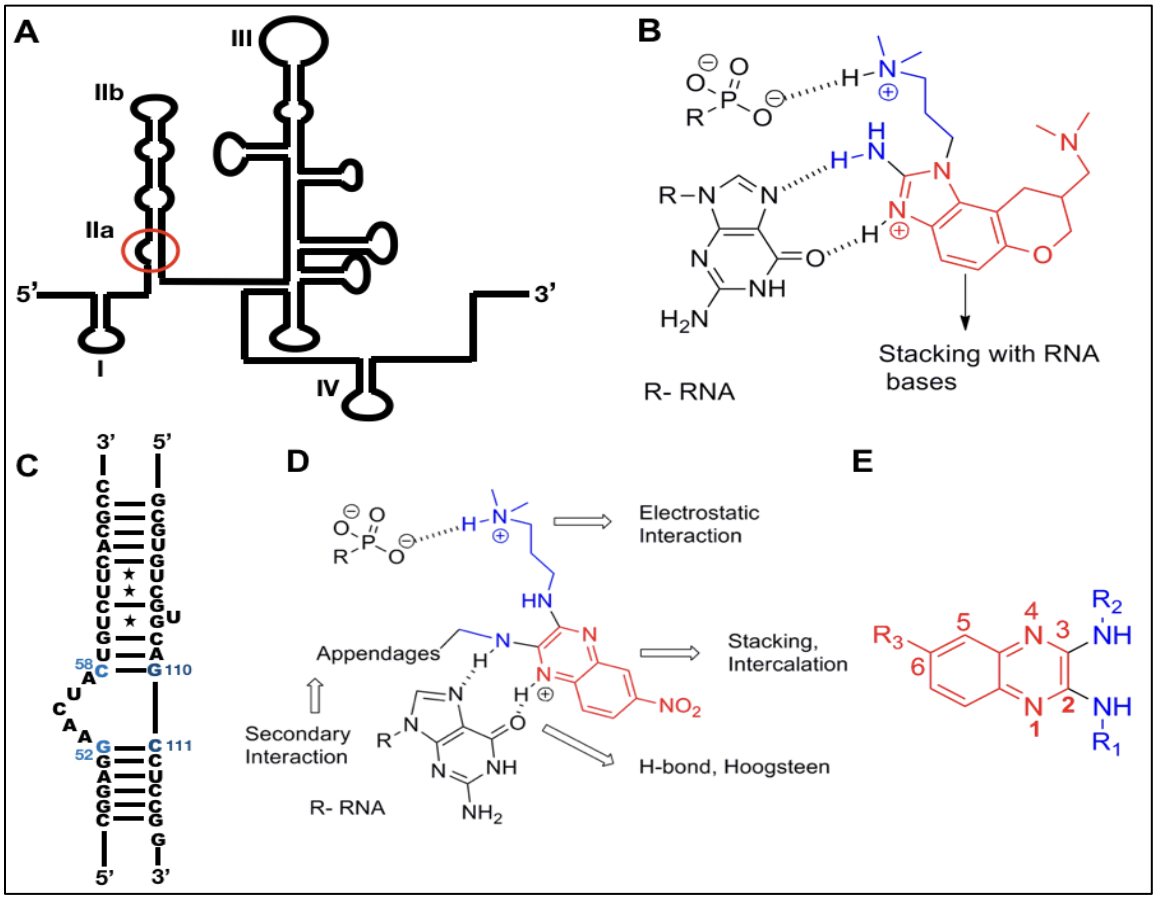

Figure 2.2: A) HCV IRES secondary structure. B) Benzimidazole-HCV IRES inhibitor complex. C) HCV IRES subdomain IIa sequence. D) Proposed interaction between HCV IRES subdomain IIa and designed monoquinoxaline compounds. E) Different substitution positions in the monoquinoxaline scaffold.

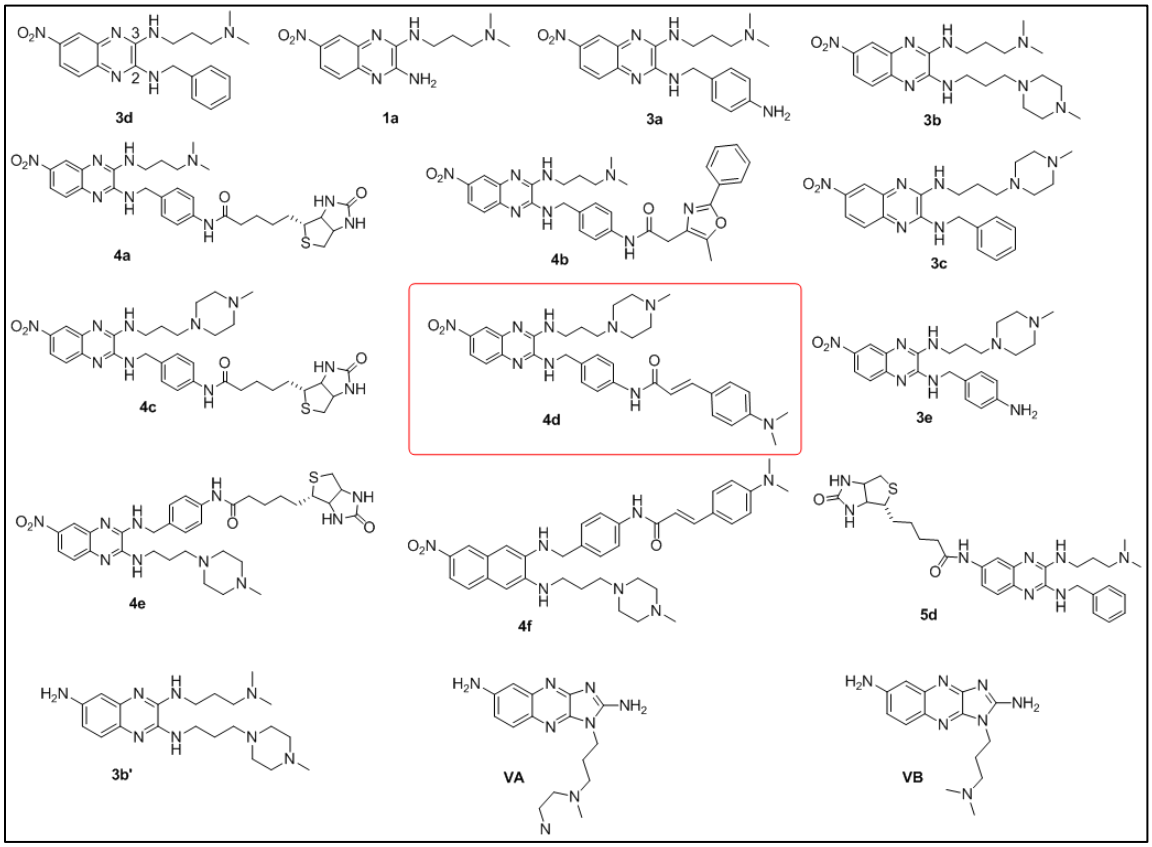

Figure 2.3: Structures of monoquinoxaline derivatives used in the study.

2.3A.2. <u>Dual Luciferase Assay:</u>

The potential to inhibit IRES-mediated translation of the designed quinoxaline small molecules was studied using Dual-Luciferase reporter-based studies. In the assay, a bicistronic reporter plasmid containing the Firefly Luciferase gene under HCV IRES control and the renilla luciferase gene (Internal Control) under the Cap promoter was taken (Figure 2.4). The Ratio of Fluc by Rluc of the compound treated was compared with the untreated. The relative percent luciferase activity was taken keeping the control as 100%. From the luciferase assay, some molecules showed promising results from which the most potent molecule was found to be was **4d**($EC_{50} \approx 7$ μM). (Figure 2.5) Results suggest that the molecules can inhibit translation by HCV IRES in Huh 7 cells.

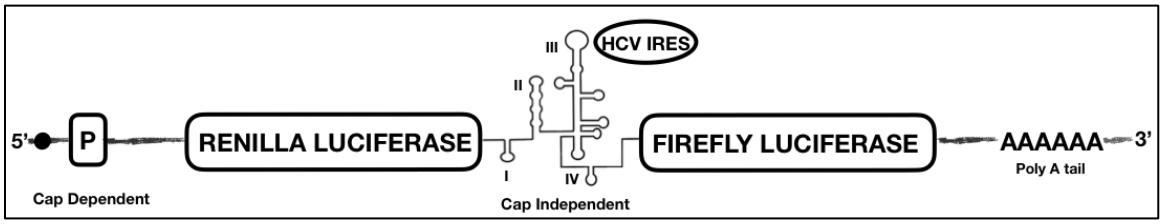

Figure 2.4: Plasmid DNA construct for Dual Luciferase assay.

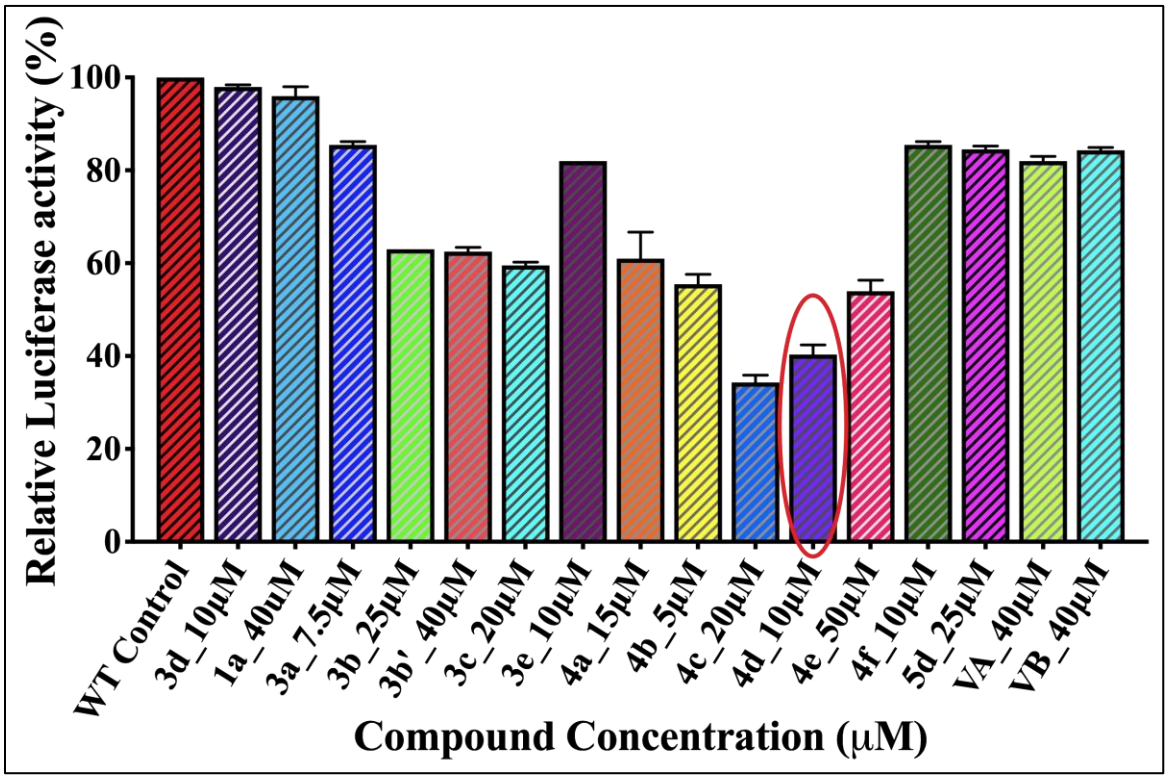

Figure 2.5: Translational Inhibition of HCV IRES by dual luciferase assay for all compounds used for the study.

2.3A.3. <u>Circular Dichroism Studies of the IRES subdomain IIa upon treatment with 4a:</u>

The HCV IRES RNA can take up many complex secondary and tertiary structures, which are mainly guided by divalent metal ions like Mg2+ and Mn2+. The structural change of any nucleic acids can be probed using Circular Dichroism spectroscopy [185-187]. Folded IRES RNA shows a characteristic positive ellipticity peak at around 262 nm and a negative ellipticity peak at around 215 nm indicative of the A form of RNA, the more predominant form of RNA present in nature [188-189]. The subdomain IIa of HCV IRES

undergoes an increase in ellipticity peak at 262 nm upon titration with an increasing concentration of $MgCl_2$ that indicates an enhancement in base stacking interaction in the L-shaped loop of subdomain IIa (Figure 2.6A) that was also supported by MD Studies (Figure 2.7). Upon treatment of this subdomain IIa with the compound **4d**, there was a significant reduction in ellipticity at ≈ 262 nm suggesting **4d** disrupts the base stacking interaction in the RNA thereby reducing the influence of HCV IRES subdomain IIa driven translation initiation in Huh 7 cells as observed from circular dichroism studies (Figure 2.6C) and Molecular simulation studies (Figure 2.8). When **4d** treated IRES was titrated with increasing concentration of $MgCl_2$ in reverse titration experiment, there was a recovery in ellipticity peak at around 262 nm suggesting **4d** was dislodged from the RNA since $Mg2^+$ competes with **4d** for the binding site at the subdomain IIa (Figure 2.6E). At a higher concentration of **4d** there was a significant base unstacking and collapsing of the subdomain IIa structure that could not be recovered upon titration with $MgCl_2$ (Figure 2.6F). The CD titration experiments of the other potent molecules are represented in Figure 2.7.

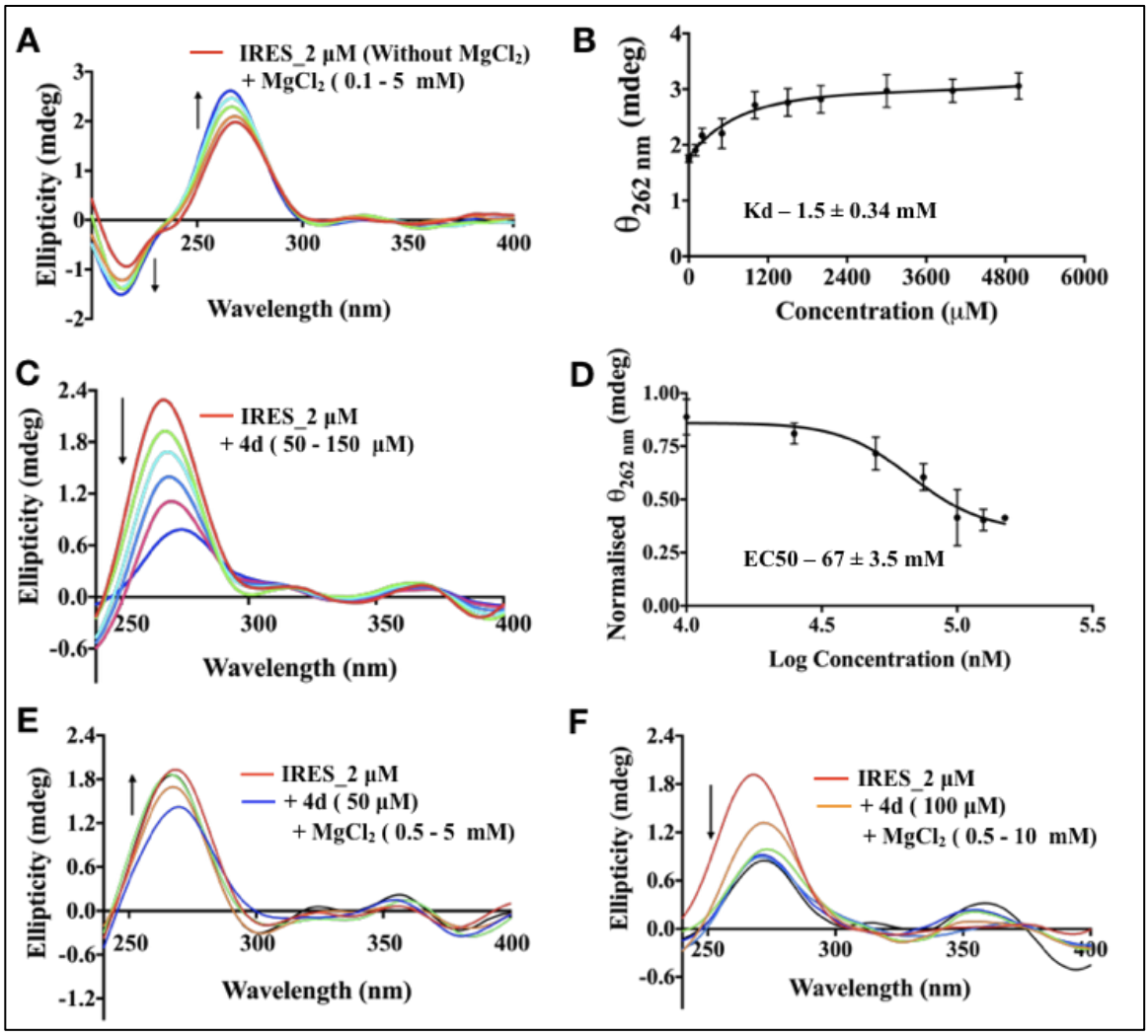

Figure 2.6: A) Circular dicroism (CD) spectra of $MgCl_2$ titrated (100µM – 5mM) HCV IRES subdomain IIa. **B)** Ellipticity plots at 262 nm for MgCl2 titrated (100µM – 5mM) HCV IRES subdomain IIa. **C)** CD spectra of **4d** treated (50 – 150 µM) HCV IRES IIa. **D)** Ellipticity plot at 262 nm for **4d** treated (50 – 150) HCV IRES IIa. **E)** CD spectra of **4d** treated (50 µM) HCV IRES IIa titrated using $MgCl_2$ (0.5 – 5mM). **F)** CD spectra of **4d** treated (100 µM) HCV IRES IIa titrated with $MgCl_2$ (0.5 – 5mM).

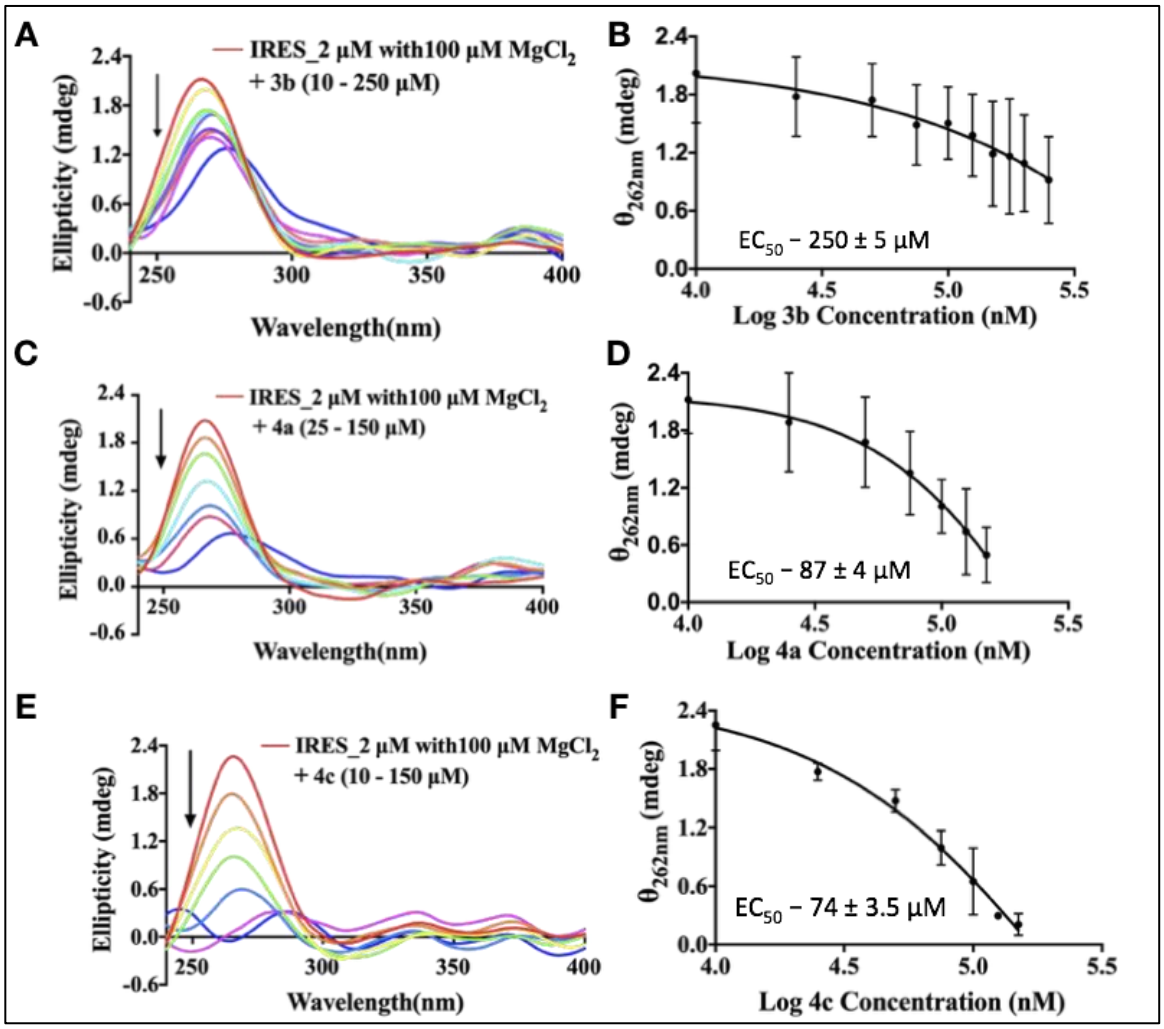

Figure 2.7: A) CD spectra of **3b** titrated (10-250) HCV IRES IIa. **B)** Ellipticity plot at 262 nm for **3b** titrated (50 – 150) HCV IRES IIa. **C)** CD spectra of **4a** titrated (25-150) HCV IRES IIa. **D)** Ellipticity plot at 262 nm for **4a** titrated (25 – 150) HCV IRES IIa. **E)** CD spectra of **4c** titrated (25-150) HCV IRES IIa. **F)** Ellipticity plot at 262 nm for **4a** titrated (10 – 150) HCV IRES IIa.

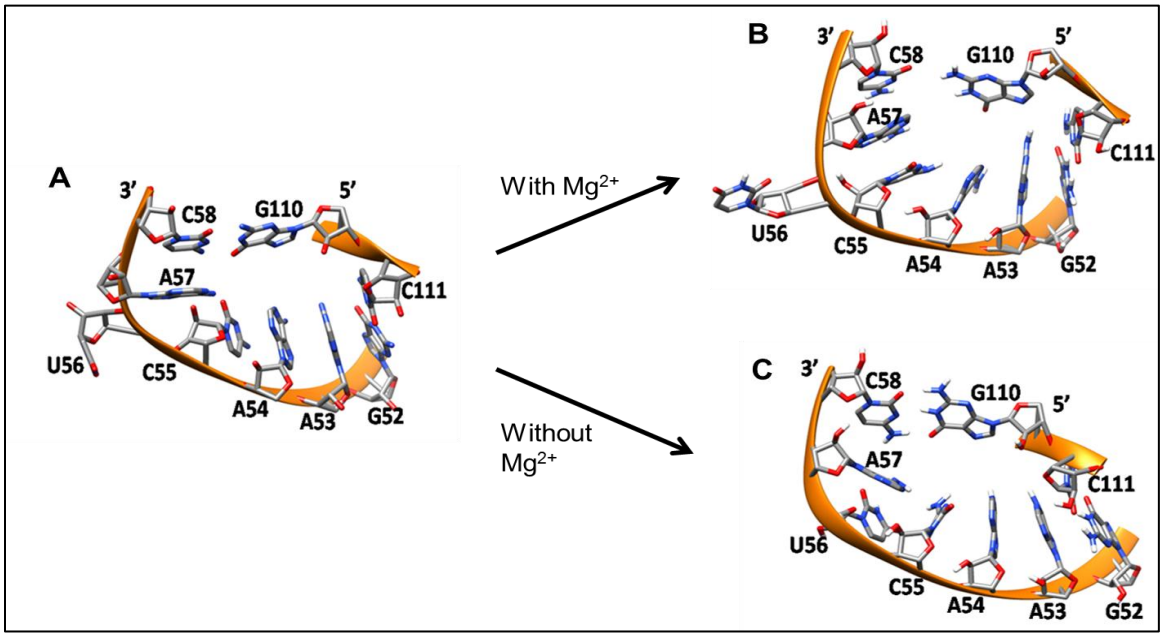

Figure 2.8: A) Base stacking interaction of IRES IIa in absence of Mg^{2+} ions pre-stimulation. **B)** Base stacking interaction of subdomain IIa in presence of Mg^{2+} ions post-stimulation (50 nano seconds). **C)** Base stacking interaction of IIa in Mg^{2+} ions absence post-stimulation (50 nano seconds).

2.3A.4. <u>HCV Replicon study:</u>

The subdomain IIa is an important player in regulating the HCV viral RNA replication [171]. The 125 nucleotides encompassing the subdomain 1 and 2 of IRES are crucial for the replication of the HCV RNA genome.[190] The HCV replication inhibition potential of the compound **4d** was therefore studied using genotype-IIa of HCV monocistronic replicon in Huh 7 cells. HCV RNA levels of treated and untreated Huh 7 cells carrying the replicon plasmid were measured to inquire the replication efficiency of the viral RNA in presence of **4d**. Using HCV RNA fold change plots it was found that **4d** could indeed reduce the production of viral replicon RNA in Huh 7 cells (Figure 2.9). This work was done in collaboration with Prof. Soumitra Das.

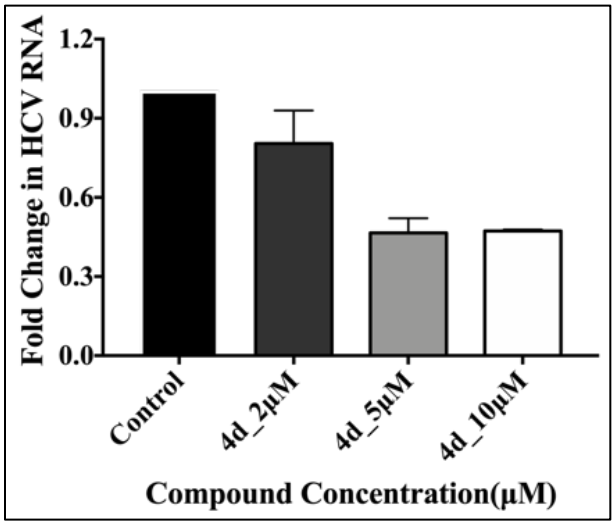

Figure 2.9: Fold change in the replication of HCV upon treatment with **4d** using an HCV replicon plasmid in Huh 7 cells.

2.3A.5. <u>Molecular docking and simulations:</u>

Molecular docking and simulation were performed from the available HCV IRES crystal structure (PDB ID: 2NOK) using various bioinformatics tools. Molecular dynamics simulations were used to understand the **4d** mediated HCV IRES subdomain IIa structural change. The docking of the most potent compounds like **4d**, **4a,** and the control compound Benzimidazole were performed with the IRES RNA IIa L-shaped structure in order to recognize their binding sites in the subdomain IIa RNA. MD simulations were further performed using the best-docked complexes. A gradual increase up to 11Å was observed within the terminus residues of the IRES RNA-**4d** docked structure similar to the one observed for Benzimidazole (8Å) suggesting that **4d** can also alter the secondary structure of subdomain IIa.

This work was done by Krishna Kumar under the supervision of Dr. Saikat Chakrabarti.

2.3A.6. **Mutational Studies:**

The sequence specificity of the most active HCV IRES translation inhibitor was performed using site-directed mutagenesis experiments. The residue Adenine 57 in subdomain IIa is vital in maintaining the HCV IRES L-shaped structure in presence of Mg^{2+}. Since the compound **4d** competes with Mg^{2+} for the binding site in the subdomain IIa we tried to decipher the effect of **4d** on an A57U mutated form of the IRES where the Adenine at the 57^{th} position is replaced by Uracil. The mutated IRES were confirmed using sequencing studies. This work was done together with Dr. Tridib Mahata (**THESIS ID- CUE-A15792-T11942**).

Translational studies using dual luciferase-based assay with the Wild Type and A57U mutated IRES showed that there was a reduction in the HCV driven IRES translation for both the wild type and A57U mutants when treated with other active compounds like **3d**, **4e**, **4f,** etc. (Figure 2.10A) but the translation inhibition potential of **4d** was lost in case of A57U mutant (Figure 2.11B) and remain active against the wild Type IRES (Figure 2.11A).

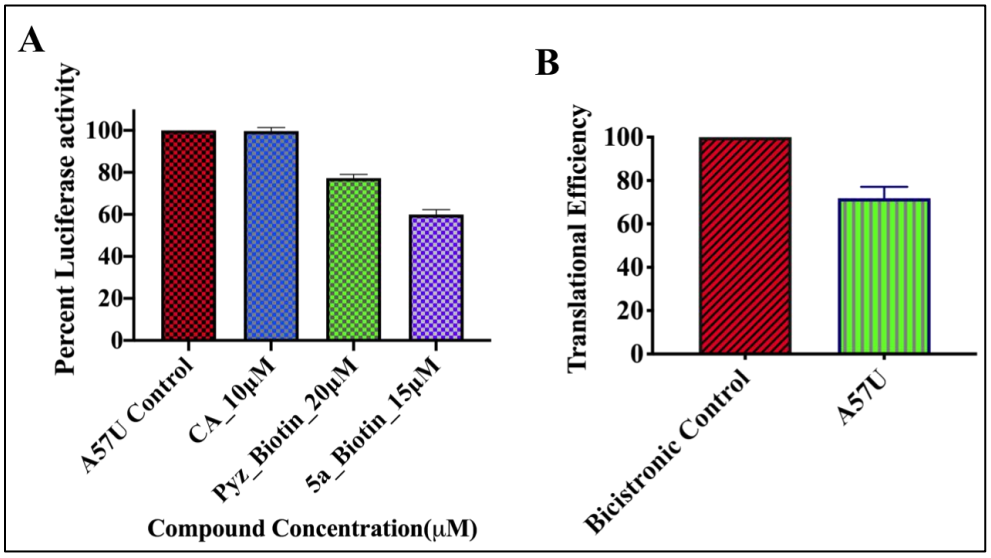

Figure 2.10: A) Dual-luciferase assay of A57U mutated plasmid DNA with compounds **4d**(CA), **4c**(Pyz Biotin) and, **4a**(5a_biotin). **B)** Translational efficiency comparison between Wild Type IRES and A57U mutated IRES**.**

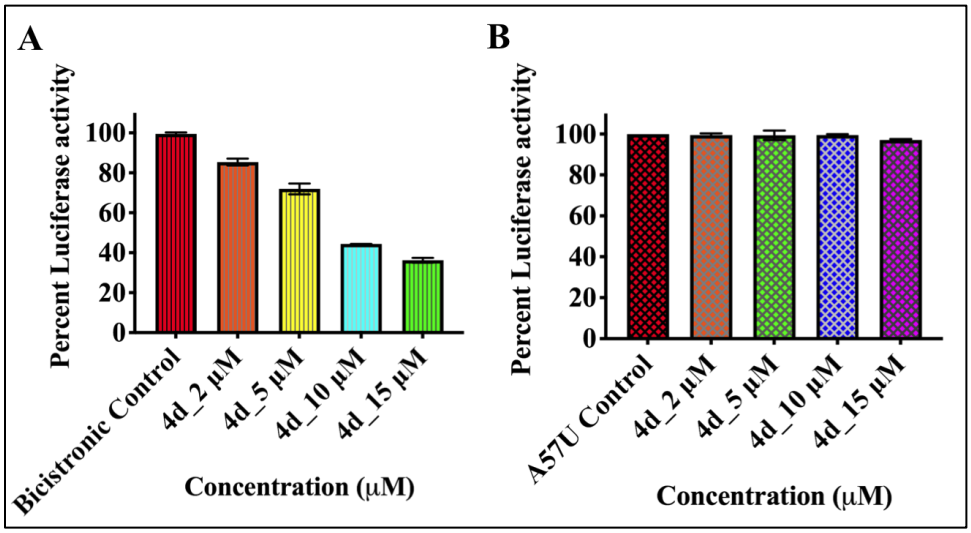

Figure 2.11: A) Dose-dependent dual luciferase assay of **4d** on wild type IRES bicistronic plasmid. **B)** Dual-luciferase assay of **4d** (dose dependent) on A57U mutated IRES bicistronic plasmid.

Circular dichroism studies with wild type subdomain IIa and A57U mutated subdomain IIa also showed that there was a reduction in the ellipticity at 265 nm for A57U mutated IRES when titrated with $MgCl_2$ in comparison to the wildtype IRES (Figure 2.12) suggesting the importance of the Adenine (57) base in maintaining the base stacking interaction of the IRES by interacting with Mg^{2+} ions.

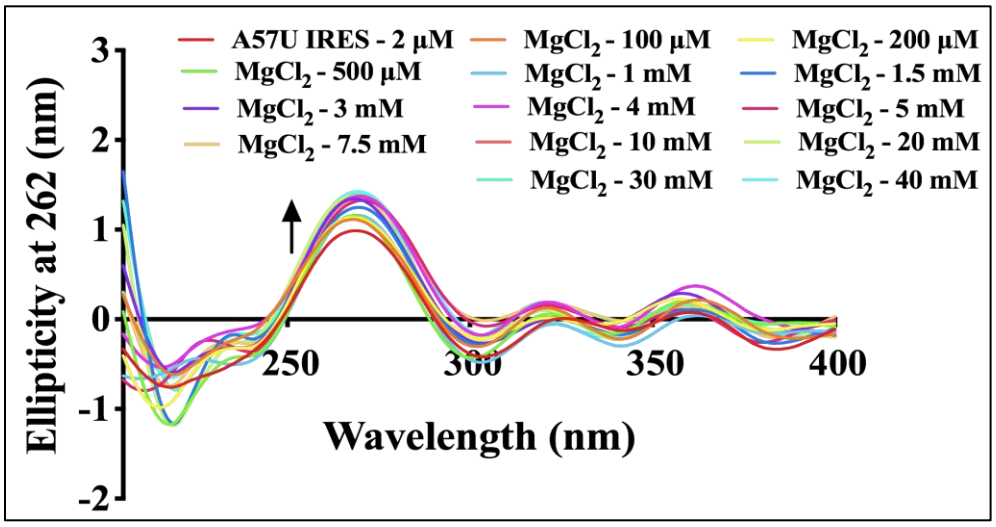

Figure 2.12: A) Circular dichroism (CD) spectra of $MgCl_2$ titrated (100µM – 40mM) A57U mutated HCV IRES subdomain IIa RNA.

2.3A.7. DNA intercalation experiments:

DNA intercalation studies like DNA Gel shift assay was carried out to investigate the effect of the most potent IRES binders on DNA. This is important since the IRES binder must have minimal off-target effects otherwise they would be highly toxic to cells which would significantly reduce their therapeutic potential as an antiviral compound. PBR 322 plasmid DNA was used for the gel shift studies. Different PBR 322: IRES binder ratios were used to study the effect of the compounds on the plasmid DNA. It was observed that the compounds did not intercalate to the ds DNA even at high molecule: PBR 322 DNA ratios (Figure 2.13) suggesting the molecules show specificity towards the HCV IRES subdomain IIa RNA.

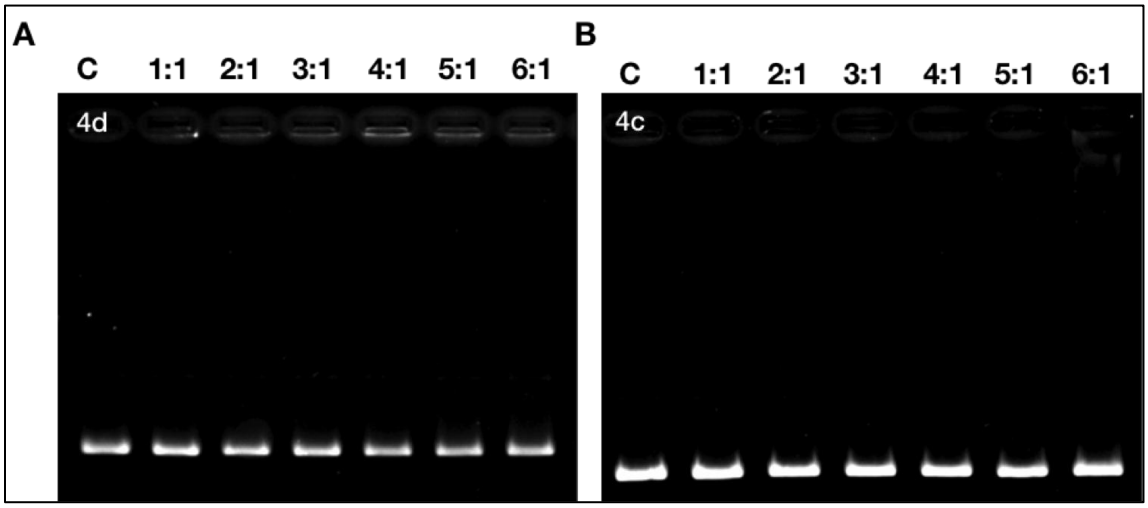

Figure 2.13: PBR 322-plasmid DNA Gel shift assay upon treatment with 4d(A) and 4c(B).

2.3A.8. Cytotoxicity studies using MTT assay:

Cell cytotoxicity studies were performed using both Hek 293 (Figure 2.14) and Huh 7 cells (Figure 2.15) using MTT assay following the standard protocol mentioned under material and methods. Different compounds showed different cell cytotoxicity in Hek 293 and Huh 7 cells. The dual luciferase assay was performed based on the cytotoxicity results of individual compounds where the compound dosage for the dual-luciferase assay was kept at a much lower concentration than their respective CC_{50} values so as to minimalize any cytotoxic effect of the compounds on the translational inhibition efficiency.

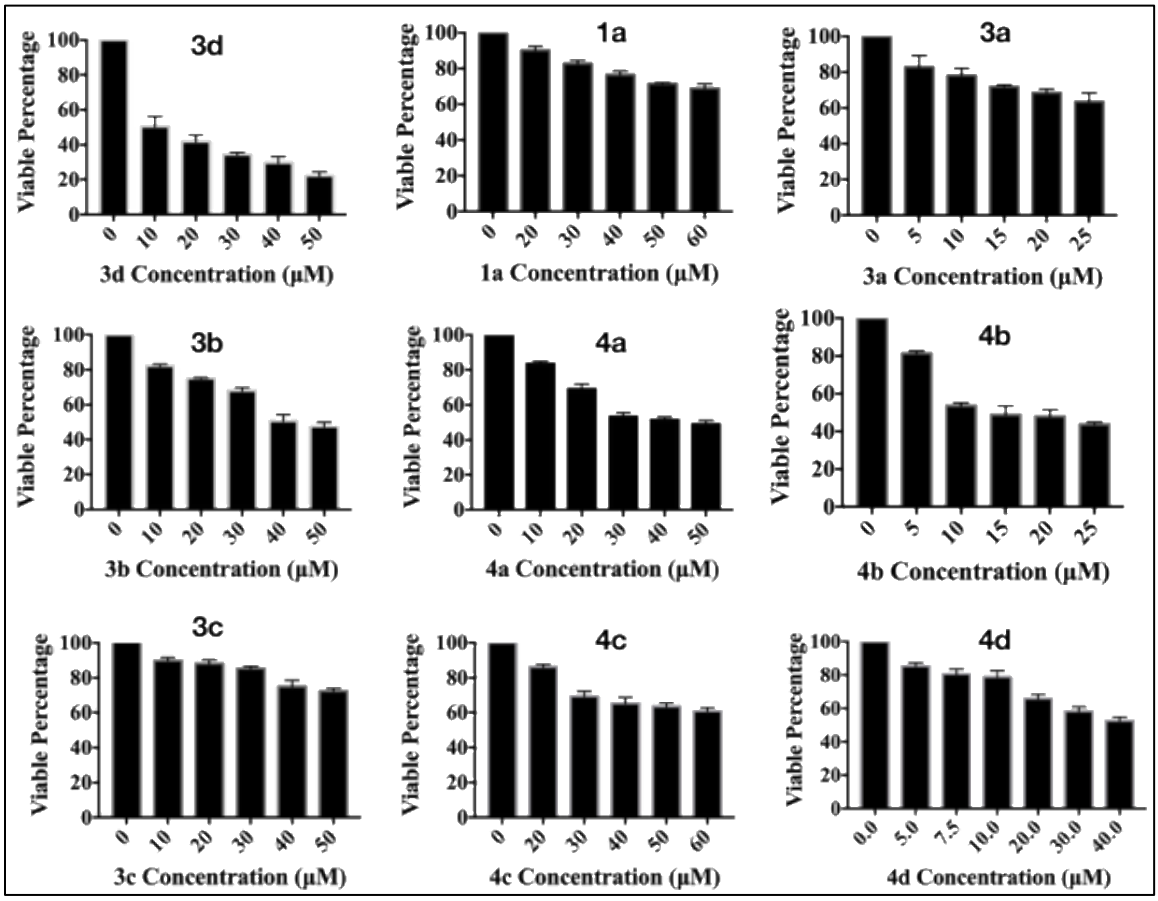
3d
Viable Percentage
100
80
60
40
20
0
0 10 20 30 40 50
3d Concentration (μM)
1a
Viable Percentage
100
80
60
40
20
0
0 20 30 40 50 60
1a Concentration (μM)
3a
Viable Percentage
100
80
60
40
20
0
0 5 10 15 20 25
3a Concentration (μM)
3b
Viable Percentage
100
80
60
40
20
0
0 10 20 30 40 50
3b Concentration (μM)
4a
Viable Percentage
100
80
60
40
20
0
0 10 20 30 40 50
4a Concentration (μM)
4b
Viable Percentage
100
80
60
40
20
0
0 5 10 15 20 25
4b Concentration (μM)
3c
Viable Percentage
100
80
60
40
20
0
0 10 20 30 40 50
3c Concentration (μM)
4c
Viable Percentage
100
80
60
40
20
0
0 20 30 40 50 60
4c Concentration (μM)
4d
Viable Percentage
100
80
60
40
20
0
0.0 5.0 7.5 10.0 20.0 30.0 40.0
4d Concentration (μM)

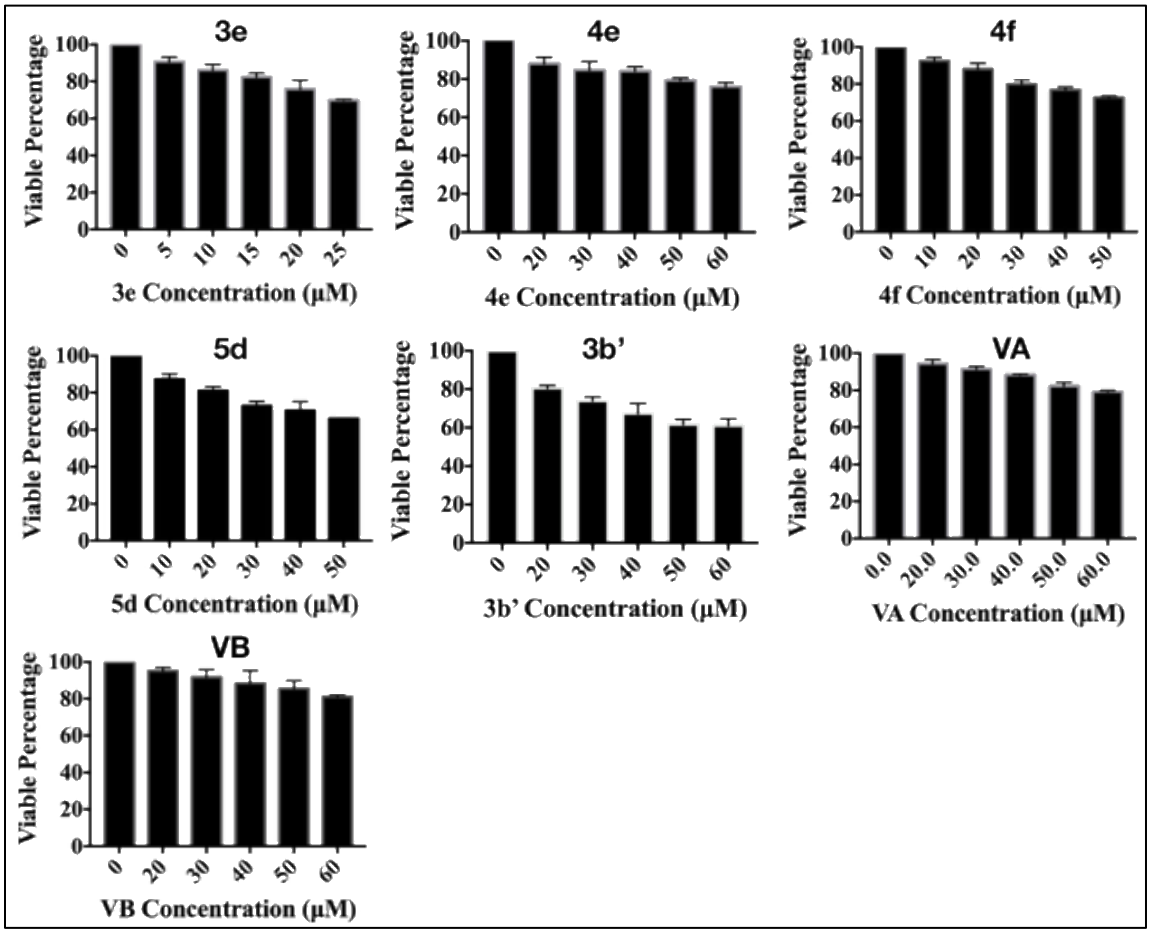

Figure 2.14: MTT assay in Hek 293 cells.

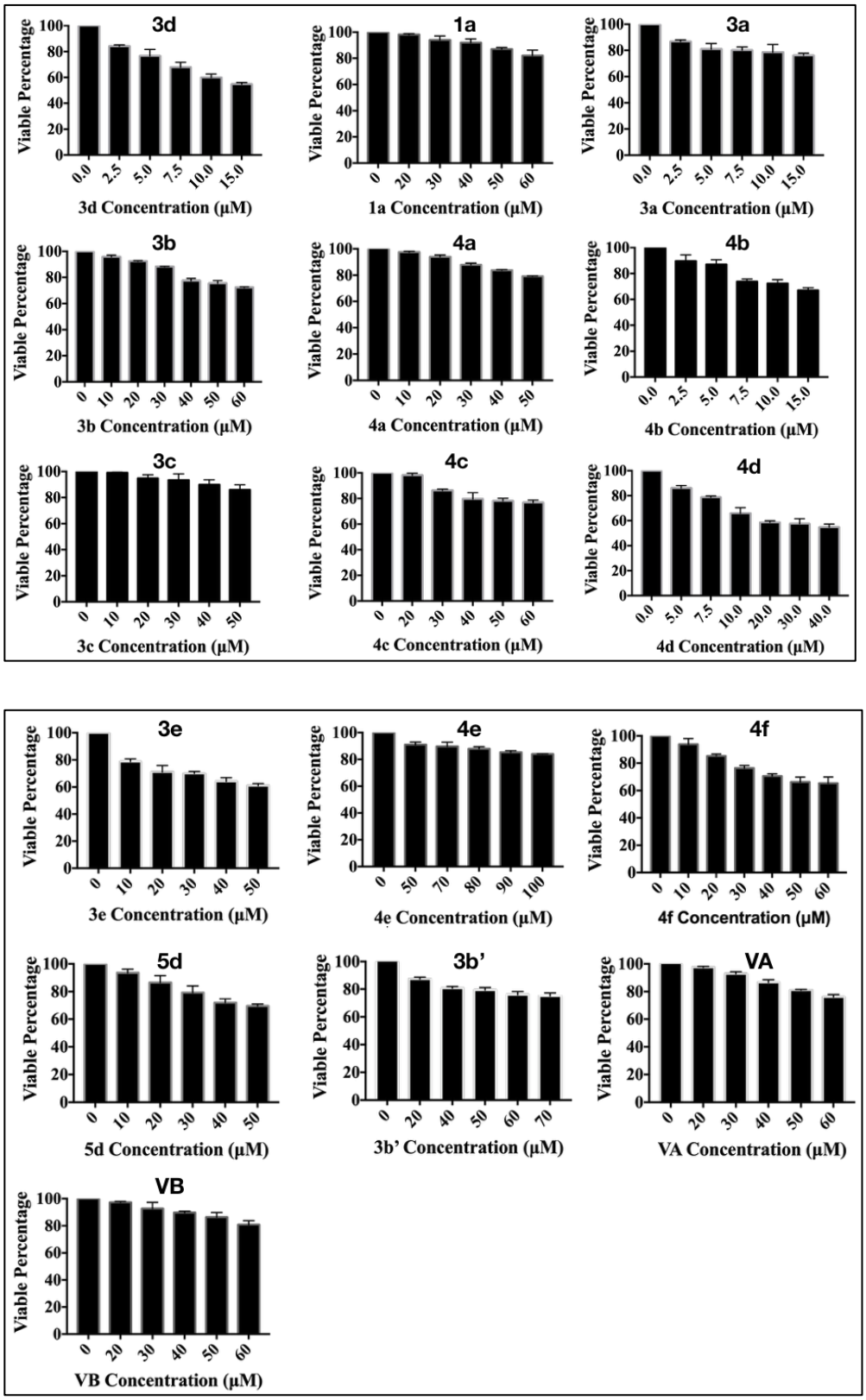

Figure 2.15: MTT assay in Huh 7 cells.

PART B

2.3B. RESULTS AND DISCUSSION:

2.3B.1. Design and synthesis of the quinoxaline derivatives:

A series of monoquinoxaline residues were synthesized by replacing the *N*,*N*-dimethyl propyl amine tail part of the compound N^2-benzyl-N^3-(3-(dimethylamino)propyl)-6-nitroquinoxaline-2,3-diamine by cyclic pyrrolidine ring (Figure 2.16) in some cases. In other cases, the benzyl part was replaced by piperazine moiety (nonbenzyl). This work was done by Dipendu Patra.

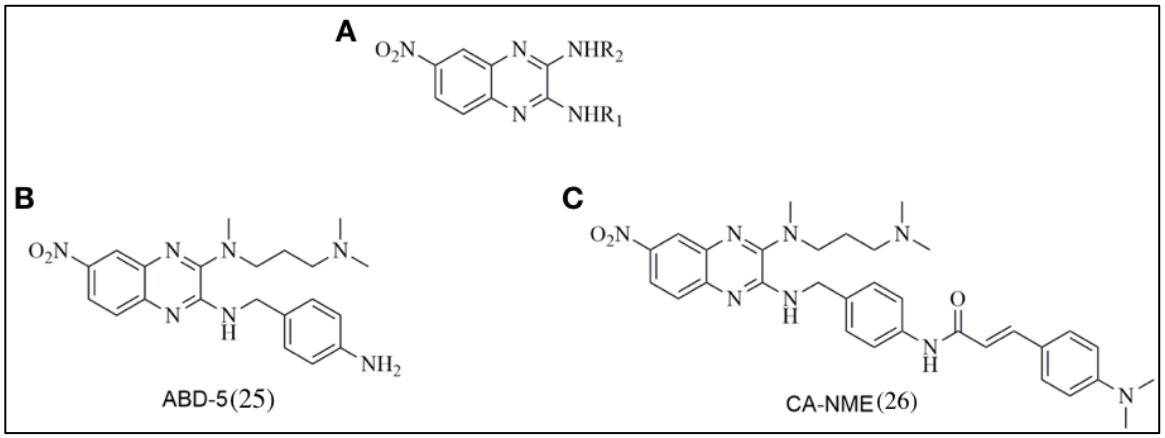

Figure 2.16: A) Monoquinoxaline scaffold used in the study. **B)** and **C)** Structures of all the two most active compounds used in the study.

2.3B.2. Cytotoxicity Studies:

Cell cytotoxicity studies were performed using MTT assay in Huh 7 and Hek 293 cells. Most of the compounds showed very little cytotoxicity **(**Figure 2.17**)**. This cytotoxicity was taken as a reference point for using the compound concentration in dual luciferase assay to eliminate the effect of cytotoxicity in the translation inhibition potential of the molecules.

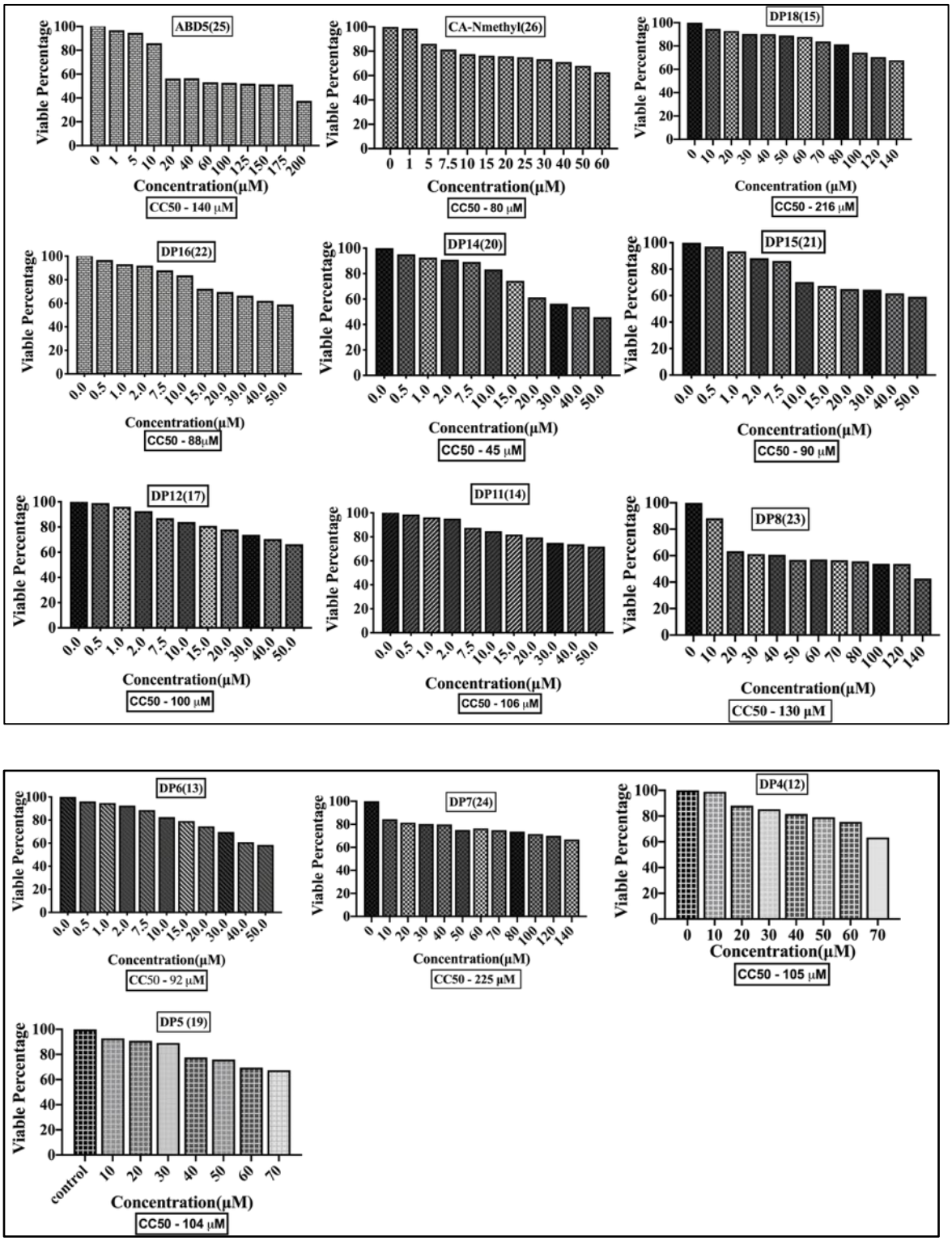

Figure 2.17: Cytotoxicity studies in Hek 293 cells with MTT assay.

2.3B.3. **Dual-Luciferase Assay:**

The synthesized molecules were subjected to dual luciferase-based reporter assay (Figure 2.18). Compound 12 where *N*,*N*-dimethyl propyl amine tail of the DNA intercalating compound N^2-benzyl-N^3-(3-(dimethylamino)propyl)-6-nitroquinoxaline-2,3-diamine (**1d**) was replaced by a pyrrolidine ring reduced HCV IRES-mediated translation efficiency by 45.94 ± 3.35% at 50µM. The most active compound was found to be **ABD5 (25)** wherein the *N*,*N*-dimethyl propyl amine tail was replaced by N,N,N′-tri methylpropane-1,3-diamine group and it decreased the HCV IRES-driven translation by 66.63 ± 6.4 at 25 µM and 77.74 ± 8.9 at 50 µM concentration. Results suggest that the synthesized derivatives can inhibit HCV IRES-mediated translation in Huh 7 cells.

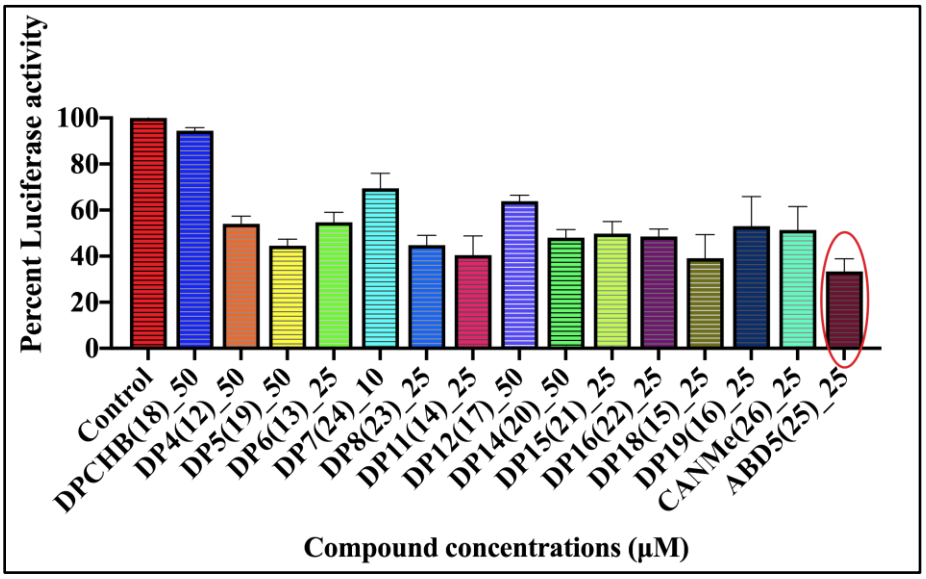

Figure 2.18: Translational Inhibition of HCV IRES by dual luciferase assay for all compounds used for the study.

2.3B.4. **Circular Dichroism studies:**

Circular dichroism studies were performed using the compound **ABD5** (**25**) (Figure 2.19) and CANMethyl **(26)** (Figure 2.20) to check whether the RNA structural alteration property of the compound was still intact using subdomain IIa RNA of HCV IRES. From both figures, it was quite evident that there was a reduction in the ellipticity peak at 265

nm suggesting compound **25** and **26** can alter the RNA structure by disrupting the base stacking interaction in the RNA.

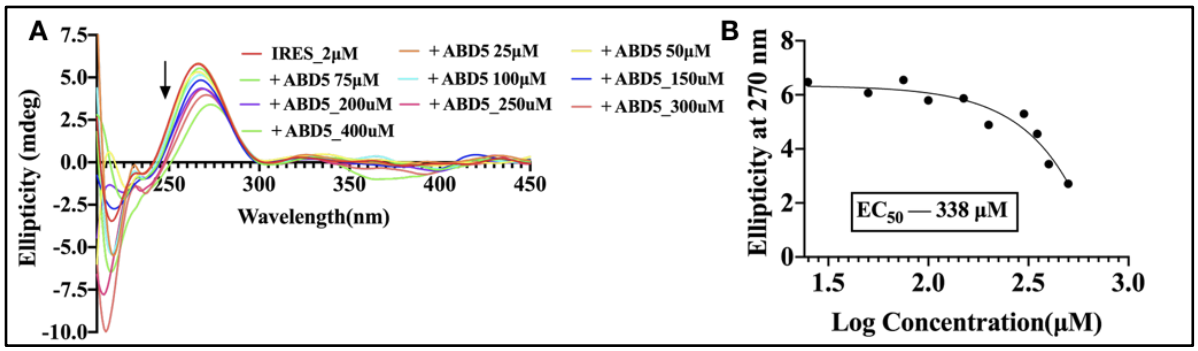

Figure 2.19: A) CD spectra of **ABD5** treated (25 – 400 μM) IRES IIa RNA. **B)** Ellipticity plot at 270 nm for **ABD5** treated IRES IIa.

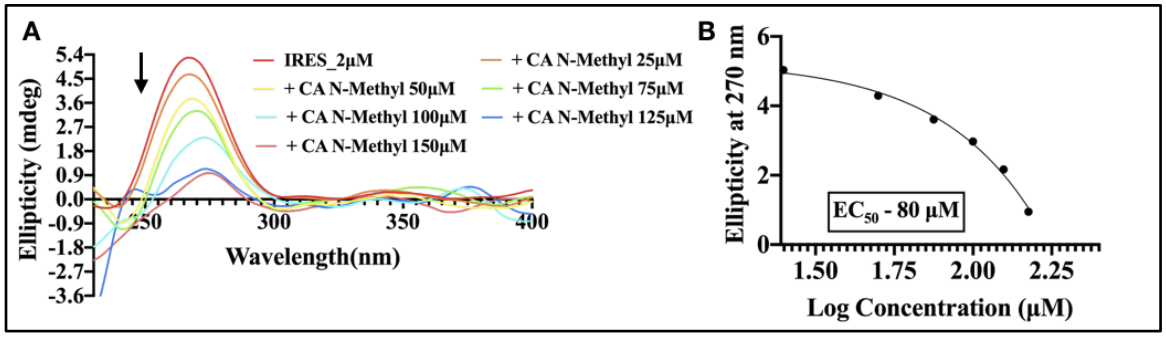

Figure 2.20: A) CD spectra of **CA-Nmethyl** treated (25 – 400 μM) IRES IIa RNA. **B)** Ellipticity plot at 270 nm for **CA-Nmethyl** treated IRES IIa.

2.3B.5. <u>DNA intercalation studies:</u>

DNA Gel shift assay was carried out to study the effect of the most potent IRES binders on DNA. The assay was performed using PBR 322 plasmid DNA. Different PBR 322:IRES binder ratios were used to study the effect of the compounds on the plasmid DNA. It was observed that the compounds ABD5 and CAN-Methyl did not intercalate to the ds DNA even at high molecule: PBR 322 DNA ratios (Figure 2.21) suggesting the molecules show specificity towards the HCV IRES subdomain IIa RNA.

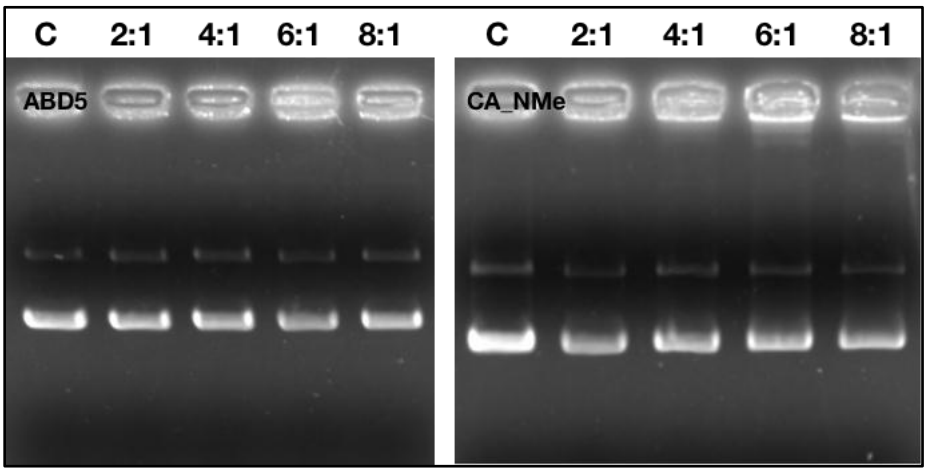

Figure 2.21: PBR 322 plasmid DNA Gel shift assay on treatment with **ABD5(25)** and **CANMe(26)**.

2.4. Conclusion:

The study shows that a group of designed 6-nitroquionoxaline derivatives was successfully synthesized that targets the HCV IRES subdomain IIa RNA. The most potent among them was found to be **4d**, a cinnamic acid derivative that reduced HCV IRES-driven translation by ≈ 60% at 10 μM. Biophysical and Molecular Dynamics analysis showed that **4d** bound to L-shaped loop of the subdomain IIa and lead to the unstacking of bases thereby resulting in the collapsing of the RNA structure. Site-directed Mutagenesis studies using the A57U mutated form of the IRES showed that there was a loss in activity of **4d** towards the A57U mutated IRES suggesting that **4d** bound to the IRES subdomain IIa at a region that is in close proximity to the Adenine 57 nucleotide of the IRES. $MgCl_2$ competitive experiments with **4d** further confirm the fact that **4d** indeed competes with Mg^{2+} for the IRES subdomain IIa binding site.

In the second part, several modifications to the scaffold **1d** were made to reduce cytotoxicity and increase activity. Although cell cytotoxicity was reduced to some extent but the translation inhibition potential was intermediate. Further modifications are required to increase the activity of the compounds before they can be used as an antiviral against HCV infections in the future.

Overall this study provides a good platform for the further development of new antivirals against HCV that can alter the HCV IRES RNA structure resulting in inhibition of HCV IRES-directed replication and translation in mammalian cells. A short model of the study is given below (Figure 2.22).

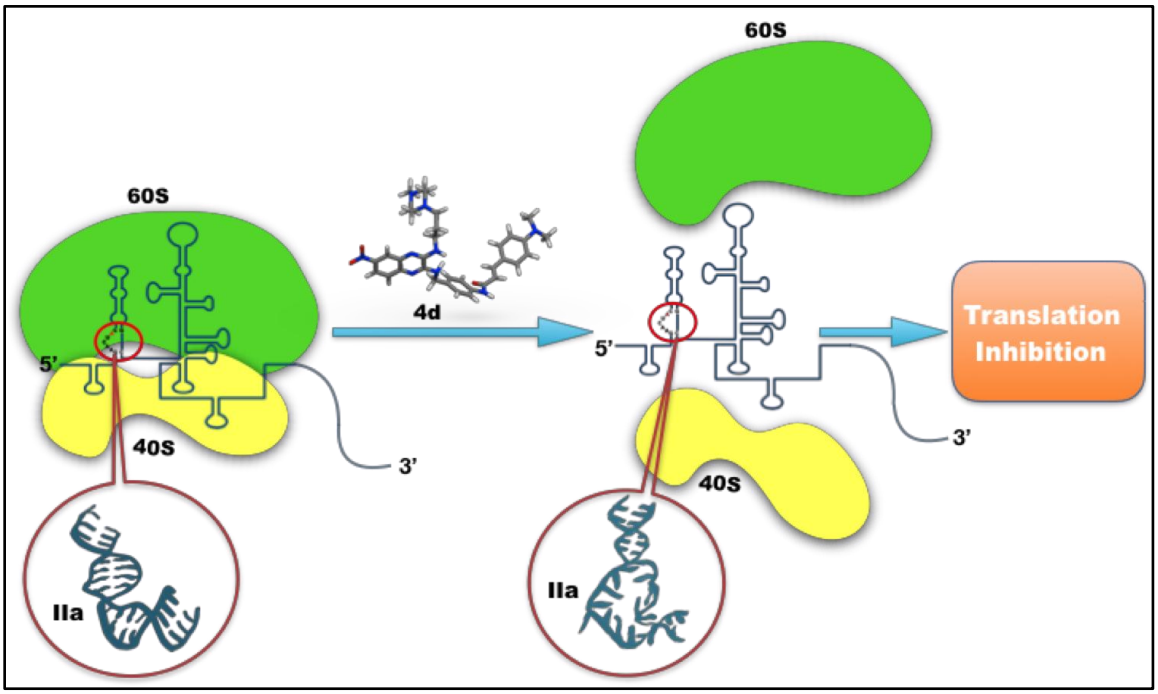

Figure 2.22: Schematic representation how **4d** disrupts the base stacking interaction in the subdomain IIa of the HCV IRES thereby reducing HCV IRES driven translation

2.5. REFERENCES:

160. Seng-Lai, T., Pause, A., Shi, Y., and Sonenberg, N. (2002). Hepatitis C therapeutics: current status and emerging strategies. Nat. Rev. Drug Discov. 1, 867.

161. Fauquet, C. M., Mayo, M. A., Maniloff, J., Desselberger, U. & Ball, L. A. Virus taxonomy: VIIIth report of the International Committee on Taxonomy of Viruses (Academic Press, 2005).

162. Hoofnagle, Jay H. "Course and outcome of hepatitis C." Hepatology. 36.S1 (2002): S21-S29.

163. Petruzziello, Arnolfo, et al. "Global epidemiology of hepatitis C virus infection: An up-date of the distribution and circulation of hepatitis C virus genotypes." World J. Gastroenterol. 22.34 (2016): 7824.

164. Filbin, Megan E., et al. "HCV IRES manipulates the ribosome to promote the switch from translation initiation to elongation." Nat. Struct. Mol. Biol. 20.2 (2013): 150.

165. Tsukiyama-Kohara, Kyoko, et al. "Internal ribosome entry site within hepatitis C virus RNA." J. Virol. 66.3 (1992): 1476-1483.

166. Brown, Edwin A., et al. "Secondary structure of the 5′ nontranslated regions of hepatitis C virus and pestivirus genomic RNAs." Nucleic Acids Res. 20.19 (1992): 5041-5045.

167. Dibrov, Sergey M., et al. "Structure of a hepatitis C virus RNA domain in complex with a translation inhibitor reveals a binding mode reminiscent of riboswitches." Proc. Natl. Acad. Sci. U.S.A. 109.14 (2012): 5223-5228.

168. Lukavsky, Peter J., et al. "Structure of HCV IRES domain II determined by NMR." Nat. Struct. Mol. Biol. 10.12 (2003): 1033-1038.

169. Dibrov, Sergey M., et al. "Functional architecture of HCV IRES domain II stabilized by divalent metal ions in the crystal and in solution." Angew. Chem. 119.1-2 (2007): 230-233.

170. Parsons, Jerod, et al. "Conformational inhibition of the hepatitis C virus internal ribosome entry site RNA." Nat. Chem. Biol. 5.11 (2009): 823-825.

171. Kim, Yoon Ki, et al. "Domains I and II in the 5′ nontranslated region of the HCV genome are required for RNA replication." Biochem. Biophys. Res. Commun. 290.1 (2002): 105-112.

172. Berman, Helen M., et al. "lN Shindyalov, PE Boume. The Protein Data Bank." Nucleic Acids Res. 28 (2000): 235-242.

173. Sastry, G. Madhavi, et al. "Protein and ligand preparation: parameters, protocols, and influence on virtual screening enrichments." J Comput Aid Mol Des. 27.3 (2013): 221-234.

174. Schrödinger, L. "Release 2017–1: LigPrep." LLC, New York, NY: Schrödinger (2017).

175. Ruiz-Carmona, Sergio, et al. "rDock: a fast, versatile and open source program for docking ligands to proteins and nucleic acids." PLoS Comput Biol 10.4 (2014): e1003571.

176. Morley, S. David, and Mohammad Afshar. "Validation of an empirical RNA-ligand scoring function for fast flexible docking using RiboDock®." J Comput Aid Mol Des. 18.3 (2004): 189-208.

177. Van Der Spoel, David, et al. "GROMACS: fast, flexible, and free." J. Comput. Chem. 26.16 (2005): 1701-1718.

178. Gil-Ley, Alejandro, Sandro Bottaro, and Giovanni Bussi. "Empirical corrections to the amber RNA force field with target metadynamics." J. Chem. Theory Comput. 12.6 (2016): 2790-2798.

179. Jorgensen, William L. "Quantum and statistical mechanical studies of liquids. 10. Transferable intermolecular potential functions for water, alcohols, and ethers. Application to liquid water." J. Am. Chem. Soc. 103.2 (1981): 335-340.

180. Zagrovic, Bojan, et al. "Unusual compactness of a polyproline type II structure." Proc. Natl. Acad. Sci. 102.33 (2005): 11698-11703.

181. Parrinello, Michele, and Aneesur Rahman. "Polymorphic transitions in single crystals: A new molecular dynamics method." j Appl Phys. 52.12 (1981): 7182-7190.

182. Van Gunsteren, Wilfred F., and Herman JC Berendsen. "A leap-frog algorithm for stochastic dynamics." MOL SIMULAT. 1.3 (1988): 173-185.

183. Darden, Tom, Darrin York, and Lee Pedersen. "Particle mesh Ewald: An N· log (N) method for Ewald sums in large systems." J CHEM PHYS. 98.12 (1993): 10089-10092.

184. Hess, Berk, et al. "LINCS: a linear constraint solver for molecular simulations." J. Comput. Chem. 18.12 (1997): 1463-1472.

185. Mahata, Tridib, et al. "The Benzyl Moiety in a Quinoxaline-Based Scaffold Acts as a DNA Intercalation Switch." Angew. Chem. Int. Ed. 55.27 (2016): 7733-7736.

186. Jaumot, Joaquim, et al. "Classification of nucleic acids structures by means of the chemometric analysis of circular dichroism spectra." Anal. Chim. Acta. 642.1-2 (2009): 117-126.

187. Chang, Yu-Ming, Cammy K-M. Chen, and Ming-Hon Hou. "Conformational changes in DNA upon ligand binding monitored by circular dichroism." Int. J. Mol. Sci. 13.3 (2012): 3394-3413.

188. Tanaka, Yoshiyuki, et al. "A′-form RNA double helix in the single crystal structure of r (UGAGCUUCGGCUC)." Nucleic Acids Res. 27.4 (1999): 949-955.

189. Miyahara, Tomoo, Hiroshi Nakatsuji, and Hiroshi Sugiyama. "Similarities and Differences between RNA and DNA Double-Helical Structures in Circular Dichroism Spectroscopy: A SAC–CI Study." J. Phys. Chem. A. 120.45 (2016): 9008-9018.

190. Friebe, Peter, et al. "Sequences in the 5′ nontranslated region of hepatitis C virus required for RNA replication." J. Virol. 75.24 (2001): 12047-12057.

SUMMARY OF WORK:

Quinoxaline small molecules are those secondary metabolites that comprise of two-quinoxaline parts attached to an octadepsipeptide ring. They intercalate double-stranded DNA in a sequence-dependent way and a few of their derivatives have been found to be very active against a wide range of bacterial species, different viruses, and other types of cancers as well. They have been used in poultry industries and fisheries in the past but their complex structures make them very difficult to synthesize. To overcome the above challenge, our lab synthesized simpler monoquinoxaline derivatives. In this work, the DNA binding, as well as antibacterial property of one of the lead molecule **3d** was explored. For the binding studies various biophysical techniques like Agarose DNA gel-shift assay using PBR 322 plasmid as well as *Staphylococcus aureus* genomic DNA were done, Circular Dichroism spectroscopy, FID (Fluorescence intercalator Displacement assay), ITC (Isothermal Titration Calorimetry) was also performed. Our study showed that the molecule bound to DNA with high affinity. AFM (Atomic force microscopy studies using PBR 322 and *S. aureus* genomic DNA were performed which showed that the lead compound **3d** led to the opening of the bases in DNA at lower compound: DNA ratios and formation of DNA superstructures and DNA condensation at high compound: DNA ratios. Circular Dichroism studies using Poly AT and Poly GC DNA showed that **3d** bound to Poly GC with high specificity.

MIC studies using five different bacteria (i) *S. aureus* (ii) *S. epidermidis* (iii) *A. chlorophenolicus* (iv) *E. coli* (v) *P. aeruginosa* showed that **3d** had good antibacterial property (low MIC) across all five bacteria when compared to other derivatives and best activity against *S. aureus*. Further studies of **3d** treated *S. aureus* cells revealed that **3d** induced replication stress in the cells and led to DNA damage as well as Nucleoid fragmentation. In cell nucleoid condensation studies showed that **3d** induces condensation of the bacterial nucleoid by around 30%. Upon treatment with **3d, a** change in the morphology of *S. aureus* cells was observed and loss in bacterial membrane integrity was also noticed leading to bacterial cell death. The potential of **3d** in disrupting Biofilms of both *S. aureus* and *S. epidermidis* was also an observable phenomenon.

In another work, differently designed and synthesized monoquinoxaline derivatives inspired from the crystal structure of Benzimidazole and domain IIa of HCV IRES was found to inhibit Hepatitis C virus-mediated translation and replication in Huh 7 cells. A lead compound **4d** was found to have activity comparable to benzimidazole. Mutational studies using an A57U mutant revealed that **4d** bound to a region in the domain IIa that was in close proximity to the A57 residue in the L-shaped pocket. Circular dichroism studies using **4d** treated IIa showed that **4d** leads to unstacking of bases in the L-shaped loop of IIa leading to collapsing of the RNA structure at a high **4d: RNA** ratio. Competitive binding experiment between **4d** and $Mgcl_2$ showed that **4d** competes with Mg for the binding site in the domain IIa**.** DNA gel shift assay using PBR 322 plasmid DNA showed **4d** had high specificity for the HCV RNA and did not intercalate into ds DNA.

PUBLICATIONS

Manuscript Published:

- **Jeet Chakraborty**,‡ Ajay Kanungo,‡ Tridib Mahata, Krishna Kumar, Geetika Sharma, Ritesh Pal, Khondakar Sayef Ahammed, Dipendu Patra, Bhim Majhi Saikat Chakrabarti, Saumitra and Sanjay Dutta*. Quinoxaline derivatives disrupt the base stacking of hepatitis C virus-internal ribosome entry site RNA: Reduce translation and replication. DOI: 10.1021/acs.biochem.8b00613**.(**‡-Authors contributed equally**)**

- Khondakar Sayef Ahammed,‡ Ritesh Pal,‡ **Jeet Chakraborty**,‡ Ajay Kanungo, Polnati Sravani Purnima, Sanjay Dutta *. DNA Structural Alteration Leading to Antibacterial Properties of 6-Nitroquinoxaline Derivatives. DOI:10.1021/acs.jmedchem.9b00599.**(**‡-Authors contributed equally**).**

- Tridib Mahata, **Jeet Chakraborty**, Ajay Kanungo, Dipendu Patra, Gautam Basu, and Sanjay Dutta*. Intercalator-Induced DNA Superstructure Formation: Doxorubicin and a Synthetic Quinoxaline Derivative. DOI: 10.1021/acs.biochem 8b00613.

Manuscript under preparation:

- Ritesh Pal,‡ **Jeet Chakraborty**,‡ Titas Kumar Mukhopadhyay,‡ Rimita Saha, Ajay Kanungo, Amit Chakraborty, Dipendu Patra, Ayan Datta,* and Sanjay Dutta.* Substituent Effect of Benzyl Moiety in Nitroquinoxaline Small Molecules upon DNA Binding: Cumulative Destacking of DNA Nucleobases leading to Histone Eviction.

- Chandra Sova Mandi, Tridib Mahata, Dipendu Patra, **Jeet Chakraborty**, Achyut Bora, Ritesh Pal, Sanjay Dutta.* Targeting DNA abasic sites by designed quinoxaline small molecule in cancer cell.

ChemComm

COMMUNICATION

View Article Online
View Journal | View Issue

Cite this: Chem. Commun., 2019, 55, 14027

Received 22nd August 2019,
Accepted 14th October 2019

DOI: 10.1039/c9cc06531h

rsc.li/chemcomm

Quinoxaline derivatives disrupt the base stacking of hepatitis C virus-internal ribosome entry site RNA: reduce translation and replication†

Jeet Chakraborty,‡[a] Ajay Kanungo,‡[ab] Tridib Mahata,[a] Krishna Kumar,[c] Geetika Sharma,[d] Ritesh Pal,[ab] Khondakar Sayef Ahammed,[a] Dipendu Patra,[ab] Bhim Majhi,[ab] Saikat Chakrabarti,[c] Saumitra Das[de] and Sanjay Dutta[*ab]

RNA-based small molecules with a monoquinoxaline core target the L-shaped structure of subdomain IIa of Hepatitis C virus internal ribosome entry site (IRES) RNA in proximity to the Mg^{2+} binding site. The binding event leads to the destacking of RNA bases, resulting in the inhibition of IRES-mediated translation and HCV RNA replication.

Hepatitis C virus (HCV) infection is one of the major liver diseases and a global health concern.[1] HCV contains 9.6 kb long positive-sense single-stranded RNA genome that acts as the template for both RNA replication and viral protein translation.[2] Highly structured 5′-untranslated region (UTR) of HCV RNA consists of a 341 nucleotides long internal ribosome entry site (IRES) that plays a crucial role in the viral cap-independent translation process (Fig. 1A).[3] Subdomain IIa (Fig. 1C) of HCV-IRES adopts an L-shaped conformation with a characteristic interhelical angle that assists in the right incorporation of subdomain IIb in the 40s ribosome E site and helps in the initiation of translation.[4] The maintenance of this L-shaped RNA structure is primarily guided by divalent metal ions as well as the stacking of the RNA bases.[5] The overall bent structure of the subdomain IIa with internal bulge, encompassing the residues G52 to C58 on one strand and G110 and C111 on the other strand of the RNA duplex, are stabilized by divalent metal ions (Mg^{2+} and Mn^{2+}).[6] Further studies have unraveled the significance of these metal ions as the key factors that help to maintain the functional bent architecture of subdomain IIa.[7] A significant structural change in the L-shaped conformation by ligand or small molecule results in the inhibition of IRES-mediated translation efficiency and is an attractive antiviral target against HCV.[7]

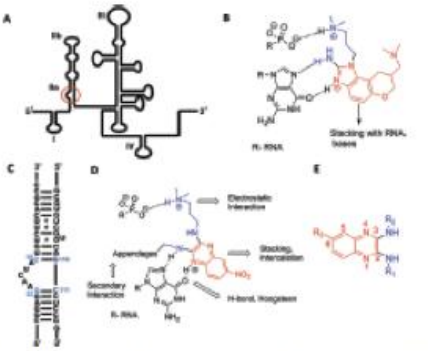

Fig. 1 (A) Secondary structure of complete HCV-IRES; (B) benzimidazole ligand forming Hoogsteen base pair with G110 RNA base of HCV-IRES subdomain IIa; (C) sequence of HCV-IRES subdomain IIa; (D) Proposed interaction of monoquinoxaline-based small molecule with subdomain IIa; (E) monoquinoxaline scaffold with different positions of substitution (C2, C3 and C6).

The design of monoquinoxaline derivatives, which can target the subdomain IIa of HCV-IRES, was inspired from the crystal structure of the subdomain IIa RNA inhibitor complex (Fig. 1B).[8] On the basis of the crystal structure, we hypothesize that the quinoxaline moiety might be involved in stacking interactions with RNA bases. Moreover, the nitrogen atoms of the quinoxaline moiety may assist *via* the formation of Hoogsteen base pairs with the guanine residues and the protonated *N*,*N*-dimethylaminopropylamine side chain will interact with the phosphate backbone, thereby increasing the affinity of the ligand toward the RNA molecule (Fig. 1D).

[a] Organic and Medicinal Chemistry Division, CSIR-Indian Institute of Chemical Biology, 4 Raja S. C. Mullick Road, Kolkata 700032, West Bengal, India. E-mail: sanjaydutta@iicb.res.in
[b] Academy of Scientific and Innovative Research (AcSIR), Kolkata-700032, West Bengal, India
[c] Structural Biology and Bioinformatics Division, CSIR-Indian Institute of Chemical Biology, India
[d] Department of Microbiology & Cell Biology, Indian Institute of Science, SERB, Biological Sciences Building, Sir C. V. Raman Avenue, Bangalore 560012, India
[e] National Institute of Biomedical Genomics, Kalyani, West Bengal, India

† Electronic supplementary information (ESI) available. See DOI: 10.1039/c9cc06531h

‡ These authors contributed equally.

Journal of Medicinal Chemistry

Article

Cite This: J. Med. Chem. 2019, 62, 7840−7856

pubs.acs.org/jmc

DNA Structural Alteration Leading to Antibacterial Properties of 6-Nitroquinoxaline Derivatives

Khondakar Sayef Ahammed,[†,§] Ritesh Pal,[†,‡,§] Jeet Chakraborty,[†,§] Ajay Kanungo,[†,‡] Polnati Sravani Purnima,[†] and Sanjay Dutta*[,†,‡]

[†]Organic and Medicinal Chemistry Division, CSIR- Indian Institute of Chemical Biology 4, Raja S.C.Mullick Road, Kolkata, 700032 West Bengal, India

[‡]Academy of Scientific and Innovative Research (AcSIR), Kolkata, 700032 West Bengal, India

Supporting Information

ABSTRACT: Structural integrity of the bacterial genome plays an important role in bacterial survival. Cellular consequences of an intolerable amount of change in the DNA structure are not well understood in bacteria. Here we have stated that binding of synthetic 6-nitroquinoxaline derivatives with DNA led to change in its global structure, subsequently culminating with over-supercoiled form through in-path intermediates. This structural change results in induction of programmed cell death like physiological hallmarks, which is dependent on substitution driven structural modulation properties of the scaffold. A sublethal dose of a representative derivative, 3a, significantly inhibits DNA synthesis, produces fragmented nucleoids, and alters membrane architecture. We have also shown that exposure to the compound changes the native morphology of *Staphylococcus aureus* cells and significantly disrupts preformed biofilms. Thus, our study gives new insight into bacterial responses to local or global DNA structural changes induced by 6-nitroquinoxaline small molecules.

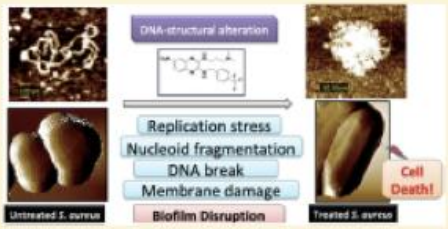

INTRODUCTION

Continuous emergence of bacterial resistance to conventional antibiotics is a serious global health concern. Bacteria that adopt resistance to antibiotics, use several mechanisms to reduce antibiotic effectiveness like drug target modifications, drug efflux from the cell, chemical modifications of the drug, or some other means.[1] More importantly some of the pathogenic bacteria can form biofilms that worsen the problem of drug resistance.[2] Biofilm formation limits drug effectiveness by reducing the penetration of antibiotics, altering their micro-environment, and neutralizing antibiotics thereby forming a multilayered defense system that contributes toward the global problem of antibiotic resistance.[3] The increasing tolerance of bacteria to antibacterial drugs reinforces the need to develop new antibacterial compounds with distinctive mechanisms.

Bacterial DNA is far longer than the average size of a bacterial cell. Inside the cell, bacteria maintain the structural architecture of their genome in a finely regulated compact form.[4] Many genome structuring proteins such as histone-like protein HU and HNS play crucial roles in maintaining the structure of the bacterial nucleoid.[5,6] Recent research indicates local supercoiling and dynamics of bacterial chromosome associated proteins regulate fundamental processes like replication, gene expression, etc.[5−7] Cellular responses to intolerable amounts of local or global structural alteration in DNA induced by small molecules have not been explored well. We have probed the physiological responses during the shock of small molecule induced structural alteration of DNA in bacterial cells.

Small molecules that bind to DNA may influence the survival of a cell by interfering with essential cellular functions. Quinoxaline based small molecules are biologically active compounds widely known as potent antiproliferative and antimicrobial agents. Quinoxaline antibiotics like triostin A (Figure 1A) are known to intercalate into dsDNA and are preferentially active against Gram-positive bacteria.[8−10] Several synthetic scaffolds using the quinoxaline moiety have been developed that have antibacterial properties against a wide range of pathogenic bacterial strains.[11−13] Quinoxaline N-oxides (QNOs) exhibit antibacterial activity by targeting DNA and inducing reactive oxygen species (ROS).[14] For a long time, quinoxaline containing antibiotics have been used as veterinary medicines for the treatment of bacterial infections in animal husbandry. Considering the moderate selectivity index, a subtherapeutic dose of QNOs (for example, OLA, 2-(*N*-2′-hydroxyethyl-carbamoyl)-3-methyl quinoxaline 1,4-dioxide; CBX, hydrazine carboxylic acid (2-quinoxalinyl-methylene) methyl ester 1,4-dioxide; or CYA, 2-formylquinoxaline-N^1,N^4-dioxide cyanocetylhydrazone) with feed additives are used as

Received: April 8, 2019
Published: August 7, 2019

DOI: 10.1021/acs.jmedchem.9b00599
J. Med. Chem. 2019, 62, 7840−7856

Biochemistry

Article

Cite This: Biochemistry 2018, 57, 5557−5563

pubs.acs.org/biochemistry

Intercalator-Induced DNA Superstructure Formation: Doxorubicin and a Synthetic Quinoxaline Derivative

Tridib Mahata,[†] Jeet Chakraborty,[†] Ajay Kanungo,[†‡] Dipendu Patra,[†‡] Gautam Basu,[*§] and Sanjay Dutta[*,†,‡]

[†]Department of Organic and Medicinal Chemistry, CSIR-Indian Institute of Chemical Biology, 4, Raja S. C. Mullick Road, Kolkata 700032, WB, India

[‡]Academy of Scientific and Innovative Research (AcSIR), New Delhi 600113, India

[§]Department of Biophysics, Bose Institute, P-1/12 CIT Scheme VIIM, Kolkata 700054, India

Supporting Information

ABSTRACT: Small molecules that intercalate DNA have tremendous therapeutic potential. Typically, DNA intercalators do not alter the overall DNA double-helical structure, except locally at the intercalation sites. In a previous report, we showed that a quinoxaline-based intercalator with a mandatory benzyl substitution (1d) induced an unusually large circular dichroism signal upon DNA binding, suggesting the formation of intercalated DNA superstructures. However, no detailed structural studies have been reported. Using atomic force microscopy, we have probed the nature of the superstructure and report the formation of a plectonemically oversupercoiled structure of pBR322 plasmid DNA by 1d, where close association of distant DNA double-helical stretches is the predominant motif. Without the benzyl moiety (1a), no such DNA superstructure was observed. Similar superstructures were also observed with doxorubicin (dox), a therapeutically important DNA intercalator, suggesting that the superstructure is common to some intercalators. The superstructure formation, for both intercalators, was observed to be GC-specific. Interestingly, at higher concentrations (1d and dox), the DNA superstructure led to DNA condensation, a phenomenon typically associated with polyamines but not intercalators. The superstructure may have important biological relevance in connection to a recent study in which dox was shown to evict histone at micromolar concentrations.

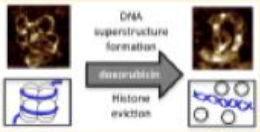

DNA regulates a plethora of biological processes. While the role of the canonical double-helical DNA structure is well-established, we are only beginning to understand the biological role of the more compact DNA superstructures.[1] Classic examples of DNA superstructure formation are DNA compaction by histones[2] and DNA condensation by polycationic species.[3] Proteins such as Hfq and H-NS also participate in DNA condensation and compaction.[4] Cationic lipids, designed for gene delivery, can also induce compaction of plasmid DNA.[5] DNA intercalation by small molecules can subtly alter the helical conformation of DNA. However, their role in DNA compaction and condensation has not been explored much. For example, DNA-intercalating agents like YOYO-1 can cause DNA condensation at acidic pH (5.7), although the mechanism is unclear.[6]

In an earlier report,[7] we showed that a simple 6-nitroquinoxaline-2,3-diamine derivative [1d (Figure 1)] acts as a DNA intercalator and brings about a large DNA conformational change at high 1d concentrations. Interestingly, no such conformational change was observed for an analogue [1a (Figure 1)] lacking a crucial benzyl substituent. The large conformational change in DNA was reflected in the unusually large induced circular dichroism (ICD) signal of the ligand that appeared in a sigmoidal fashion accompanying ligand binding at a high ligand:DNA ratio. However, ICD only indirectly reports any underlying structural change. In contrast, atomic force microscopy (AFM) can provide a direct high-resolution image of single DNA molecules, free or ligand-bound, at nanometer resolution. Here, we report the morphological changes in DNA at varying ligand:DNA ratios (1d and 1a) and show that supercoiled plasmid DNA converts into an oversupercoiled plectonemic structure with an increase in the 1d:DNA ratio, finally leading to DNA condensation, not observed for 1a. The appearance of the superstructure is sequence-dependent (GC-specific). Similar DNA superstructure formation, followed by DNA condensation at high ligand:DNA ratios, was also observed for doxorubicin [dox

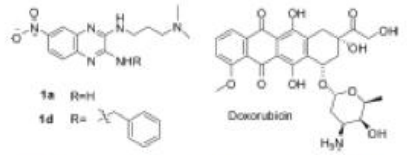

Figure 1. Molecular structures of 1a, 1d, and doxorubicin (dox).

Received: June 1, 2018
Revised: August 11, 2018
Published: August 31, 2018

DOI: 10.1021/acs.biochem.8b00613
Biochemistry 2018, 57, 5557−5563